• U C •

FCTUC FACULDADE DE CIÊNCIAS
E TECNOLOGIA
UNIVERSIDADE DE COIMBRA

Pâmela Cristina Carvalho Borges

Development of a new electromechanical probe for hemodynamic parameters assessment

Dissertation presented to the University of Coimbra in order to complete the necessary requirements to obtain the master's degree in Biomedical Engineering.

Project Coordination

Advisor PhD Professor Carlos M. B. A. Correia
Co-Advisor Eng. Helena Catarina Pereira

Coimbra, September 2014

Research Units

This work was developed in collaboration with:

CI-GEI

Centro de Instrumentação - Grupo de Electrónica e Instrumentação

Departamento de Física

FCTUC

(http://lei.fis.uc.pt)

Strength does not come from physical capacity but from an indomitable will.

(Mahatma Gandhi)

Acknowledgements

I would like to thank all the GEI team especially to PhD Prof. Carlos M.B. A. Correia, PhD Prof. Luís Requicha Ferreira who guided me throughout this journey. Thanks for the patience, time and professionalism.

I also want to thank my parents, Maria Teresa J. V. Carvalho and Fernando Jorge L.T. Borges, and my sister Gisela Tavares Borges for being the sense of my world, my support and inspiration.

I must not forget all my grandparents who have always been there for me, ready to enrich my world with their wise words and life stories full of meaning and lessons.

To all, my sincere thanks.

Pâmela Cristina Carvalho Borges

September, 2014

Abstract

Cardiovascular Diseases (CVDs) have been causing millions of death every year, being the main cause of death worldwide.

Hypertension is one of the most relevant CVD risk factors. The development of an easy, low-cost and accurate diagnostic technique capable of detecting early alterations on the cardiovascular system performance is very important, since it allows increasing the survival probability. The analysis of central blood pressure (cBP) waveform provides relevant clinical information since cardiovascular pathologies alter its shape.

This research project is focused on the development of a new, non-invasive hemodynamic probe which integrates a piezoelectric (PZ) sensor and an accelerometer connected to a demodulator circuit. The probe assesses the waveform of carotid blood pressure simulated through test bench systems, developed along this project. Result signals are acquired by using, at first stage, an USB NI-6008/USB NI-6210 module in association with an arbitrary waveform generator (Agilent), a power source and a computer. At a later stage it was used a multifunctional instrument capable to generate, record, convert, measure and analyze analog and digital signals (Digilent module) and a computer. Algorithms capable to process the acquired signals were developed through *Matlab* software.

The results of the system performance evaluation, including the validation tests performed on bench systems are presented, as well as the abbreviated signal analysis methodology applied. Experimental test proved the efficiency of the developed acquisition box and the last version of the test bench system whose allowed assessing, accurately, the APW and ABP.

Keywords

Cardiovascular Disease, Hypertension, Carotid Blood Pressure Waveform,
Piezoelectric sensor, Accelerometer, Modulation, Demodulation.

Resumo

As doenças cardiovasculares (DCVs) causam milhões de mortes todos os anos, sendo a principal causa de morte no mundo inteiro.

A hipertensão é um dos mais relevantes factores de risco das doenças cardiovasculares. Assim sendo, é muito importante o desenvolvimento de um método de diagnóstico que seja barato, fácil utilização, preciso e capaz de detectar alterações precoces da performance do sistema cardiovascular, permitindo, desta forma, aumentar a probabilidade de sobrevivência. A análise da forma de onda da pressão sanguínea central fornece informações clínicas relevantes uma vez que patologias cardiovasculares alteram a sua forma de onda.

Este projecto de investigação foca-se no desenvolvimento de um novo sensor hemodinâmico não-invasivo que integra um sensor piezoeléctrico e um acelerómetro ligados a um circuito demodulador. O sensor acessa a forma de onda da pressão sanguínea, simulada através das bancadas de teste desenvolvidas ao longo deste projecto. Numa fase inicial, os sinais resultantes são adquiridos recorrendo á utilização dos módulos de aquisição USB NI-6008 ou USB NI-6210 associado a um gerador arbitrário de formas de onda (Agilent), a uma fonte de alimentação e a um computador. Numa fase posterior foi utilizado um dispositivo multifuncional capaz gerar, guardar, converter, medir e analisar sinais analógicos e digitais (Digilent) e um computador. Algoritmos capazes de processar os sinais foram desenvolvidos utilizando o *Matlab.*

Os resultados das avaliações da performance do sistema são apresentados ao longo da dissertação, incluindo os testes de validação efectuados nas bancadas de teste e a descrição da metodologia aplicada à análise dos sinais recolhidos. Testes experimentais provaram a eficiência da caixa de aquisição e da última versão da bancada de teste, permitindo adquirir, com precisão, sinais referentes à pressão arterial e à sua forma de onda.

Palavras-Chave

Doenças Cardiovasculares, Hipertensão, Forma de onda da pressão sanguínea da Carótida, Sensor Piezoeléctrico, Acelerómetro, Modulação, Desmodulação.

Contents

List of Figures

List of tables

Acronyms

ABP	Arterial Blood Pressure
ABPD	Arterial Blood Pressure Device
Aix	Augmentation Index
AM	Amplitude modulation
OpAmp	Operational Amplifier
AP	Arterial Pulse
APW	Arterial Pressure Waveform
AS	Arterial Stiffness
CVD	Cardiovascular disease
cBP	Central Blood Pressure
DBP	Diastolic Blood Pressure
ECG	Electrocardiogram
FM	Frequency modulation
MAP	Mean Arterial Pressure
NIBP	Non-invasive Blood Pressure Device
PCB	Printed Circuit Board
PM	Phase modulation
PPG	Photoplethysmography
PTT	Pulse Transit Time
PWV	Pulse wave velocity
PZ	Piezoelectric
pABP	Peripheral Arterial Blood Pressure
RMSE	Root mean square error
SBP	Systolic Blood Pressure
Vpp	Voltage pick to pick
WHO	World Health Organization

Chapter 1

Introduction

Contents

1.1 Motivation

Cardiovascular diseases (CVDs) are the main cause of death worldwide. According to the World Health Organization (WHO), at least 17.3 million people died from CVDs in 2008, representing 30% of all death. Statistics relative to developed countries are more disturbing, revealing that CVDs are responsible for 40% of all death against 28% on underdeveloped countries [4, 53]. Because of the high mortality and morbidity, it's very important to detect with high precision the early manifestation of these diseases.

Hypertension is the main CVD risk factor where the arterial blood pressure (ABP) is a parameter that plays a significant role on the cardiovascular condition assessment. Through its waveform analysis, abundant, reliable and important clinical information about cardiovascular system performance is achieved, because cardiovascular pathologies affect the arterial pressure waveform (APW) in many ways [54].

The main methods for clinical ABP measurement are expensive and difficult to operate, even for professionals. In intense care units an intravenous catheter is used to assess the ABP. Despite its accuracy, it is an invasive method, the discomfort is very high and it has some risks to the patient. Non-invasive methods such as the Riva-Rocci 'sphygmomanometer, automated devices based on the oscillometry and auscultation method using a stethoscope, are mainly used in non-critical clinical situations. These techniques have some weaknesses: the measurement process is slow and limited, they have methodological and observer errors and some of them measure the peripheral ABP, which has a lower predictive value [6, 37].

The measuring method that is proposed in this project is non-invasive, low-cost, easy and practical to use and it has already proved its feasibility in test bench and in vivo conditions [7, 58].

This work intends to introduce some methodological improvements on the hardware and software and to develop of a strong algorithm capable to extract decisive clinical information from the ABP waveform, allowing an easy and quick patient assessment and diagnosis.

1.2 Main Contribution

This project allowed the improvement of a low-cost, small and portable prototype capable of easy and accurately detecting carotid blood pressure waveform. Algorithms were developed to extract relevant clinical information from the shape analysis.

1.3 Content by Chapter

On this section a brief content resume of each chapter will be presented in order to guide the reader throughout this thesis.

Chapter 1 – Introduction: This chapter introduces the framework and objectives of this project, describing its structure.

Chapter 2 - Theoretical Background: Physiological concepts about cardiovascular system, arterial pressure and relevant hemodynamic parameters are presented. A brief approach about PZ sensors and accelerometers are also found at the end of this chapter.

Chapter 3 – Process methodology: The Chapter describes the two different acquisition systems developed during this project, indicating the several constituents that integrate them and their respective function. Some theoretical support concepts are also presented.

Chapter 4 – The Hemodynamic probe: In this chapter a detailed description of the hemodynamic probe design, constitution and performance is done. Experimental tests results are presented and analyzed.

Chapter 5 – Amplitude Demodulator: This chapter presents theoretical information about modulation and demodulation processes, focusing on envelope detector circuit design and performance. Experimental tests of the demodulator, both on the breadboard and printed circuit board (PCB) are detailed as well as their result and analysis.

Chapter 6 – Test bench system: This chapter focuses on the description of the two different test bench systems developed during this project in order to simulate the

ABP waveform. The result signals obtained from the experimental tests are analyzed.

Chapter 7 – Conclusion: This chapter shows the general conclusions from this work, future ideas and suggestions that may improve results.

Appendixes: Several documents are presented, detailing the specificities of devices used during this project for a better comprehension of the reader.

Chapter 2

Theoretical Background

Contents

2.1 Cardiovascular System Physiology

2.1.1 The Heart

Located in the thoracic cavity, medial to lungs, posterior to the sternum and superior to the diaphragm, the heart is a muscular organ surrounded by pericardium that weighs $250 - 300\ g$ and which size approximates a closed fist. Its function is to pump blood throughout the body's tissues, removing carbon dioxide and providing them oxygen and nutrients [60].

According to the figure 2.1 the heart anatomy consists of four compartments: the right and left atria; the right and left ventricles. Left ventricle's free wall and septum are thicker than the right ventricle wall since it's responsible to pump blood trough the systemic circulation, needing higher pressure than for respiratory circulation [56, 60].

It also contains four valves classified on two main types:

- Atrioventricular
  - Tricuspid valve: located between the right atrium and ventricle;
  - Mitral valve: stands between the left atrium and ventricle;
- Semilunar
  - Pulmonary valve: found between the right ventricle and pulmonary artery;
  - Aortic valve: lies in the outflow tract of the left ventricle controlling the blood flow to aorta [56].

Figure 2.1 shows the cavities and the movement route of the blood inside the heart.

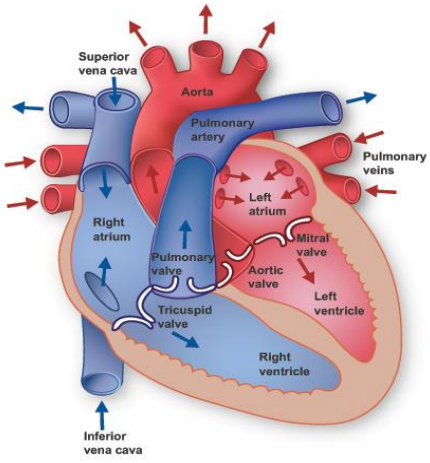

Figure 2.1: The anatomy and physiology of the heart. The image illustrates the anatomical structure of the heart, showing all the cavities, valves and main arteries. It's also possible to see the courses followed by the blood during a heart cycle [8].

The greater vessels are the superior and inferior vena cava, the pulmonary artery and veins, as well as the aorta.

2.1.2 Cardiac cycle

A cardiac cycle refers to any heart event related to blood flow and blood pressure from the beginning of one heartbeat to the beginning of the next one. A single heartbeat, which duration is approximately one second, has five main stages. At the first two stages, both considered as "Ventricle Filling" stages, the blood moves from atria to ventricle. The next two stages involve the blood movement from ventricle to pulmonary artery (right ventricle) and aorta (left ventricle) during isovolumetric contraction and ejection phase. What follows is the quiescent phase where an isovolumetric relaxation on early ventricle diastole occurs [56].

The figure below shows the variation of the pressure, ventricular volume, heart sounds and electrocardiogram signal during a single cardiac cycle.

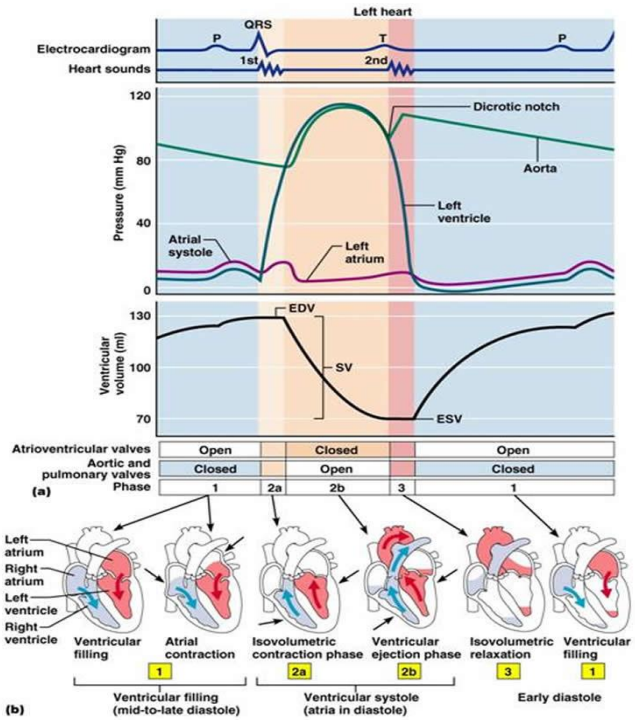

Figure 2.2: Cardiac cycle diagram and its stages. At the first two stages the ventricle is filled with blood. The three next stages correspond to the movement of the blood to pulmonary artery (right ventricle) and aorta (left ventricle). During a cardiac cycle contraction and relaxation there are changes on the aortic pressure, left ventricle pressure (LVP), left atrial pressure (LAP), left ventricle volume (LV Vol) and heart sounds. All those changes are time related to the electrocardiogram (ECG) [16, 24].

The heart pumping leads the blood to have two main circulatory routes: the systemic and respiratory [15].

- Respiratory circulation

Deoxygenated blood from all over the body enters the right atrium through superior and an inferior vein cave. Then, it is pumped through the tricuspid valve into the right ventricle. From the right ventricle, the blood is pumped through the pulmonary valves into pulmonary trunk.

At the lung the carbon dioxide is released and oxygen is absorbed. After gases exchange, oxygenated blood returns to heart through pulmonary arteries, filling the left atrium [56].

- Systemic circulation

The blood that arrives on the left atrium from lungs goes to the left ventricle passing through mitral valve. After ventricle systole the blood is pumped through the aortic semilunar valve into the aorta. From the aorta, blood enters into systemic circulation throughout the body tissues, providing oxygen, until it returns to the heart via the vena cava [55, 56].

- Coronary circulation

The myocardium also has its vital needs. The right and left coronary arteries which arise from the ascending aorta and encircle the heart are responsible to reach heart 'cells with oxygenated blood [56].

Figure 2.3 presents the main circulatory routes, the respiratory and the systemic one.

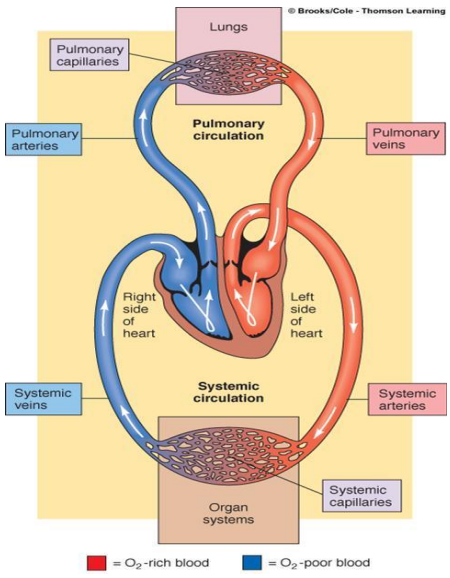

Figure 2.3: Blood circulation during a cardiac cycle. At the right atrium venous blood arrives from all over the body which is then pumped through the respiratory circulation where gases exchanges are made, reaching the blood with oxygen. The left side receives the oxygenated blood from the lungs and pumps it to the all body, through the systemic circulation [16].

2.2 Cardiovascular Diseases

2.2.1 General concepts

CVD is a class of disease caused by disorders of the heart and blood vessels (arteries, capillaries and/or veins) [2, 61]. It includes several diseases as:

- Coronary heart disease: troubles on blood vessels supplying heart muscle;
- Cardiomyopathy: problems with the heart muscles itself;
- Cerebrovascular disease: problems on blood vessels supplying the brain;
- Cardiac Dysrhythmias: Abnormalities on the heart rhythm;
- Peripheral arterial disease: when blood vessels that supply arms and legs are compromised.
- Rheumatic heart disease: damage on the heart muscle and heart valves from rheumatic fever, caused by streptococcal bacteria;
- Congenital heart disease: birth malformations on the structure of the heart;
- Deep vein thrombosis and pulmonary embolism: blood clots in the leg veins, which can dislodge and move to the heart and lungs [61].

Some situations can lead to heart diseases but the most common are the atherosclerosis and hypertension. Atherosclerosis corresponds to artery hardening and blockage due to accumulation of fatty materials such as cholesterol and triglycerides in the inner wall of the blood vessel, named atheromatous plaque [19]. On the other hand, hypertension is a chronic medical condition in which blood pressure in arteries is elevated [17, 18].

2.2.2 Risk Factors

Some behaviors may constitute a risk to the cardiovascular health. Unhealthy diets, physic inactivity, harmful use of alcohol and tobacco promote metabolic risk factors such as raised blood glucose, raised blood lipids, overweight, obesity, diabetes mellitus, and raised blood pressure. That contributes to heart diseases and stroke [26, 57, 61, 64].

2.2.3 Statistics

WHO statistics show that CVDs correspond to the main cause of death worldwide. In 2008, 30% of all death was due to CVD representing an amount of 17.3 million people, 7.3 million due to coronary disease and 6 million due to stroke [4].

In 2030 statistics predict that an amount of 23.3 million people will die from CVD [4].

2.2.4 Hypertension

Hypertension corresponds to a constant high blood pressure, beeing one of the major risk factors for stroke, coronary heart disease, congestive and renal failure, peripheral and vasculular disease [2, 37, 42, 45, 61].

The risk of hypertension may be caused by the high systolic blood pressure (SBP), the high diastolic blood pressure (DBP) or by their combination, both high systolic and diastoolic blood pressure. However, high SBP contributes more for eventual complications.[2, 43].

It is highly recommended to measure blood pressure, at least, twice, on separate occasions. A person is only labeled as having hypertension if the average of two readings is at or above 140/90 mmHg [44]. The table below presents the standard values used to classify the different levels of hypertension on adults.

Table 1: Recommendations for classifying and defining blood pressure levels for adults [37].

Category	SBP (mmHg)	DBP (mmHg)
Normal	<130	<85
High Normal	130-139	85-89
Hypertension - Stage 1 (mild) - **Stage 2 (moderate)** - **Stage 3 (Severe)** - **Stage 4 (Very severe)**	140-159 160-179 180-209 ≥ 210	90-99 100-109 110-119 ≥120

Therefore, it is imperative that the diagnosis of hypertension be based on accurate, representative, and reproducible measurements.

2.3 Arterial pressure Waveform

2.3.1 General Concepts

Throughout the arterial tree, while cross-sectional area increases the average diameter reduces, reflecting an increase on the number of arterial bifurcation toward arterioles and capillaries. The force that commands the blood flow is a result of the pressure created by the heart.

During heart systole, left ventricle contraction ejects blood into ascending aorta and, since it is elastic, it stores part of this blood leading to its wall distension and formation of an arterial pressure [27]. Then it recovers its original size resulting on a pulse wave that propagates throughout the arterial tree with a velocity that depends on a stiffness of the arteries. Pliability and compliance are some artery's properties that allow formation of a palpable pressure wave [19].

The pulse is one of the most critical signals of human life and it may be felt in various parts of the body where the arterial pulsation is transmitted to the skin surface, especially when it's compressed against a bone structure. Some measurement sites include the temporal artery at the sides of the forehead, facial artery at the angle of the jaws, carotid artery in the neck, brachial artery, radial artery at the wrist, femoral artery the groin, popliteal artery behind the knees, posterior tibial artery and dorsalis pedis artery over the foot [25]. The next figure shows the several measurement sites mentioned below.

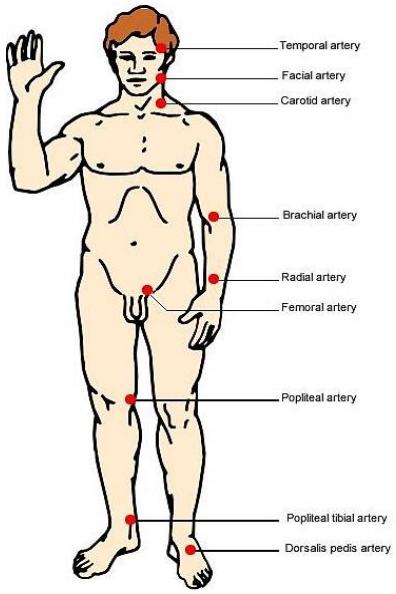

Figure 2.4: Arterial pulse (AP) measurement sites. The image presents different parts of the body where AP measurement is convenient since the arteries are at a superficial level and most of them can be compressed again a bone structure [25].

2.3.2 The morphology

The shape and amplitude of the pulse wave varies according to the measurement site. However the most analyzed pulse shape is the aortic one, presented on the next figure.

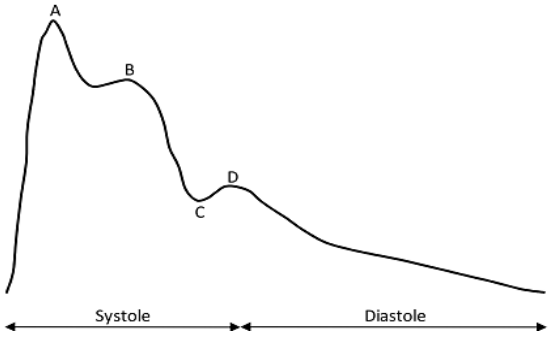

Figure 2.5: Aortic pulse waveform. Each peak on the pulse shape has a physiological meaning. A- Systolic wave; B- Reflected wave; C- Dicrotic incisura; D- Dicrotic wave; [21]

The first peak is the most significant in terms of amplitude and it's due to blood ejection into aorta, by left ventricle. This pressure wave is reflected on first ramification of the aorta returning to the measurement site forming peak B. Reflected wave is caused not only for discontinuity on arterial wall but also for high vessel resistance. The dicrotic incisura is the depression that follows reflected wave peak and that occurs at the end of a systole, when artery's wall starts recovering its initial size. Peak D appears due to closure of aortic valve that exerts a small pressure forcing blood to return to aorta, producing a small dilatation on its walls [57].

Arterial pressure wave changes its shape while it travels down the aorta. Increasing the distance from heart SBP augment, DBP slightly falls and the amplitude oscillation between SBP and DBP, pulse pressure, doubles [27, 57]. Figure 2.6 shows the different APW from central to peripheral artery

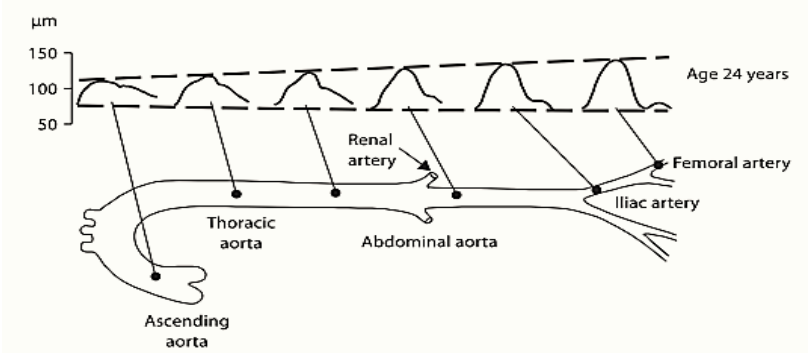

Figure 2.6: APW along the arterial tree. The shape of pulse wave changes through the arterial tree since SBP increase, DBP slightly reduce and pulse pressure doubles [27].

APW measured at carotid has a higher cardiovascular predictive value than that measured at peripheral arteries since it is very close to the aorta and heart. Measurements made at peripheral sites such as radial or brachial arteries require a transfer function to reconstruct aortic waveform besides the lower data accuracy. However, peripheral arterial blood pressure (pABP) measurement reveals to be helpful when carotid artery is difficult to access, for example, in obese patients with major atherosclerotic plaques. cBP measurement necessitates a higher degree of technical expertise however a transfer function is not necessary [22].

Abundant and consistent clinical information about the cardiovascular system may be extracted from the cAPW.

Arterial vascular diseases such as atherosclerosis, stenosis, sclerosis, functional circulatory disturbances, arterial spams and occlusions, hypertension and coronary heart disease are examples of pathological condition that may be detected analyzing AP wave since they affect its shape in different way such as the strength, reflection and frequency. Figure 2.7 shows the modification of the APW caused by several CVDs.

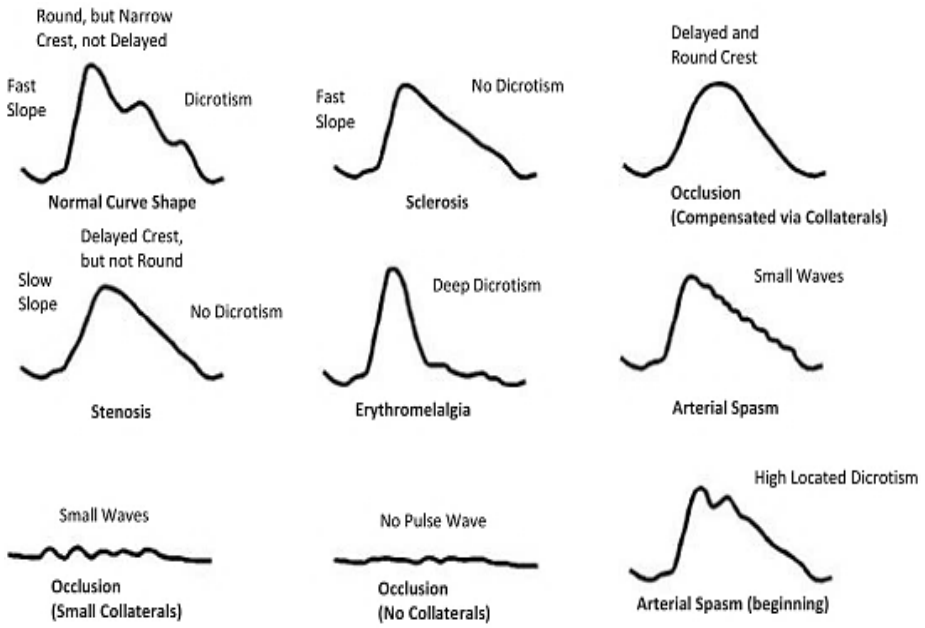

Figure 2.7: Different APW due to different cardiovascular pathologies. APW shape analysis provide valuable information about the cardiovascular system state and performance [21, 54].

2.3.3 Arterial pressure waveform typology

Murgo JP et al (1980) proposed a criteria that classify APW in four main types [31]:

- **Type A**

Inflection point occurs before systolic point. The value of augmentation index (Aix) is positive representing a stiffer artery.

Aix is an important parameter that varies significantly, according to the APW and contributes widely to CVD assessment [22, 31]. This parameter is explained, with fully details on section 2.4.4.

- **Type B**

Inflection point occurs shortly before the peak systolic and indicates smaller arterial stiffness (AS). Just like the type A APW, Type B as a positive AS.

- **Type C**

The inflection point occurs after peak systolic. The value of Aix is negative meaning that the artery is relatively elastic and healthy.

- **Type D**

Waveform is similar to type A pulse wave velocity (PWV), but inflection point cannot be observed visually because reflected wave arrives early in systole and merge with the incident wave.

The figure below presets the four main APW types.

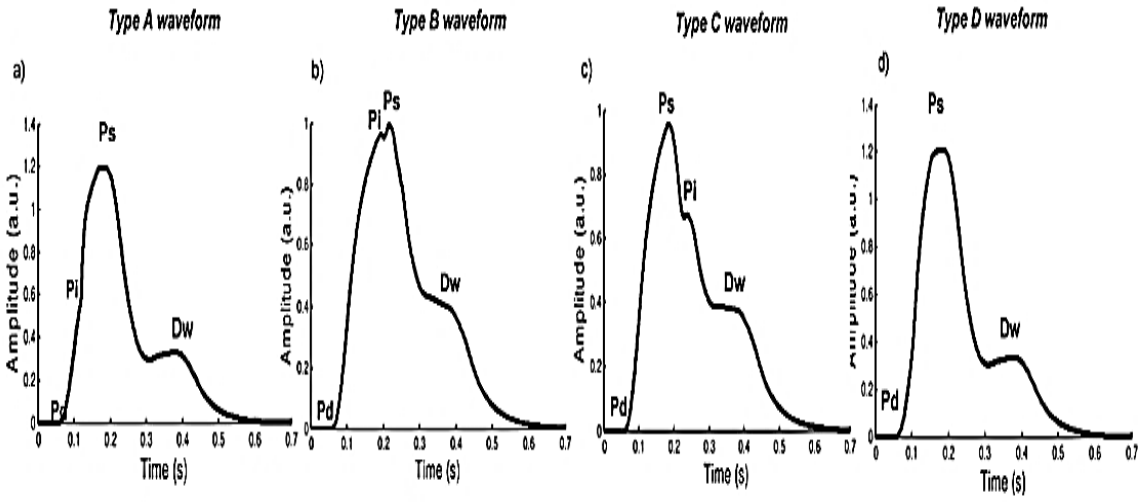

Figure 2.8: Different types of APW according to Murgo JP, et al, (1980). Pd: DBP; Ps: Systolic pressure; Pi: Inflection point [22, 31].

2.3.4 Measurement Device

ABP is an important vital sign which allows assessing the cardiovascular system state.

Direct intra-arterial measurement using a catheter is the gold standard of ABP measurement. However it is not practical or appropriate for repeated measurements outside a hospital. Besides being an invasive method, it has some risks to the patient and the discomfort is very high [37].

Indirect measurement techniques still rely almost exclusively on applanation tonometry where artery is squeezed against the underlying bone structure. Despite being less accurate and less reproducible, indirect methods are still simple, practical, low in cost and non-invasive [37].

Sphygmomanometer is a common indirect method, introduced on 1896 by Riva Rocci, constituted by an occluding cuff, a stethoscope and a manometer with a calibrated scale for measuring pressure. The cuff is inflated to a level above arterial pressure in order to occlude the artery and then is gradually deflated. As the pressure in the cuff is reduced, pulsatile blood flow reappears through the partially compressed artery, producing repetitive sounds generated by the pulsatile flow (Korotkoff sounds). The pressure level at the first Korotkoff sound is the SBP while the level of pressure at which the sounds disappear permanently, when artery is no longer compressed, is the DBP [37, 38, 40].

Despite being a very simple method, it has a big disadvantage: it requires skilled professionals to use it and the subjectivity of the reads requires standardization [39].

Automated devices are based essentially on the auscultation and oscillometric techniques. The oscillometric method detects the oscillations of an occluded artery's lateral walls while the cuff is deflated. The oscillations start at the level of SBP and reach their greatest amplitude at the level of mean arterial pressure (MAP). Systolic blood pressure value measured through this technique is accurate but the diastolic pressure is not, besides being a derivative value [37, 41].

These devices have some serious restrictions once they present a wide fluctuation in ABP readings resulting from the high sensitivity relative to the position (it may be positioned in the wrist or pulse) [37].

Doppler devices, which amplify the Doppler signal from flowing blood, are also used with standard sphygmomanometers and obviate the need for a stethoscope.

Photoplethysmography (PPG) is a non-invasive optical technique that consists on the measurement of infrared light transmission through a finger, an ear or a toe in order to detect pulsatile physiological waveform attributed to cardiac synchronous changes in the blood volume with each heartbeat [68].
It provide valuable information about the cardiovascular system, being used to measure parameters such as oxygen saturation, heart rate, blood pressure and cardiac output allowing assessing autonomic functions and detecting peripheral vascular disease[68].

2.4 Arterial stiffness

2.4.1 General concepts

In recent years a great emphasis has been placed on AS role on the development of CVD, being increasingly used on patient diagnosis [62].

A material may be classified as being elastic or plastic if, after removing an applied force, the material recovers its original size or retain the deformation, respectively. Arterial walls are classified as “viscoelastic”, where pressure represents mechanical stress and the strain is the alteration of vessel diameter or volume. AS is the inverse of arterial elasticity [27, 28].

2.4.2 Proximal vs Distal arterial stiffness

Proximal arteries are more elastic while distal ones are stiffer. This is caused by the variation on the composition and arrangement of the materials that make up the vascular wall structure leading to APW variation along arterial tree, from aorta to periphery [65].

In a young, normal and healthy person, medial fibrous elements of thoracic aorta contain more elastin than collagen but, increasing the distance from heart, at peripheral arterie, proportions reverse quickly prevailing the amount of collagen over elastin. An increase of 25% of AS from carotid to radial arterie is observed in healthy patients [27, 29].

An artery with no reflection sites has a pressure wave that diminishes progressively with an exponential decay along it. However when the viscoelastic artery has numerous branches, pressure is progressively amplified from central to distal conduit arteries due to wave reflections. The result is a pressure wave with higher amplitude in peripheral arteries than in central ones. This is called "Amplification phenomenon" [29].

2.4.3 Pathophysiological changes of arterial stiffness

Direct injuries, atherogenic factors and hemodynamic flow changes may lead to modifications on the arterial wall leading to activation, proliferation and migration of vascular smooth muscles cells, increase of arterial lumen and wall thickness and rearrangement of extracellular matrix and cellular elements [27].

Acute changes in tensile and sheers stress induce adjustments on vasomotor tone and arterial diameter while chronic changes on mechanical forces lead to alteration of geometry and composition of vessel's wall [27, 63].

Tensile stress $\boldsymbol{\sigma}$, according to Laplace Law, is defined by:

$$\sigma = \frac{P \times r}{h} \qquad (1)$$

Where $\boldsymbol{h}$ is the wall thickness; $\boldsymbol{r}$ is the arterial radius and $\boldsymbol{P}$ is the arterial transmural pressure. On the other hand sheer stress $\boldsymbol{\tau}$ is mathematically defined as:

$$\tau = \frac{Q \times \eta}{\pi \times r^3} \qquad (2)$$

Where $\boldsymbol{Q}$ represents blood flow, $\boldsymbol{\eta}$ is the blood viscosity and $\boldsymbol{r}$ is the arterial radius.

The ABP rises tends to increase the arterial radius. To maintain the tensile stress the heart and vessels walls become thicker. Although sheer stress is major mechanical factor in atherosclerosis development and tensile stress is present on patients with hypertension, both are interconnected. Any alteration on arterial radius caused by blood flow change affects tensile stress. Arterial blood flow augmentation induces the increase of vessel lumen leading to arterial inner diameter reduction [27, 63].

Age is the major determinant factor in increase AS. By the sixth decade of life, accumulation of cyclic stress of more than 2 billion aorta expansions due to heart

systoles causes fatigue, eventual fracturing of artery elastin, proliferation of collagen and deposition of calcium. Arteriosclerosis is a degenerative and pathological process that consists on central arterial stiffening. As such, older patients present a loss of artery compliance, SBP increase and diminution of peripheral amplification [46]. The following figure shows the modification on APW with age.

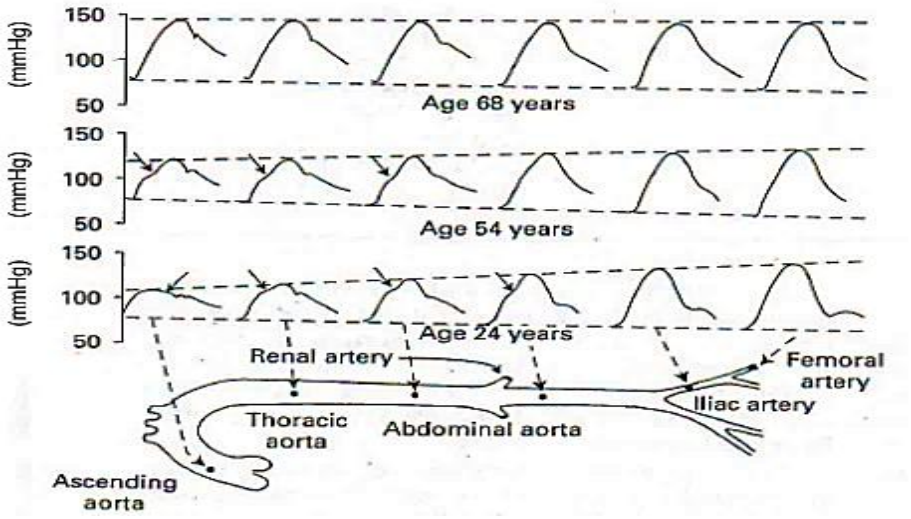

Figure 2.9: APW along the arterial tree in a human with 68, 54 and 24 years old, respectively. It is possible to see that peripheral amplification diminish with years. Older patients, due to a stiffer central artery, have a higher cABP leading to lower peripheral amplification. [46]

2.4.4 Arterial Stiffness assessment

Vascular artery wall includes smooth muscle cells and extracellular matrix which is responsible for passive mechanical properties, mathematically defined from a cylindrical artery model. Several indices are used to assess AS and most of them are measured non-invasively and in-vivo using echo-Doppler techniques with high resolution and high degree of reproducibility. Table 2 summarizes some of them.

Table 2: Important indices to assess AS [27].

Indices	Definition	Mathematical Formula	SI Unit
Pulse wave velocity	Speed of pulse travel along an arterial segment.	$\frac{Distance}{\Delta t}$	cm/s
Arterial Distensibility	Relative diameter or area change for a pressure increment; The inverse of elastic modulus.	$\frac{\Delta D}{(\Delta P \times D)}$	$mm\,Hg^{-1}$
Arterial Compliance	Absolute diameter or area change for a given pressure step at fixed vessel length.	$\frac{\Delta D}{\Delta P}$	$cm/mmHg$ $cm^2/mmHg$
Elastic modulus	Intrinsic elastic properties of wall material.	$\frac{\Delta P \times V}{\Delta V \times h}$	$mmHg/cm$
P, pressure; **D**, diameter; **V**, volume; **h**, wall thickness; **t**, time.			

Moens and Korteweg was the first to define PWV using arterial wall elastic modulus($\boldsymbol{E}$), its thickness($\boldsymbol{h}$), radius ($\boldsymbol{r}$) and blood density ($\boldsymbol{\rho}$), through a mathematical formula:

$$PWV = \sqrt{\frac{E \times h}{2 \times r \times \rho}} \qquad (3)$$

Later, Bramwell and Hill described the association in terms of relative change in volume and pressure during ex vivo experiments [30]:

$$PWV = \sqrt{\frac{\Delta P \times P}{\Delta V \times \rho}} \qquad (4)$$

To assess PWV it's more adequate to use the definition presented on table 1 according with, the velocity of the pulse pressure propagation is calculated from the distance between two different BP recording sites along arterial tree and the transit time which is

the time travel of the foot of the wave over a known distance (figure 2.10). The foot of the wave occurs at the end of diastole, when the steep rise of the wave front begins.

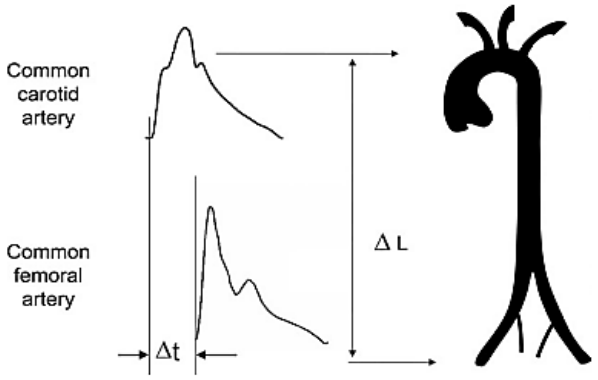

Figure 2.10: Carotid-femoral PWV measurement using foot to foot method. Foot to Foot method calculates PWV value using distance between two different BP recording sites and the time delay between them [62].

Another very useful parameter for pressure wave analysis is the augmentation index which is defined as the strength of the reflected wave relative to the total pressure waveform, as presented on figure 2.11. The key to its estimation is to identify the inflection point where reflected wave imparts to the pressure waveform [22].

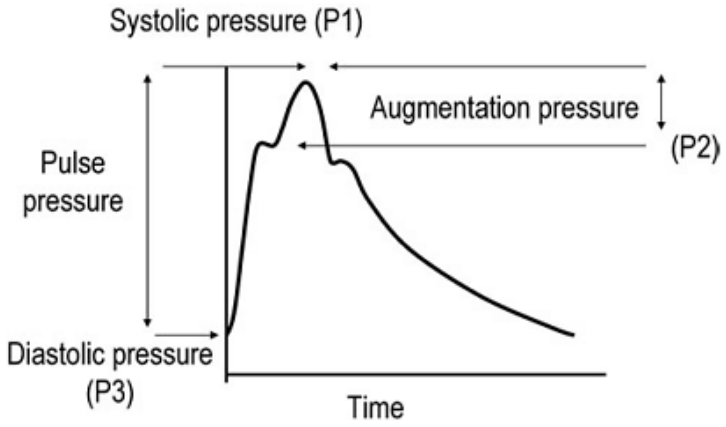

Figure 2.11: Representation of augmentation pressure on carotid pressure waveform. Systolic peak (P1) above the inflection (P2) defines the augmentation pressure and the ratio of augmentation pressure to PP defines Aix (in percentage) [62].

Augmentation pressure (ΔP) corresponds to the difference between the peak of systolic wave and reflected wave, while augmentation index is defined as the ratio of augmentation pressure to pulse pressure [29, 30].

$$Alx = \frac{\Delta P}{PP} \qquad (5)$$

2.5 Sensors

2.5.1 Piezoelectric Sensor

Piezoelectric (PZ) sensors are important tool which are, nowadays, widely applied in various measurement processes. According to PZ effect this sensor type converts mechanical energy into electrical charge and vice-versa [68].

Single crystals and PZ ceramics are examples of materials used as transducers on PZ sensor. PZ crystals are composed by aligned cells and each cell has an electrical dipole [68]. The following figure illustrates the structure of PZ crystals.

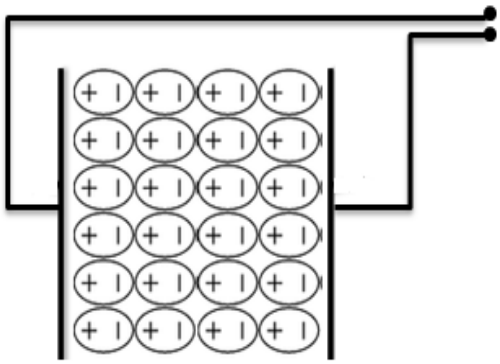

Figure 2.12: Internal structure of a PZ crystal. It is possible to see several dipoles perfectly aligned resulting in a null differential potential since there's no stress over it [68].

In absence of stress, crystal's cells orientation remains perfectly balanced so, no potential difference is produced. When subjected to mechanical deformations, as a consequence of applied pressure, acceleration, strain or force, a proportional electrical charge is produced as output due to the unbalance on the electrical dipoles orientation. This results in a temporary excess of surface charge, which subsequently is manifested as a voltage, which is developed across the crystal [21]. As such:

$$V = \frac{Q_c}{C} \tag{6}$$

Where, Q_c is the charge produced by applying force and C is the capacitance of the material.

Inverse PZ effect is the opposite process where the material deforms when a certain voltage is applied. Figure 2.13 illustrates the direct and indirect piezoelectric effect.

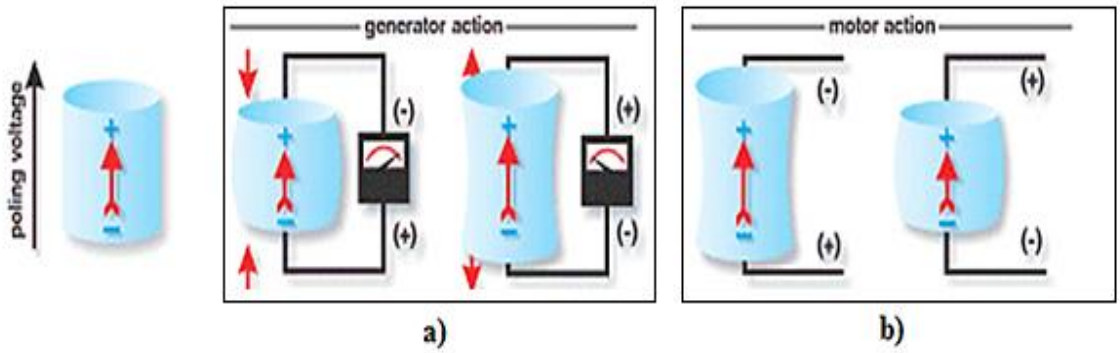

Figure 2.13: Direct and inverse PZ effect. Image a) presents the direct PZ effect where electrical output charge is produced proportionally to the mechanical deformation applied by the PZ material. At image b) is possible to see the inverse PZ effect that occurs when the PZ material deforms by applying an input voltage [20].

Pressure is one of the physical quantities measured by a PZ sensor. This sensor type has a sensing diaphragm with a constant area that transfers the force produced by the fluid pressure to the transduction element. It's important to ensure that the transduction element is loaded in one direction. The output is an electrical charge proportional to the pressure.

A PZ sensor works as a differentiator and has an equivalent RC circuit. The output is related to mechanical force as if it had passed through the equivalent circuit.

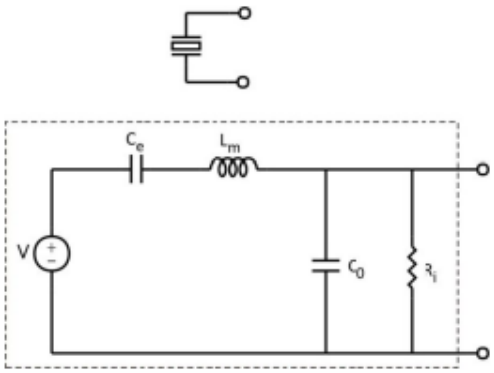

Figure 2.14: Schema of a PZ sensor equivalent RC circuit. [21].

The equivalent circuit above include PZ sensor imperfections due to mechanical construction and others reasons. The impedance $\boldsymbol{L_m}$ represents the seismic mass and sensor's inertia. $\boldsymbol{C_e}$ is inversely proportional to the sensor mechanical elasticity, $\boldsymbol{C_0}$ characterizes the static capacitance of the transducer and $\boldsymbol{R_i}$ is the insulation leakage resistance of the transducer element.

2.5.2 Accelerometer

An accelerometer has many applications on industry and science, being used to measure motions, vibrations, accelerations, orientation, tilt or shocks [6, 66].

Some aspects such as its low-cost, robustness, small size, light weight and the ability to deliver 1, 2 or 3 measurement-axes with a wide frequency range, from DC to very high values, makes its use very popular among the technological areas [66].

Most accelerometers have two transduction elements: a seismic mass which is responsible to convert acceleration into displacement and a second transducer that transforms, proportionally, the displacement into electrical charge. Since the seismic mass is constant, when subjected to acceleration, it produces a force proportionally to the body's acceleration, according to Newton' second law [67]. The displacement occurs due to a spring-mass system integrated on the accelerometer, which respects Hooks' law:

$$F = m \times a = K \times x \qquad (7)$$

Where $\boldsymbol{F}$ is the force exerted by the seismic mass $\boldsymbol{m}$ when it is accelerated ($\boldsymbol{a}$), producing a displacement $\boldsymbol{x}$ on the spring with a stiffness constant, $\boldsymbol{K}$.

On the next system is possible to see a spring-mass system which integrates two transducers responsible to convert acceleration into displacement and displacement into voltage.

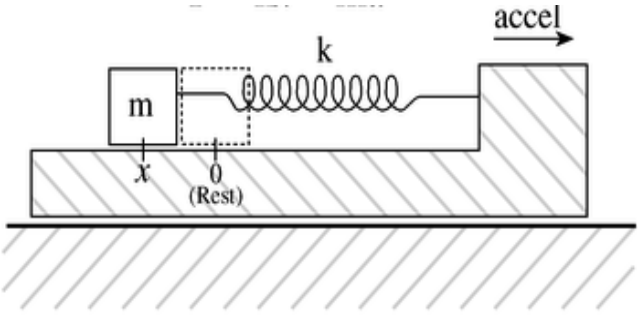

Figure 2.15: The spring-mass system that integrates accelerometer as a transducer. This system permits to produce, according to Hook and Newton' second law, a displacement that is proportional to the body acceleration. The displacement is then proportionally converted to an electrical charge by another accelerometer transducer [23].

The system presented above only measures acceleration along the spring length. To measure acceleration of more than one axe, more than one spring-mass system is required, one to each axis.

Chapter 3

The hemodynamic Probe

Contents

3.1 Introduction

It is very important to have a robust hemodynamic probe to detect with high accuracy our target parameters: APW and ABP.

Constituted by two sensors, its performance is based on concepts such as piezoelectricity, accelerometry and demodulation. The output signal is a modulated signal.

This chapter focuses, not only, on probe design description but also on experimental tests and results to confirm its good performance.

3.2 Support Concepts

3.2.1 Resonance frequency

Resonance frequency or system's resonant frequency is defined as being the frequency at which the amplitude response is a relative maximum, meaning that the system's oscillation is bigger. Figure 3.1 shows an example of resonance frequency.

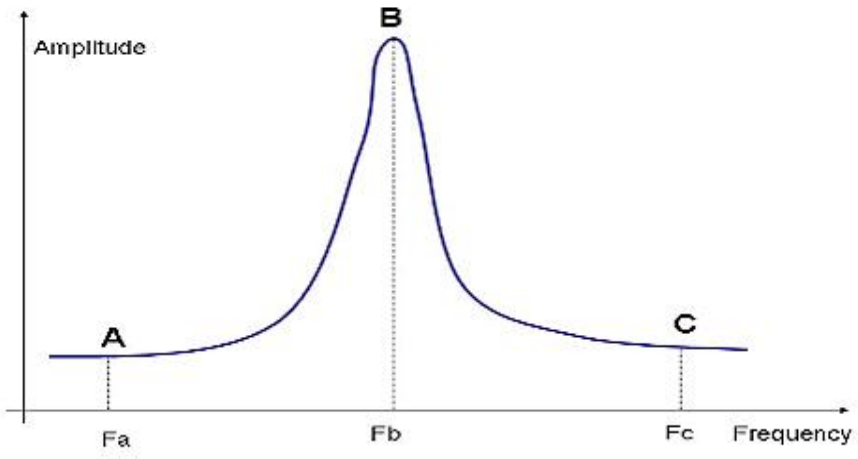

Figure 3.1: Resonance frequency simple case. The amplitude at F_b is larger than in F_a and F_c.

The resonance phenomenon occurs when the system is able to store and easily transfer the energy between two or more different storage modes. That's the reason why even small periodic driving forces can produce large amplitude vibrations.

When damping is small the resonance frequency is approximately equal to the system natural frequency, the frequency of free vibrations. [32]

3.3 Probe Design

The hemodynamic probe corresponds to the association of two sensors: a PZ sensor and an accelerometer, presented on the figure below.

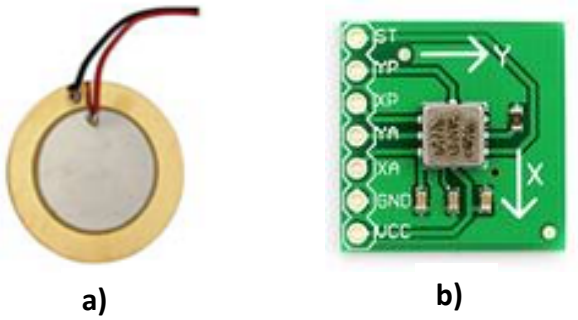

Figure 3.2: PZ sensor and accelerometer. Image a) shows the PZ sensor while image b) corresponds to the accelerometer.

The PZ sensor used has a diameter equivalent to 27 mm and its resonant frequency, according to the manufacturer, corresponds to 4.6 KHz $\pm$ 0.5 KHz; the accelerometer is an ADXL203 dual-axis analog device, supplied by an operating voltage equivalent to 5 V. Full specifications about the sensors may be found on Appendix D and E.

Figure 3.3 presents a picture of the developed hemodynamic probe, based on a PZ-accelerometer unit.

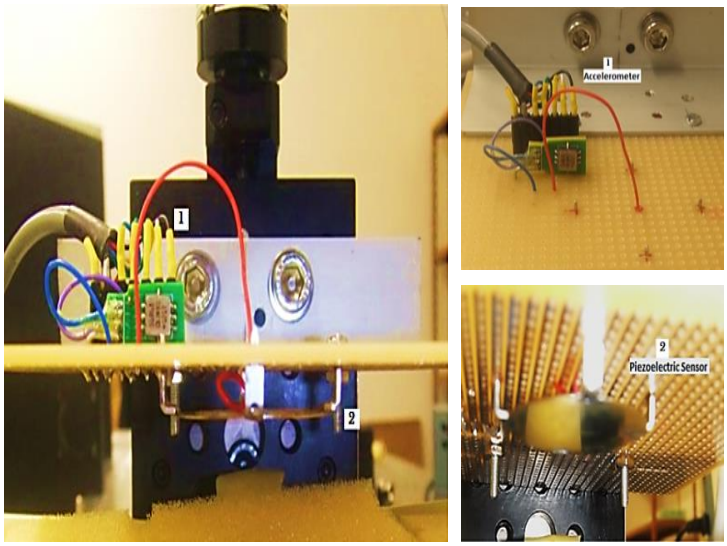

Figure 3.3: APW hemodynamic probe. It is constituted by two sensors PZ sensor and an accelerometer, and which images are also shown above.

Posteriorly, some improvements were done on the hemodynamic probe, adding an INA126 that is a precision instrument amplifier.

By using it, it is possible to analyze the hemodynamic probe current, to improve data acquisition process and to obtain acute and low noise signals.

It works with very low quiescent current and a wide operating voltage range of ±1.35V to ±18V.

Figure 3.4 shows a photo of the hemodynamic probe after improvements.

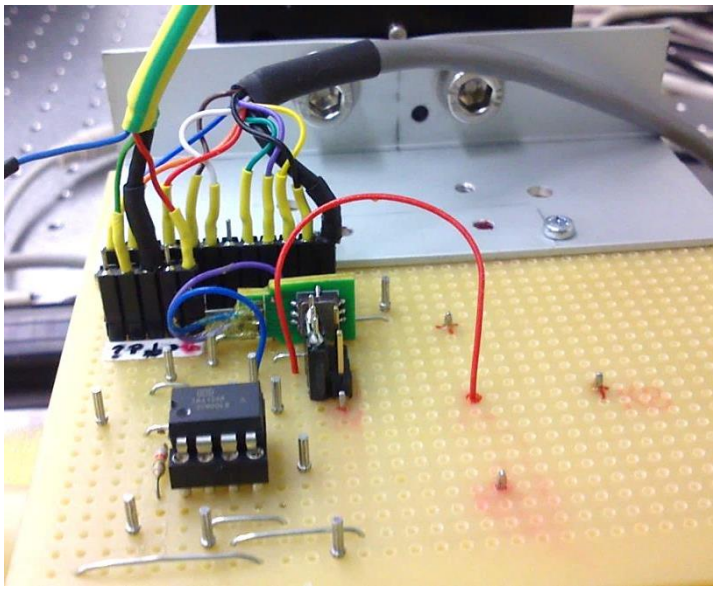

Figure 3.4: Hemodynamic probe after improvements. An INA126 electronic amplifier was introduce on the hemodynamic probe in order to allow current measurement and to enable better signal acquisitions.

3.4 Probe performance

According to piezoelectricity concepts, by stimulating the PZ sensor it proportionally vibrates. This input stimulus is a high frequency signal provided by a waveform generator device (Agilent).

By exerting pressure over the PZ sensor, its vibrational amplitude varies proportionally. That way, properties of the external exerted pressure become inherent to variation of PZ sensor vibrational amplitude. Figure 3.5 illustrates the probe functioning.

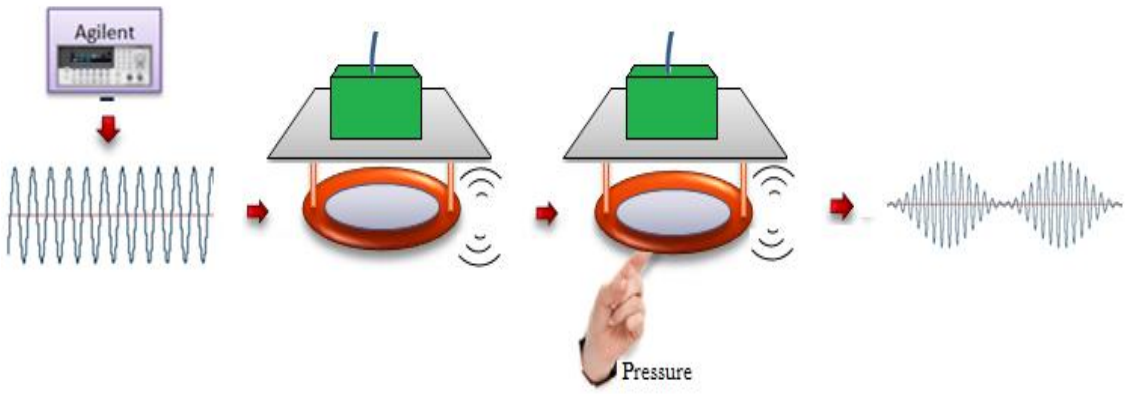

Figure 3.5: Illustration of hemodynamic probe performance. An Agilent stimulates the PZ sensor with a high frequency sinusoidal signal causing a proportional vibration. By exerting pressure over the PZ sensor, its vibrational amplitude varies proportionally, and it is detected by an accelerometer

The pressure detection also depends on the accelerometer since it converts the PZ sensor vibration into electrical signal, agreeing with accelerometry laws. Despite detecting PZ sensor vibration three-dimensionally, only the vibration in the direction of vessel's movement is considered.

That way, the hemodynamic probe output is a modulated signal, where the higher frequency signal is the carrier wave and it corresponds to the PZ sensor vibrational signal while the envelope wave corresponds to the external exerted pressure.

The external pressure which actuates over PZ sensor is produced in a dedicated test bench system assembled to emulate the dynamics of the arterial system, namely wave travel, reflection phenomenon and ABP variations. Chapter 6 is dedicated to the description of several test bench systems developed during this thesis project. However, the first tests to emulate the probe's performance used a finger to actuate over the PZ.

The hemodynamic probe is attached to a tri-axial position monitoring system device that allows doing translation movements with a micrometric precision. To be more specific, the system consists of three linear positioners (T-LA28A, Miniature linear activator) and each has a precision equivalent to $0.099\ \mu m$ and its command may be done manually or through parallel *Matlab* programing.

Figure 3.6 show a picture of the tri-axial position monitoring system device at which the hemodynamic probe is attached.

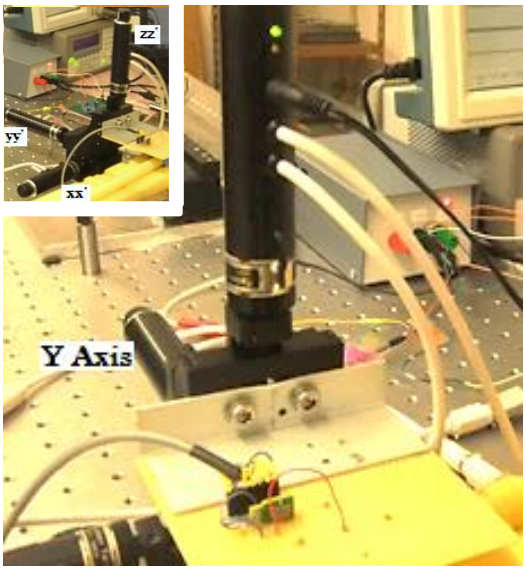

Figure 3.6: Tri-axial position monitoring device based on a *Zaber* linear positioner. The hemodynamic probe is attached to *Zaber* which, besides acting as a support, allows precise milimetric translations of the probe.

3.5 Probe Resonance Frequency

The input signal used to stimulate the PZ sensor is characterized by a high frequency which must be equal to the resonance frequency of the probe in order to maximize its sensitivity. However, the resonant frequency of hemodynamic probe slightly differs from the PZ sensor resonant frequency since other elements beyond it integrate the probe.

To determine the hemodynamic probe's resonance frequency some tests were made in two different situations: with the probe attached to its support, the tri-axial position monitoring system, and with the probe suspended.

Using unitary dirac impulses characterized by a frequency equal to 2.5 kHz and an amplitude equivalent to 400 mV were provided to the probe and its response was recorded.

All the result signals were recorded at a sampling frequency of$250KHz$, being submitted to frequency analysis (Fourier analysis).

Figure 3.7 shows the signals acquired on the two aforementioned situations.

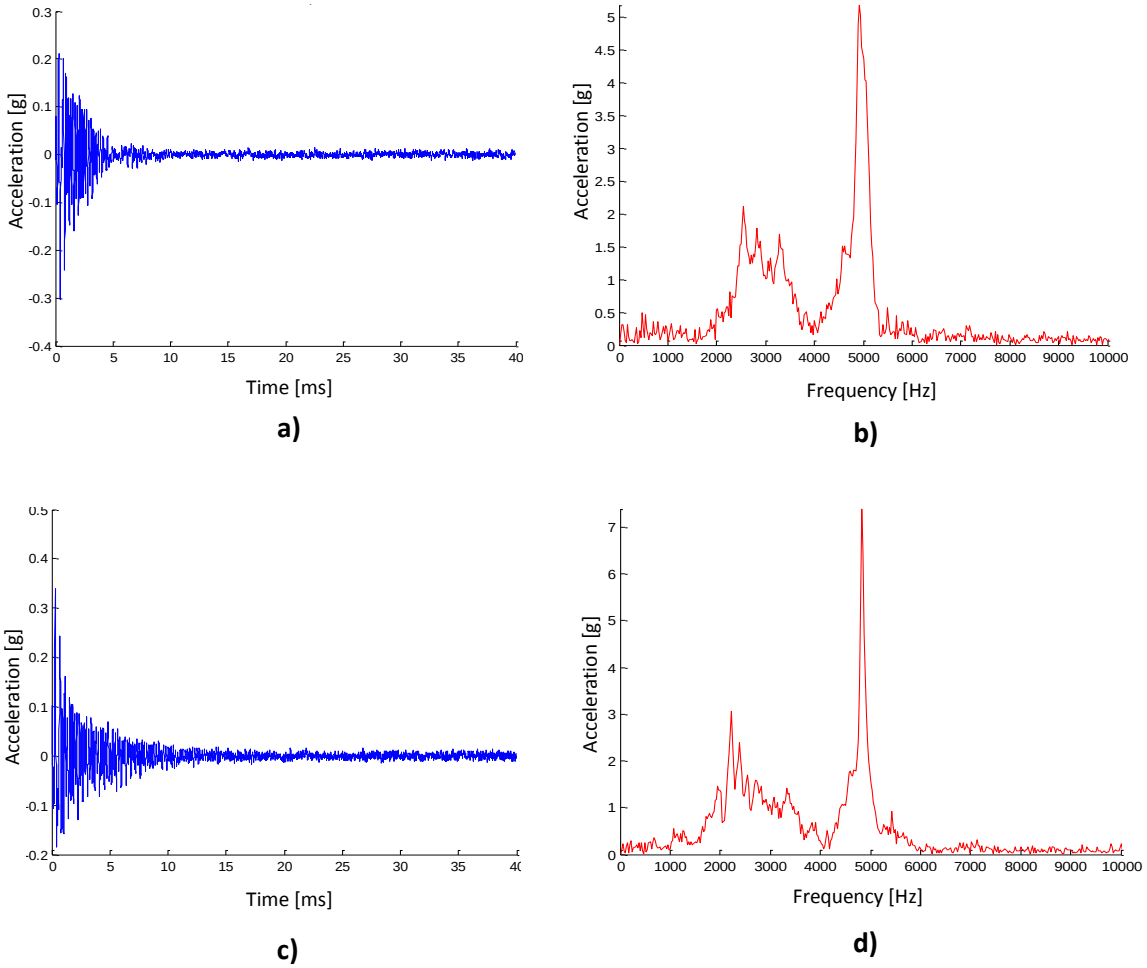

Figure 3.7: Time and frequency domain analysis of the probe's output signal. On the first row, images a) and b) refer to the test made when the sensor was attached to its support, a *Zaber* device; the second row which contains images c) and d) are related to the test made when the probe was suspended.

Considering the maximum amplitude values in the frequency domain, is possible to conclude that the resonant frequency of the hemodynamic probe is $4825\ Hz$ when suspended and $4926\ Hz$ when attached to its support.

3.6 Probe's functioning tests

After finding the system resonant frequency, some tests were done in order to evaluate the probe functioning.

This test corresponds to a reproduction of the schema presented in figure 3.5. Result is presented below on figure 3.8. The test consists on pressing the previously activated PZ sensor with a finger and then analyse the produced output signal which must be an amplitude modulated wave signal.

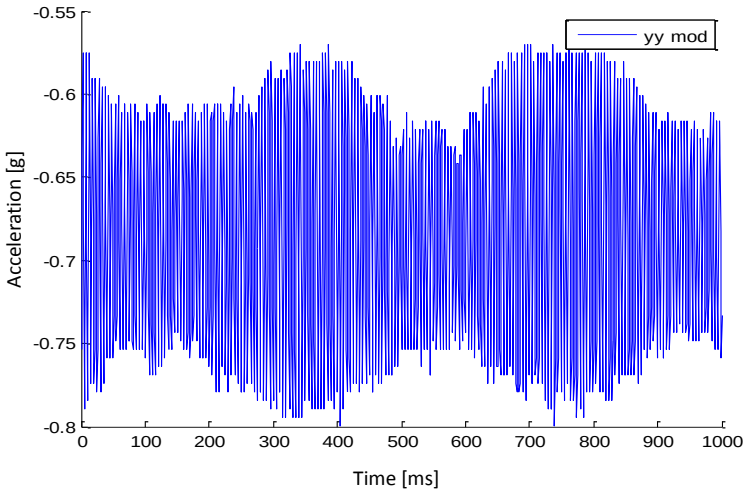

Figure 3.8: PZ sensor output signal modulated in terms of amplitude. This signal was a result of tests made to evaluate the performance of PZ sensor. A finger was used to actuate over a previously activated sensor, exerting pressure.

The developed hemodynamic probe detects external pressures correctly. Analyzing figure 3.8, it is easily observed that the probe output is a high frequency signal whose amplitude is proportionally modulated by an external pressure.

Chapter 4

Amplitude Demodulator

Contents

4.1 Introduction

The hemodynamic probe output is a modulated signal. In order to obtain demodulated signal, an envelope detector circuit was planned and developed.

Detailed description of its constitution, performance and experimental tests results are exposed on the following subchapters.

4.2 General concepts

4.2.1 The demodulation method

The modulation process consists on the variation of the carrier wave's properties according to the modulating signal.

The carrier signal is a periodic and sinusoidal wave characterized by a high frequency and the modulating signal corresponds to a lower frequency signal which constitutes the information to be transmitted.

Figure 4.1 illustrates the modulation process described above.

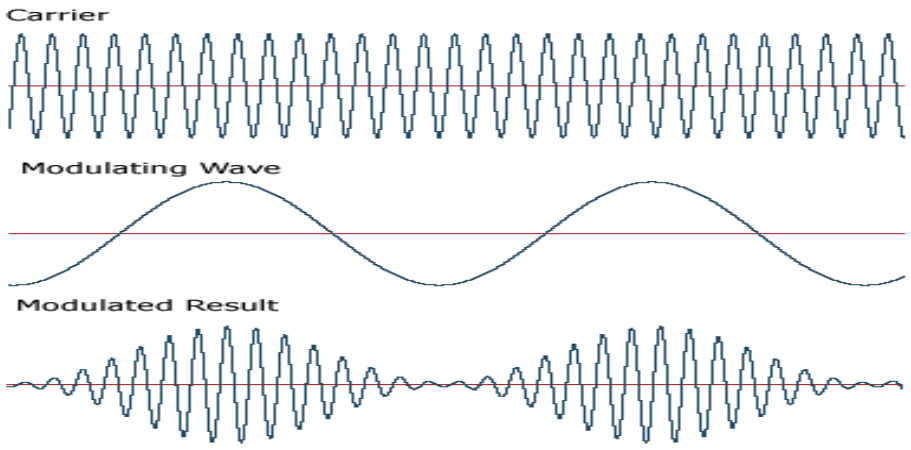

Figure 4.1: Modulation process. The signal with a higher frequency corresponds to the carrier signal. The modulating wave has a lower frequency and it contains the information to be transmitted [9].

There are different types of modulation. The main difference between them relies on the way how the properties of the modulating signal are transmitted on the carrier wave. The most common types are:

- Amplitude modulation (AM)

This modulation type is done by varying the amplitude and strength of carrier signal waveform according to the information contained on the modulating signal.

- Frequency modulation

It's obtained when the carrier wave property which varies is the instantaneous frequency.

- Phase modulation (PM)

It encodes information by varying the instantaneous phase of the carrier wave.

The next figure presents three different types of modulation: amplitude modulation, frequency modulation and phase modulation.

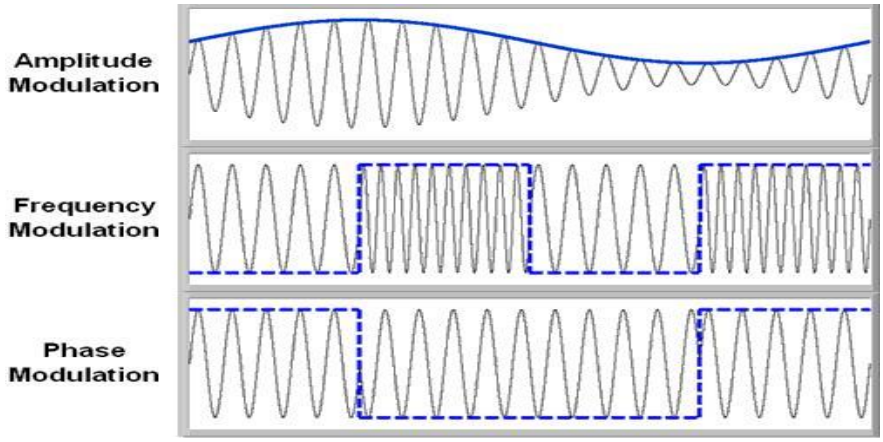

Figure 4.2: Different types of modulation. The amplitude of the carrier signal changes according to the modulator signal. The second graph represents the frequency modulation and it is easily detected the variation of carrier wave frequency while on the third graph the carrier wave's property which changes is the phase [10].

The variation of the modulation relative to the original signal level is a parameter named modulation depth, h, defined as:

$$h = \frac{peak\ value\ of\ m(t)}{A} \text{ x } 100 \qquad (8)$$

Where $m(t)$ and A are the modulator and the carrier wave, respectively. Modulation depth is expressed in percentage, (%). The following figure presents different degree of modulation.

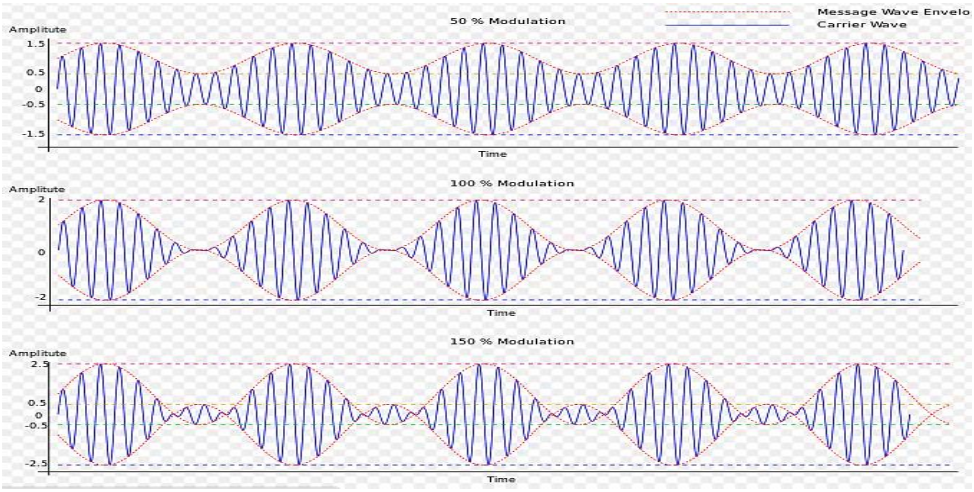

Figure 4.3: Different depths of amplitude modulated signals. The signals represented above have, respectively, 50%, 100% and 150% AM depth [11].

Demodulation is the inverse process of modulation and consists on the separation and extraction of the original information, modulating signal, inherent to the modulated signal. A demodulator, also called detector, is an electronic circuit whose constitution depends on how the input signal is modulated. For each kind of modulated signal a different electronic circuit is required.

4.2.2 Amplitude Demodulator

There are two types of amplitude demodulators:

- Product detector

To obtain the demodulated signal the input wave is multiplied by a local oscillator signal with the same frequency and phase of the carrier's incoming signal. Then, the signal is filtered obtaining its envelope.

- Envelope detector

The input modulated signal is first passed through a rectifier, a non-linear device, and then through a filter to eliminate the high frequencies. The rectifier plays an important role on the envelope detector. In its absence, after filtering the signal, the positive and negative envelopes cancel each other, becoming impossible to recover the original information once they are 180º out of phase.

Figure 4.4 illustrates the performance of an envelope detector, detailing its component funtions.

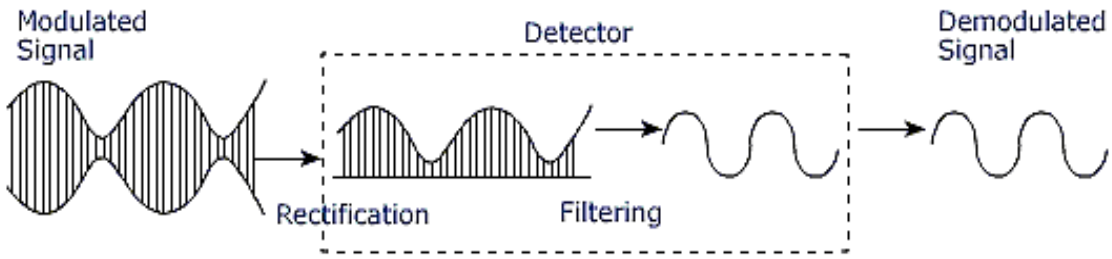

Figure 4.4: Function of the envelope detector's components. The input signal first passes through a rectifier and then over a RC low-pass type of filter [12].

The rectifier may be constituted by a single diode or be more complex. In order to obtain the envelope signal it is essential to convert the alternating signal into an, approximately, continuous one. To achieve that, a capacitor is placed parallel to a resistance on the rectifier; it loads during carrier wave's semi-circles selected by the rectifier, and discharges during the time between those consecutive semi-circles. When its voltage value matches with the voltage value of the next rising semi-circle it restarts to load repeating the cycle.

This process originates what is called ripple, characterized by a time constant RC which value is very important to the detector. In order to obtain a satisfactory demodulated signal, its ideal value stands between the carrier wave period and the maximum modulator signal variation [13].

$$\frac{1}{f_{carrier}} \ll RC \ll \frac{1}{W} \qquad (9)$$

$f_{carrier}$: Carrier wave frequency

W: Maximum modulator signal variation.

If the RC constant is smaller than the carrier wave period, the capacitor discharges rapidly. On the other hand, if the RC constant is much bigger than the maximum variation of the modulator signal the capacitor discharges too slowly. In both situations, the detector is not able to properly detect the envelope signal.

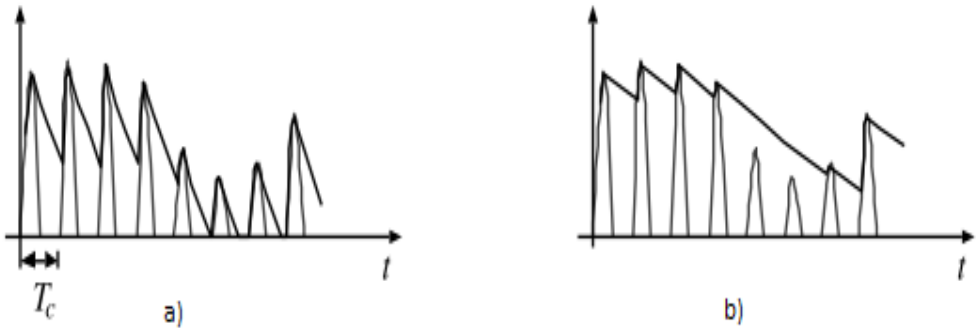

Figure 4.5: Capacitor discharging behaviors. The figure illustrates the capacitor behavior when: a) RC constant is lower than the carrier wave period; b) RC constant is bigger than maximum modulator variation [13].

4.3 Amplitude demodulator

4.3.1 The electronic circuit

The main task in this subchapter was to understand, produce, mount and test the circuit on breadboard and on the PCB. The envelope detector electronic circuit is represented on the Appendix-A.

The envelope detector is constituted by two units for each accelerometer axis. However, only YY' axis signal was used. Each unit is responsible to demodulate the positive or negative half-side of modulated input signal.

To succeed on that, a half-wave inverter rectifier was used. The diodes' orientation on each unit defines which side of the modulated signal is selected and which one is cut.

Unit 1 of the demodulator circuit has a rectifier with two diodes directly polarized, allowing demodulating the negative half-side of the modulated input signal. Unit 2 does the opposite and demodulates the positive half-side of the modulated signal, since both diodes are inversely polarized.

Analyzing each unit's output signal is possible to see that they suffer an inversion. This is explained by the existence of an inverter operational amplifier (OpAmp) with a unitary gain, -1.

The temporal RC constant used on the circuit design is between $0.25\ ms$ and $333.33\ ms$.

After passing the signal through a rectifier, the signal must be filtered in order to eliminate the high frequency signal remaining only the envelope, a lower frequency signal. It was designed a RC low-pass filter whose cut-of frequency is equivalent to:

$$f_c = \frac{1}{2\pi RC} = 318.31\ Hz \qquad (10)$$

$\boldsymbol{f_c}$: Cut-off frequency;

$\boldsymbol{R}$: Low-pass filter's resistance value;

$\boldsymbol{C}$: Low-pass filter's capacitor resistance.

During the electronic circuit experimental test phase, the low-pass filter revealed itself useful reducing the noise and allowing obtaining the demodulated signal. The signals obtained are presented on the next subchapter.

However, when introduced into the real acquisition system, during experimental test, on bench conditions, it revealed to have an unstable behavior. On that phase, it was discarded once it was possible to apply a low-pass filter using the *Matlab* Software.

4.3.2 Demodulator experimental tests

4.3.2.1 *Input* signal specifications

To test the envelope detector circuit on the breadboard and PCB, a modulated input signal produced by arbitrary waveform generator (Agilent) was used.

The carrier signal was a high frequency sinusoidal wave while the modulating signal simulated a type C APW, characteristic of a healthy person, as presented on figure 4.6.

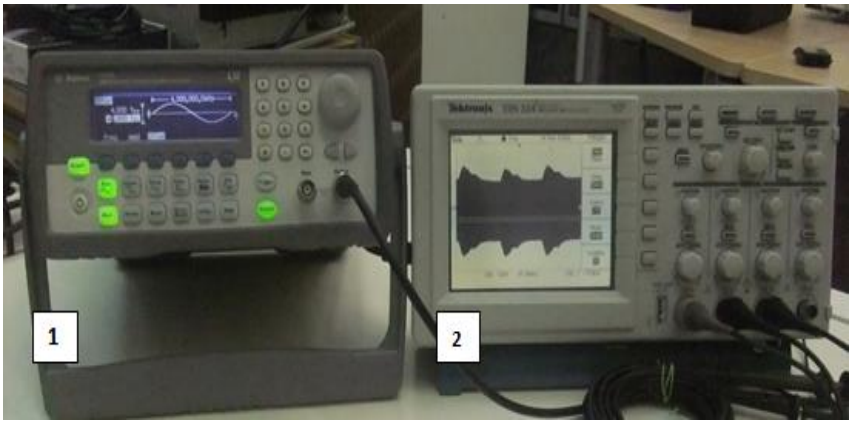

Figure 4.6: Input signal used to test the envelope detector, produced by an arbitrary waveform generator (Agilent). The image shows a waveform generator device (Agilent) (1) which produces the input signal, visualized in real-time using an oscilloscope (2). The input is a modulated signal which envelope is a type C APW.

Ideal values for the input signal parameters were achieved through a trial and error process, combining different values of frequency, amplitude, amplitude depth and offset.

Varying the Amplitude depth of the modulator signal, demodulation may occur with high quality or not. Since signals are inverted after passing through the rectifier, higher peaks will correspond to very low carrier waves' amplitude. As such, this leads to a problem: very low absolute carrier wave amplitudes are not demodulated correctly.

Accep.table values for input signal's parameters are shown on the table 4.

Table 3: Characteristics of the input modulated signal. The table presents the values for parameters of input signal used to test the demodulator circuit at the breadboard and PCB.

	Frequency (*Hz*)	Amplitude (*Vpp*)	Amplitude ($V_{pp_{RMS}}$)	Offset Voltage (*Vpc*)	AM Depth (%)
Carrier Signal	4000	4	2.828	0	---------
Modulator Signal	3	---------	---------	0	50

4.3.2.2 Data Processing Results

After confirming the good performance of the envelope detector on the breadboard and on the PCB, analog output signals were converted into digital data. Posteriorly, they were processed and visualized using *Matlab* software.

The signal processing required the development of an algorithms, leading to an easier analysis of the output signals. Their functions consist on the following steps:

Step 1: Overlap of positive and negative demodulated signals;

Step2: Unitary normalization of both signals;

Step 3: Segmentation and overlap of the several detected ABP pulses, on each demodulated signal;

Step 4: Determination of the mean AP for each demodulated signal;

Step 5: Calculus of root mean square error (RMSE) values associated to each mean AP.

4.3.2.2.1 Output signals from the Breadboard

The demodulator's electronic circuit was first tested on a breadboard. Figure 5.7 shows a photo of the breadboard with the electronic circuit assembled, during experimental tests.

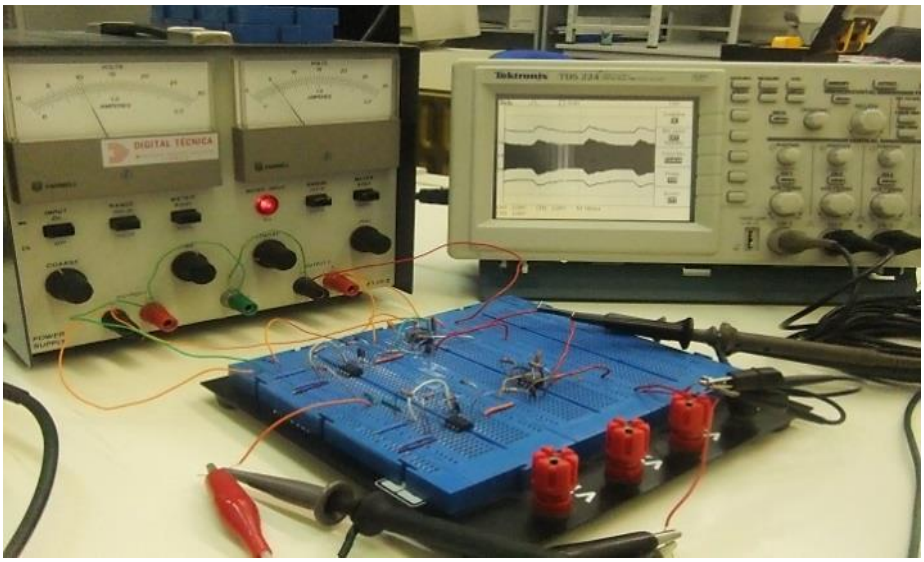

Figure 4.7: Envelope detector test on breadboard. On the right is possible to see the Agilent which is responsible to provide the input modulated signal and, on the left, a power source.

Signals resulting from software processing, according to the steps previously described, are presented below.

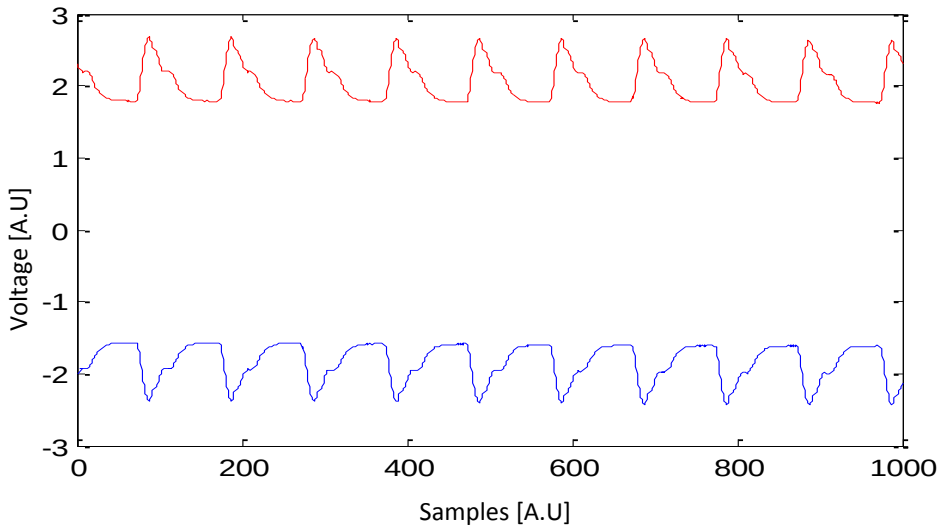

Figure 4.8: Demodulated output signals from breadboard. The blue and red signals result, respectively, from demodulation of the positive and negative half-side of the input signal

The following figure corresponds to posive and negative output signal overlap and normalization, respectively.

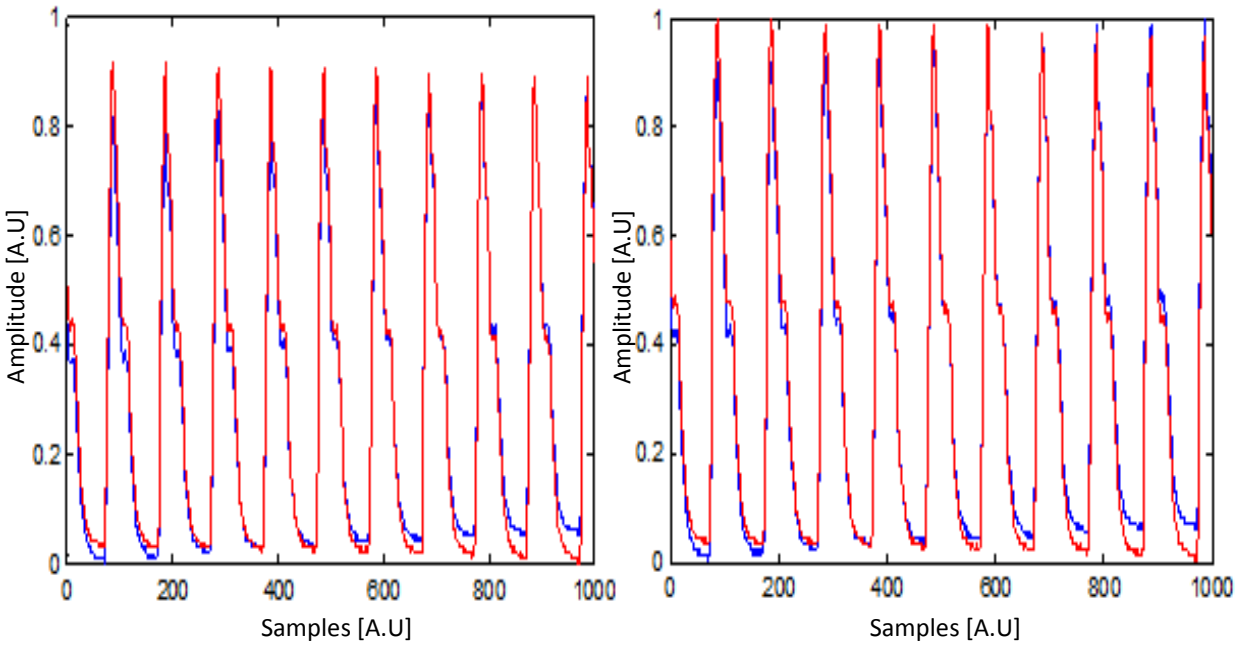

Figure 4.9: Overlap and normalization of the positive and negative demodulated output signals obtained in breadboard. Graphic a) shows the overlapping of the two positive and negative output signals and Graphic b) shows the same signals after normalization. The blue and red signals correspond to the negative (after inversion) and positive demodulated signal respectively.

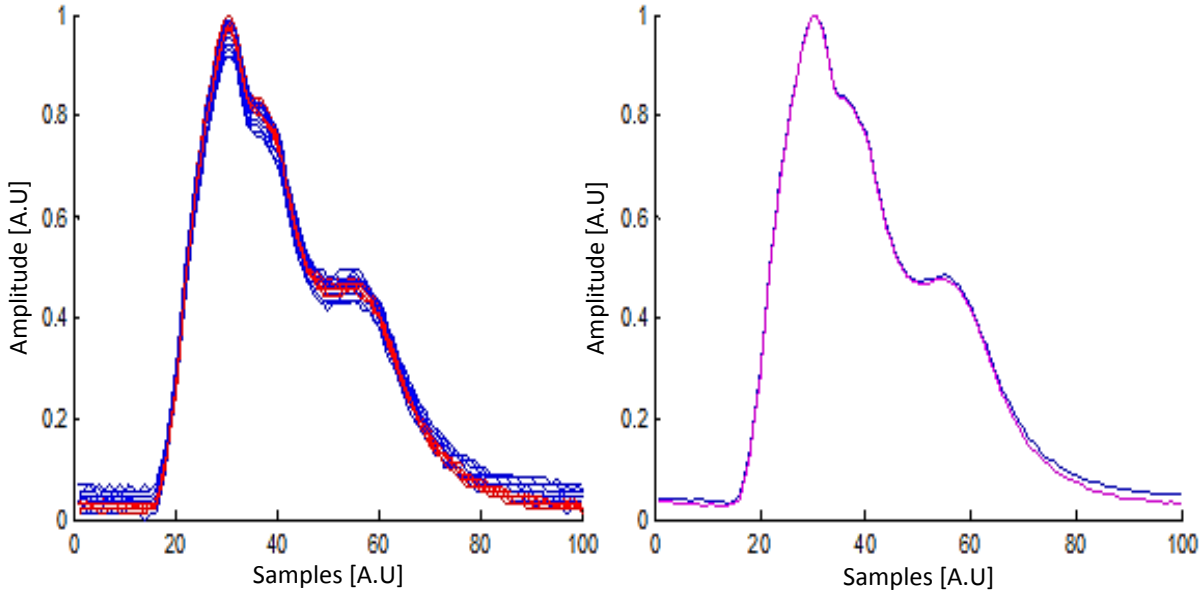

Figure 4.10: Overlap of the several AP after segmentation and their mean signals at breadboard. Graphic a) presents the overlapping of the several sectioned ABP pulses of the signals obtained after demodulation. On the other hand, graphic b) shows the mean AP for each demodulated signal. The blue and red signals correspond to the negative (after inversion) and positive demodulation respectively.

The mean AP was determined with a RMSE equivalent to 1.069%.

4.3.2.2.2 Output signals from the printed circuit board

The following figure is a photo of the envelope detector circuit on the PCB, during experimental tests.

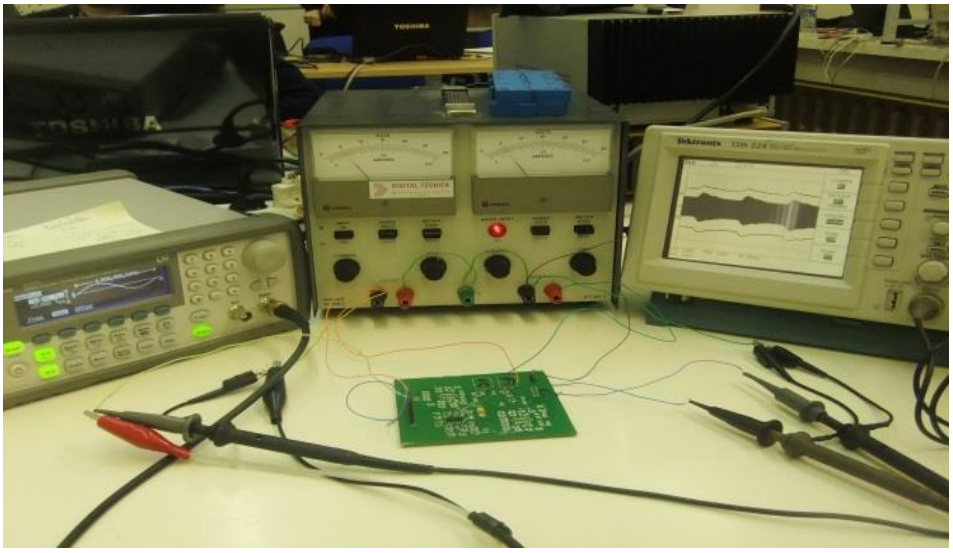

Figure 4.11: Envelope detector test on PCB. On the right, is possible to see the arbitrary waveform generator (Agilent) device which is responsible to provide the input modulated signal and, in the middle, a power source.

The signals resulting from *Matlab* processing are presented on the next three figures.

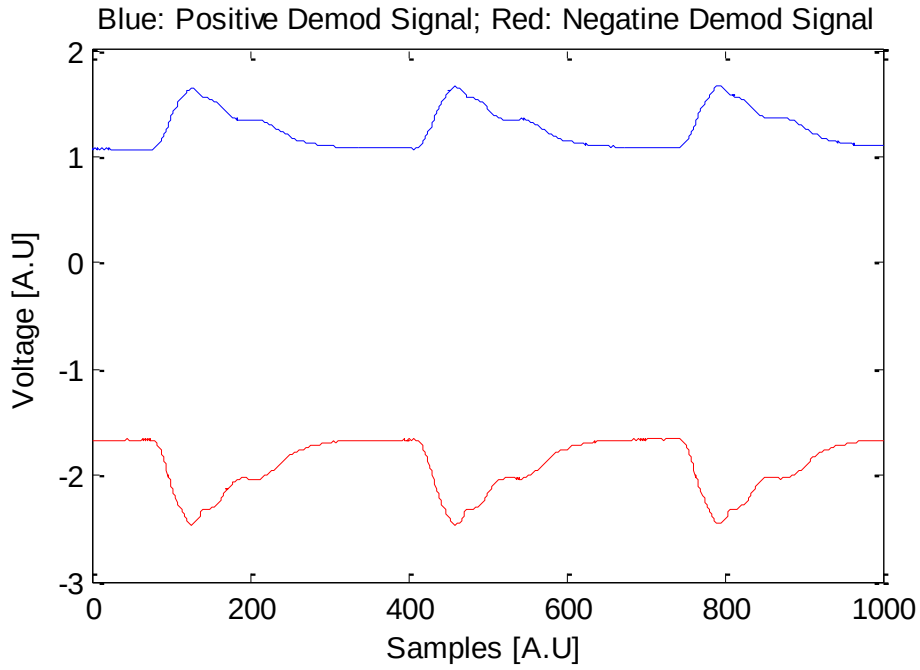

Figure 4.12: Demodulated output signals from the PCB. The blue and red signals result from demodulation of positive and negative half-side of the input signal, respectively.

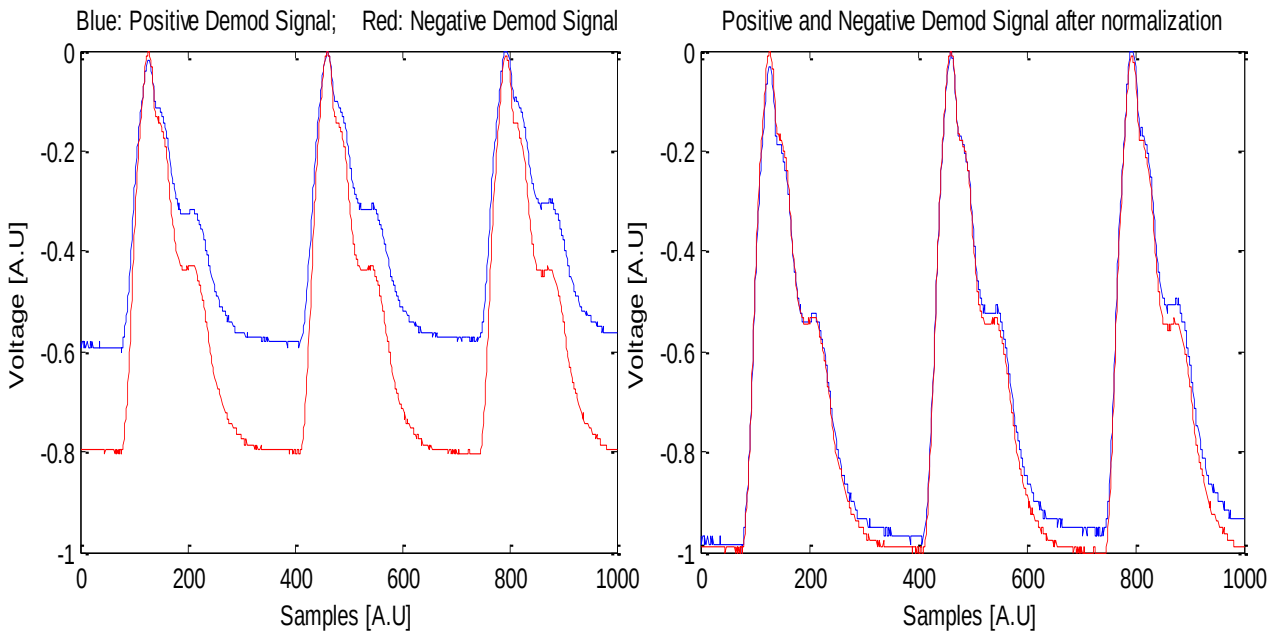

Figure 4.13: Overlapping and normalization of the positive and negative PCB demodulated output signal. The first graphic shows the overlapping of the positive and negative demodulated signals and second graphic shows the same signals after normalization.

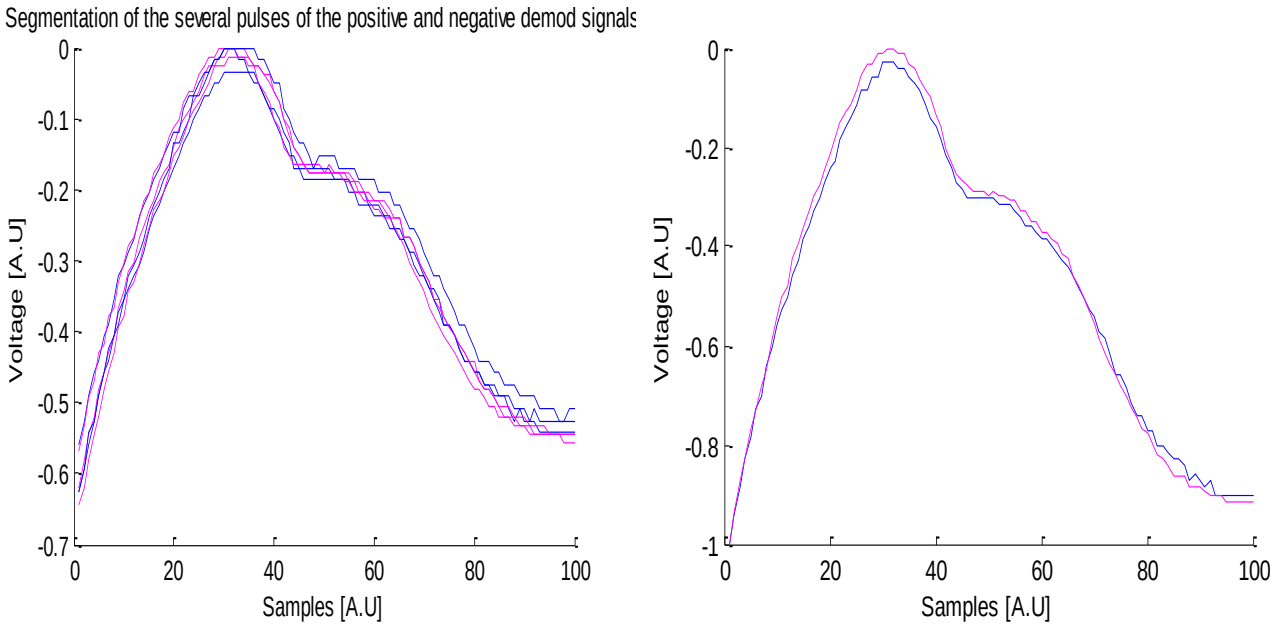

Figure 4.14: Overlapping the several ABP pulses and their mean signal at PCB. . Graphic a) presents the overlapping of the several sectioned ABP pulses of the signals obtained after demodulation. On the other hand, graphic b) shows the mean AP for each demodulated signal.

The mean AP was determined with a percent error of 1.2952.

4.3.2.2.3 Comparison between software and hardware printed circuit board demodulation

As mentioned above, the probe output is a modulated signal whose demodulation is done using the envelope detector circuit. However, it also may be done through software using algorithms capable of detecting the envelope signal.

By comparing both signals it is possible to analyze how close to ideal is the performance of the developed envelope detector. Software demodulation has already proved its effectiveness in extracting modulating signals in bench conditions with errors less than 2% [7, 58], while the demodulation from hardware has imperfections.

The next two figures compare demodulated signals obtained from hardware and software demodulation processes.

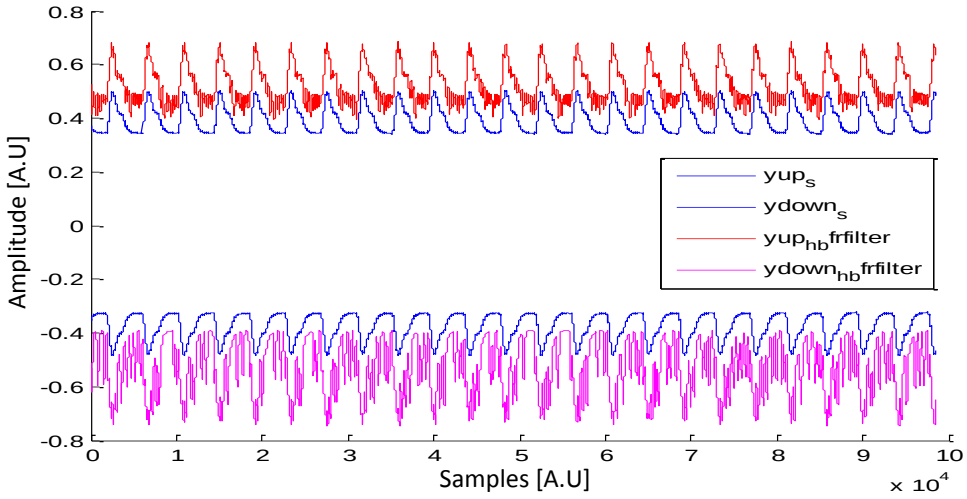

Figure 4.15: Comparison between software and hardware demodulation. The blue signal results from software demodulation and the others are the demodulation obtained from hardware.

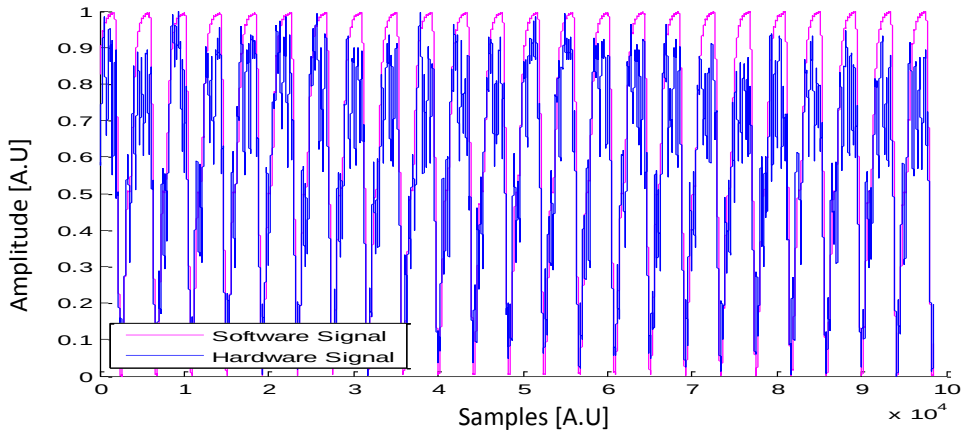

Figure 4.16: Software and Hardware comparison after *Matlab* processing. The processing consists on the subtraction of the positive and negative demodulation and their posterior normalization.

To compare the software and hardware demodulated signals it was necessary to process them previously. The main steps were based on:

Step 1: Overlap the positive and negative demodulated signal obtained through hardware;

Step 2: Overlap the positive and negative demodulated signal obtained through software;

Step 3: Normalization of both hardware and software demodulated signals;

Step 4: Comparison between the software and hardware demodulated signal and calculus of RMSE value.

The RMSE between the two demodulated signals was equivalent to 16.56 %.

4.3.2.3 Conclusion

Experimental tests on breadboard and PCB proved the correct functioning of amplitude demodulator circuit which, successfully, detected the envelope that surround the modulated input signal.

The comparison of hardware demodulation and software demodulation demonstrated the limitation of hardware demodulation; its output signals are affected by a significant noise. In further implementations digital filters will be used.

Chapter 5

Process Methodology

Contents

5.1 Introduction

The purpose of this project is to develop a hemodynamic probe capable to detect carotid dynamic, more specifically APW and extract, from it, relevant clinical information. However it is indispensable to have a support acquisition system responsible to acquire, convert and store the data for signal visualization and analysis.

Two different acquisition systems were developed along this project. This chapter is focused on their description, explaining in detail their main constitution and successive improvements.

5.2 Acquisition System version I

The design of the first acquisition system version includes a hemodynamic probe, an amplitude demodulator, an acquisition module box and a personal computer.

The association between the hemodynamic probe and the PCB containing the demodulator circuit allows detecting ABP waveform; the function of the acquisition module is to acquire and log analog signals, converting them to digital, yielding ".txt" data file; the computer allows data storage, processing and analysis using softwares such as *NI LabVIEW SignalExpres* and *Matlab*.

Additional instruments such as an arbitrary waveform generator (Agilent), a power source and an oscilloscope also integrate the system supporting all the acquisition process. The Agilent is responsible to stimulate the PZ sensor by providing a high frequency sinusoidal signal and the power source supplies the pressure sensor and the hemodynamic probe, more specifically the accelerometer and the demodulator circuit.

Specifications about the design and performance of the hemodynamic probe are exposed in detail in chapter 3.

Below, on figures 5.1 and 5.2, an illustrative schema of first acquisition system and a photo took after its assembly, are presented.

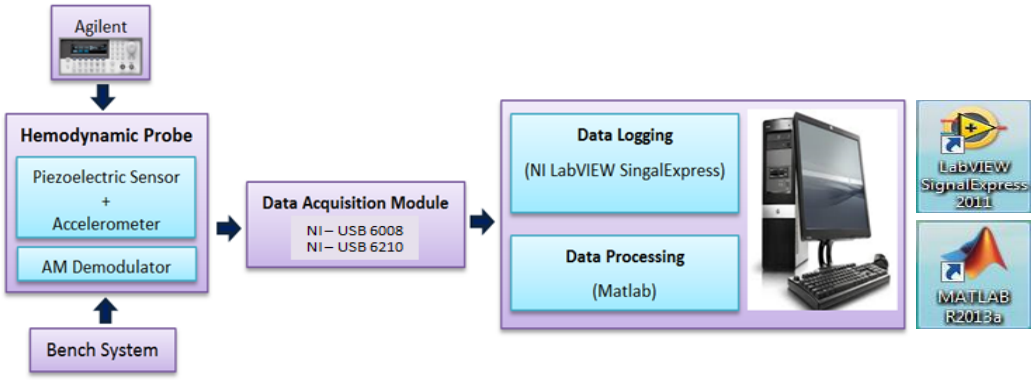

Figure 5.1: Schema of the first acquisition system version. The schema presents the design of the acquisition system and indicates the mains parts that integrate it. Its main components are the hemodynamic probe, the demodulator, the data acquisition module and a personal computer. The Agilent function is to stimulate the PZ sensor. A power source and an oscilloscope are also required to support the acquisition process.

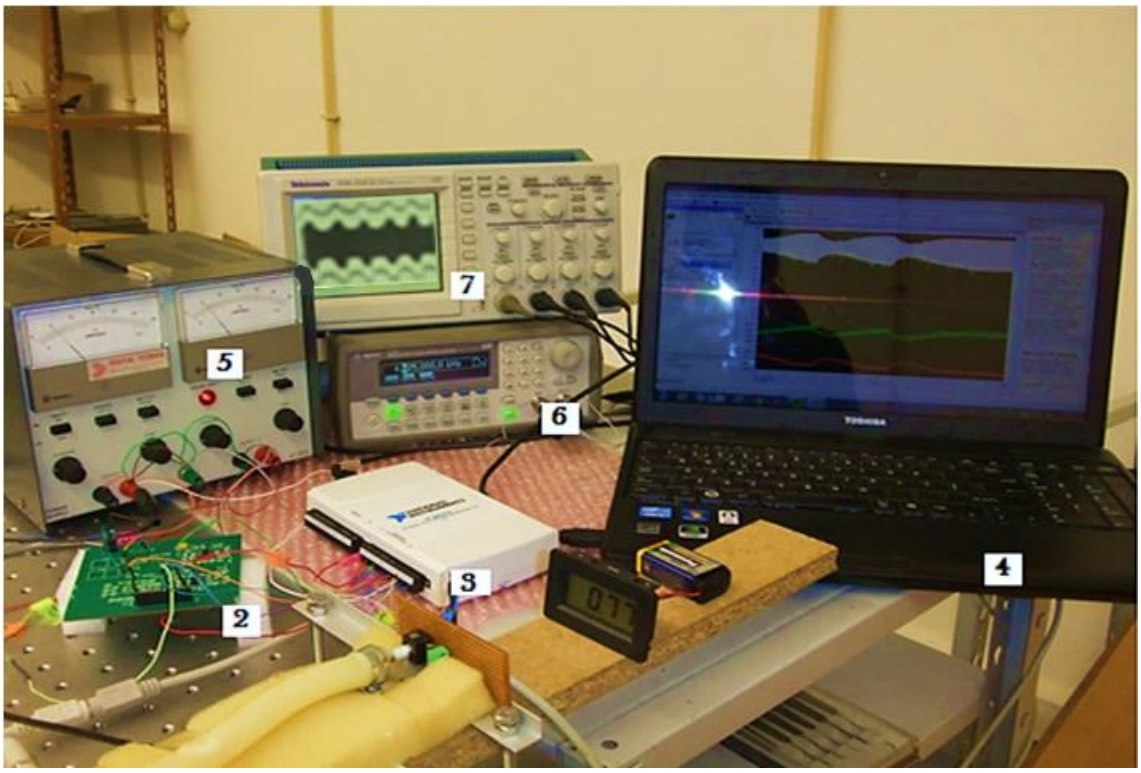

Figure 5.2: Photo of the first acquisition system version. 2- Demodulator circuit; 3- Acquisition module; 4- Personal computer; 5- Power voltage source; 6- Arbitrary waveform generator (Agilent); 7- Oscilloscope.

The acquisition, log in and conversion of analog into digital data was first done by using the NI-6008, a USB based data acquisition device characterized by 8 analogical input channels, 12 bits and a sampling rate equivalent to 10 KS/s (Kilo samples per second).

Posteriorly, it was replaced by a NI USB-6210, since it allowed acquiring, simultaneously, an increased number of signals with higher sampling rate.

NI USB-6210 is a data acquisition device which presents 16 analog input channels, 16 bits and a sampling rate equal to 250 KS/s.

Figure 5.3: Different data acquisition devices. The image shows the two different data acquisition devices used to convert analogic to digital data. Image a) NI USB-6008; Image b) NI USB- 6210.

Additionally, it was also necessary to replace the power supply due to some functioning problems.

Despite its correct functioning, this acquisition system version had some weaknesses related to its non-portability, high cost, and inability to be used in in-vivo trials. As such, a new and improved system version was developed.

5.3 Acquisition System version II

5.3.1 Support concepts

5.3.1.1 Digilent

Digilent is a multifunctional instrument capable to generate record, convert, measure and analyze both analog and digital signals. Its inputs and outputs, which may be analogic or digital, connect to electronic circuits using simple wire probes [47, 52].

It may be controlled by using *Matlab* or PC–based $WaveForms^{TM}$ softwares which allow configuring the digilent in order to accomplish several tasks.

The following figure shows the external and internal aspects of a Digilent.

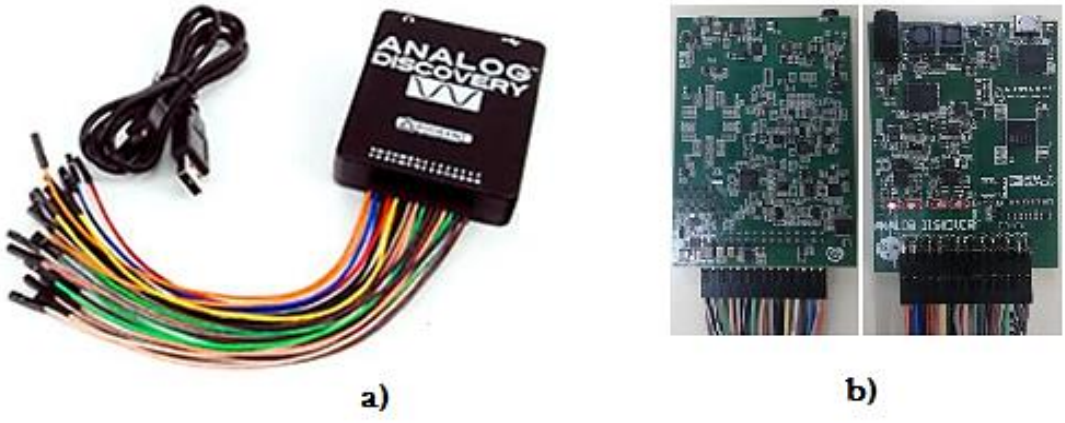

Figure 5.4: Digilent external and internal aspect. Image a) show the Digilent external aspect while in image b) shows a picture of the Digilent PCB. [48, 49]

The most important properties that characterize the Digilent is the existence of 2 oscilloscope channels, 2 waveform generator channels, 16 logic analyzer channels, 16 digital pattern generator channels , ±5V DC power supplies, a spectrum analyzer, a network analyzer, a voltmeter and a digital I/O [47,48].

These specificities reveal digilent as a multifunctional device able to perform several tasks such as reading data from the two oscilloscope channels (analog input), control and generate data for the two waveform generators (analog output), characterize integrated circuits, measuring its behavior and analyzing its components, configure the sampling rate of the device, trigger the start of the data acquisition or find and display digilent Analog Discovery device settings. [47]

Detailed information about Digilent specifications are presented on the table 3.

Table 4: Detailed specifications of a Digilent system. This table presents detailed information about Digilent digital I/O, analog input and output. [47]

	Analogue Inputs	**Analogue Outputs**	**Digital I/O**
Characteristics	AD9648 dual: - 14bits; - 105 MSPS; - 1.8 V dual analog to digital converter	AD9717 dual: -14-bits; - 25 MSPS; - Low power digital to analog converter	16 Signals shared between logic analyzer, pattern generator and discrete I/O devices ions per pin

Characteristics	2-channel differential (±20V max)	2-channels: - Single-ended; - Arbitrary waves up to ±4V	Crosstriggering with scope channels
	250 µV to 5V per division	Standard and user-defined waveforms	
	Variable gain setting	Sweeps, envelopes, AM and frequency modulation (FM)	
	100MSPS; 5MHz bandwidth	100MSPS; 5MHz bandwidth; 16Ksamples/Channel	

5.3.1.2 Multiplexer

Multiplexing is a generic term used to describe the operation of sending one or more analogue or digital signals over a common transmission line.

The device capable of doing that is called Multiplexer, a combinational logic circuit designed to switch one of several input lines through to a single common output line.

The multiplexer may be digital or analogic. Digital ones are made up from high speed logic gates which switch digital or binary data while, analogic type normally use transistors, MOSFET's or relays to switch the currents or voltage inputs to a single output. [50]

The Multiplexing process may be classified according to the applied input recognition technique. Examples are:

- Frequency Division Multiplexing: Each input has its own well-defined spectral band;
- Time Division Multiplexing: Each input has its predefined time to use the transmission line;
- Statistical Time division Multiplexing: Communication channel is divided into an arbitrary number of variable bit-rate digital channels or data streams. The link

sharing is adapted to the instantaneous traffic demands of the data streams that are transferred over each channel;

- Wavelength Division multiplexing: Each input has a different wavelength, directly related to the frequency;
- Code Division Multiple access: Each input signal is identified by an initial code which allows recognizing it. [50, 51]

Figure 5.5 illustrates the basic principle of a multiplexer switch, selecting from several inputs options an individual signal to pass through the single and common output line.

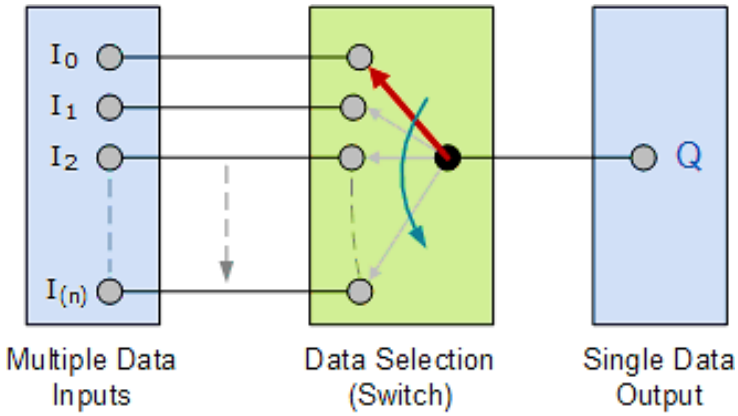

Figure 5.5: Multiplexer's basic functioning principle. The image shows the way how multiplexer works, through switching process that allow choosing one of the several signals available as input to pass through a single output line. [52]

The selection of each input line on the multiplexer requires additional input set called *Control Line* or *Select Lines.* According to the binary condition of these control inputs the appropriate input is connected directly to the output.

Usually, a multiplexer has a number of inputs equivalent to 2^N where N is the number of bits.

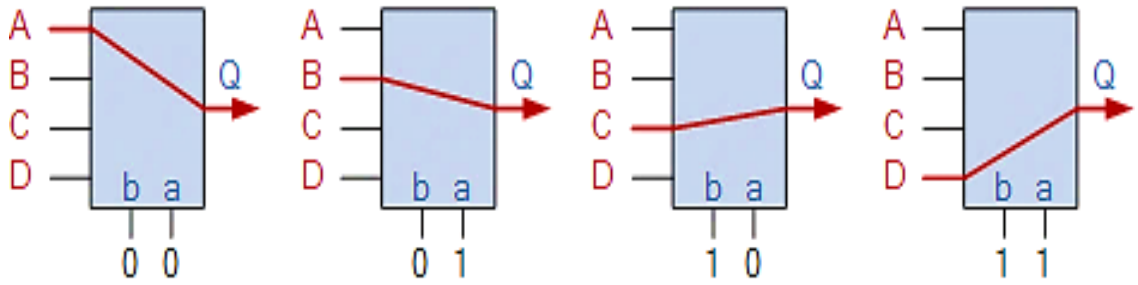

Figure 5.6: Multiplexer Input line selection based on binary condition. To select the desired input signal, ignoring the others a binary logic condition is used on the control input lines. Multiplexer always has a number of inputs equivalent to 2^N, granting the possibility of selecting anyone of the available input. [52]

The multiplexer usage is advantageous since it allows reducing the number of logic gates required on circuit design.

The developed design of this new acquisition system requires two different types of multiplexers: two 8-to-1 and two dual 4-to-1 multiplexers. Further explanations about the reasons for their use and details about architecture of the new acquisition system will be presented on the following subchapter.

5.3.2 Architecture of the second acquisition system version

The innovations implemented in this new acquisition system version are the use of a digilent device and the integration of multiplexers on the envelope detector electronic circuit which architecture was restructured.

The designed acquisition system corresponds to a single box which integrates the PCB with the envelope detector circuit connected to a Digilent. A Db15 female connector allows to login signals into the system and two female connectors, a USB 2.0 Micro B and a DC barrel jack, permit powering the system and transferring data to a computer.

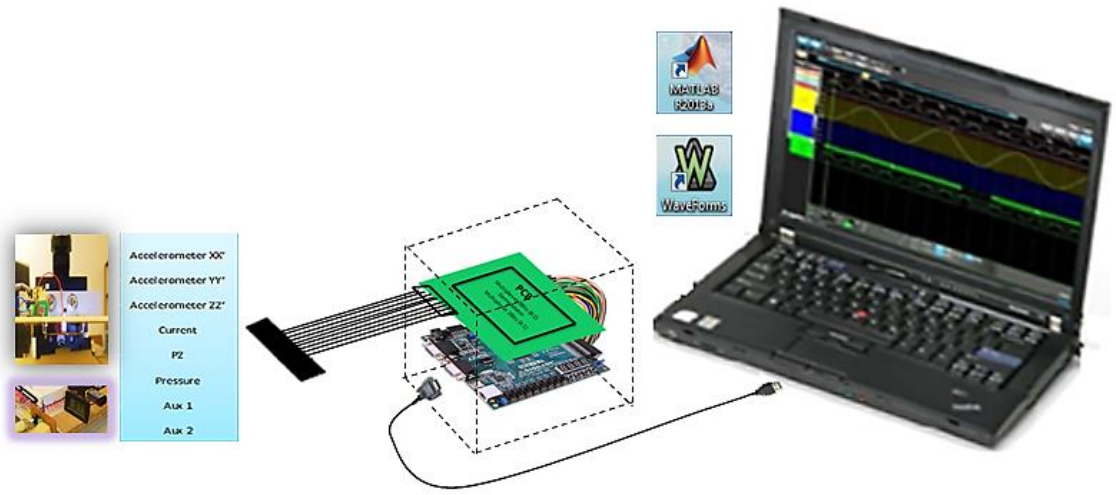

Figure 5.7: Schema of the second acquisition system version. In this new acquisition system, signals which come from the hemodynamic probe and pressure sensor are processed on the developed PCB. Output signals enter the Digilent which enable to visualize, analyze and store ".cvs" data files. Further information about the PCB architecture will be presented posteriorly.

The input signals are collected from the pressure sensor and hemodynamic probe, more precisely signals from X, Y and Z accelerometer axes and PZ sensor. Information about

the current is also important since it plays a crucial role on system calibration. Three more signals are available at input channels: +5V, +15V and -15V.

As described above, the Digilent is a multifunctional device capable to realize several functions, specific to others traditional instruments such as the oscilloscope, Agilent and acquisition module (USB NI-6008 / USB NI-6210). By using the Digilent these instruments became no longer necessary on signal acquisition process.

However, the Digilent has a disadvantage: it only has two oscilloscope channels meaning that is only possible to visualize record and analyze, simultaneously, two signals. Considering this fact, some adjustments were done on the architecture of PCB which contains the demodulator circuit in order to enable choosing, for both digilent channels, any signal to observe, analyze and record.

For each Digilent channel an 8-to-1 multiplexer, an envelope detector circuit and a 4-to-1 multiplexer are assembled together. The first multiplexer selects, from several available inputs, the target signal which may keep its original form or enter the demodulator circuit to obtain the positive and negative envelope. Multiplexer 4-to-1 allows selecting any of these chosen signal versions and sends it to a specific digilent channel.

Figure 5.8 depicts a schema of the architecture designed for the envelope detector PCB. A more detailed schema may be found on point c) of Appendix-A.

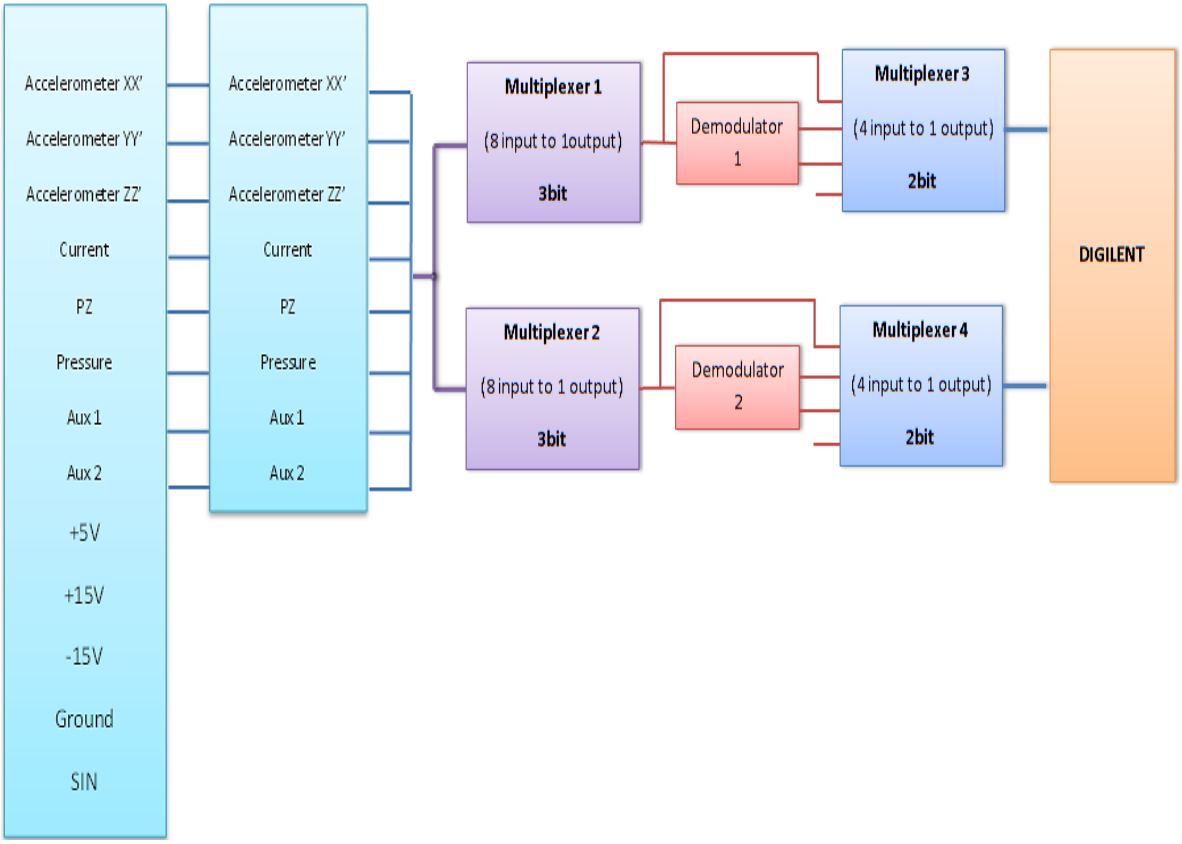

Figure 5.8: schema of the PCB architecture containing envelope detector. The PCB was architected in such a way to permit choosing any one of the several available input signals, either in its original version, its positive or negative demodulated version. Two different type of multiplexer were used: an 8-to-1, 3 Bits and a double 4-to-1, 2 Bits multiplexer.

The selection of signals in any multiplexer requires signal addressing codes. The developed algorithm allows addressing the signals, activate the digilent which acquires the selected signals and convert them from analog to digital yielding ".csv" data file. This way is possible to visualize both signals, analyze and compare them.

On Figure 5.9 is possible to see a photo of the acquisition box and the PCB with the envelope detectors circuit while figure 5.10 shows a picture of the second acquisition system version.

Figure 5.9: Photo of the acquisition box and the PCB containing the demodulator circuit. The acquisition box integrates not only the demodulator PCB but also the digilent. Observing the PCB it is possible to see an increase on the circuit complexity. There are two demodulator, one for each digilent channel. The electronic components marked with *"M"* correspond to multiplexers.

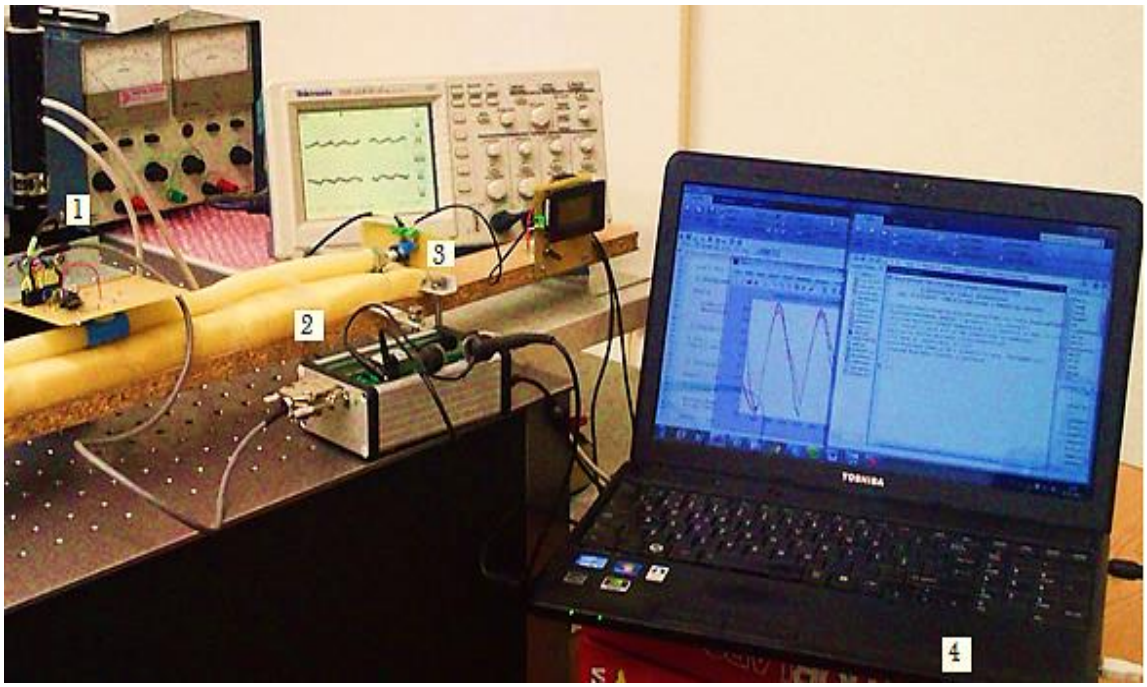

Figure 5.10: Picture of the second acquisition system version. It only includes the acquisition box and a computer. Input signals are collected from the hemodynamic probe (1) and pressure sensor (3) being sent to the acquisition box (2). The analog output signals are converted into digital thanks to the digilent. The result data files are sent to the computer (4) where they are processed using *Matlab* software.

5.3.3 Advantages and improvements introduced by the new acquisition system version

The modification of the acquisition system architecture represented a great improvement and advance to the viability of this project providing several advantages:

- Reduction of monetary costs since very expensive devices such as Agilent, oscilloscope, power supply and modules USB NI-6008 or USB NI-6210 were no longer necessary;
- Considerable reduction on all system dimensions and weight;
- A decrease of energy waste;
- An easier system management due to the new developed architecture;
- Increase of system mobility;

Chapter 6

Test bench System

Contents

6.1 Introduction

The test bench system is a powerful tool used to do experimental tests during a probe's development and algorithms validation. In this project it is used to simulate the dynamic of a human carotid artery, reproducing the local ABP and APW;

Two different bench systems were developed during this project, differing from each other on the syringe size and the way how its piston is moved, manually or mechanically.

6.2 Support Information

Physiological and mechanical arterial walls properties have a decisive influence on the blood flow, being a crucial factor on hemodynamic parameters assessment. This explains our concern on reproducing, with high fidelity, artery walls.

Latex models of arterial vessels have been previously used in medical researches. Tests to compare latex models and human arteries were done and parameters such as compliance, PWV and Young's modulus were evaluated. Results proved their similarities except for the increased compliance of latex model at high pressure [33, 34].

Feng and Khir constructed an experimental setup made of a piston pump connected at a latex tube. At Brunel University, another group of researchers have used latex tubes to model arterial waves [35, 36]. In GEI-CI group (Instrumentation Center- Electronic and Instrumentation group), latex tubes have also been used in programmable test bench systems for hemodynamic studies [68, 69, 70].

Considering the literature we were encouraged to do, in this project, experimental tests using a latex for arterial modeling.

6.3 First Test bench system version

6.3.1 Instrumentation

The first bench system's design consists on a 49 cm long flexible latex rubber tube attached to a pressure sensor and a syringe at one and another extremity, respectively. The syringe diameter is equivalent to 6.7 cm and its length is equal to 5 cm. Both the tube and the syringe are filled with water.

The pressure sensor is a 40PC015G1A (Honeywell S&C) type and it is used to detect tube inner pressure. According to specifications on its datasheet, available on Appendix E, the pressure sensor needs +5V power supply to operate; 170 mmHg is the maximum detectable pressure and the range of analog output voltage goes from 0.5 to 4.5V, being linearly proportional to the input pressure.

The pressure conversion into voltage values is done according to the following formula:

$$P_{mmHg} = \frac{V_p - V_{Null}}{0.2667} \text{ x } 51.715 \qquad (11)$$

P_{mmHg}: Tube inner pressure measured in *mmHg;*

V_P: Voltage value displayed on LCD when pressure is exerted;

V_{Null}: Minimum output voltage.

0.2667 mV/psi is the device sensitivity and 51.715 corresponds to 1 *psi* converted to *mmHg*.

It is necessary to control the force that is applied on the syringe piston, since the range of pressure that matters to the experimental tests goes from 50 to 160 mmHg. The piston movements are caused by an eccentric attached to a DC motor rotation axis (figure 6.1).

In order to obtain the desired range of pressure, it is required a previous study of eccentric's shape and dimension. It was used a circular eccentric whose diameter equals to 11.8 cm and that contains a slot passing through its center, allowing its position adjustment to a DC motor rotation axis.

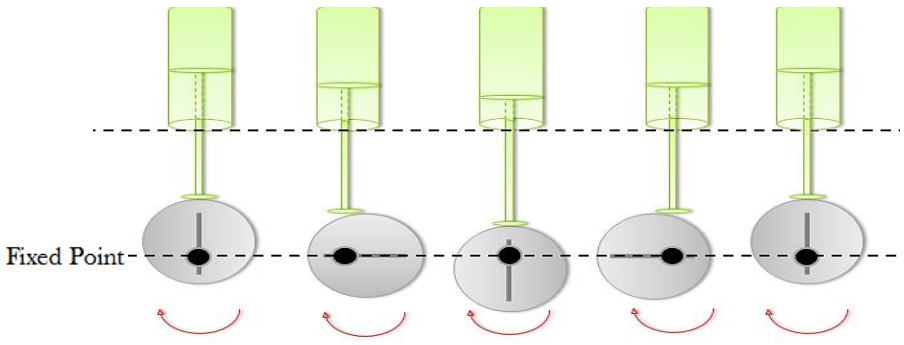

Figure 6.1: schema of the eccentric's design and performance over syringe's piston. The slot on the eccentric allows adjusting its position on the motor rotate axis and controls the exerted pressure.

The following figure represents a schema of the test bench system design.

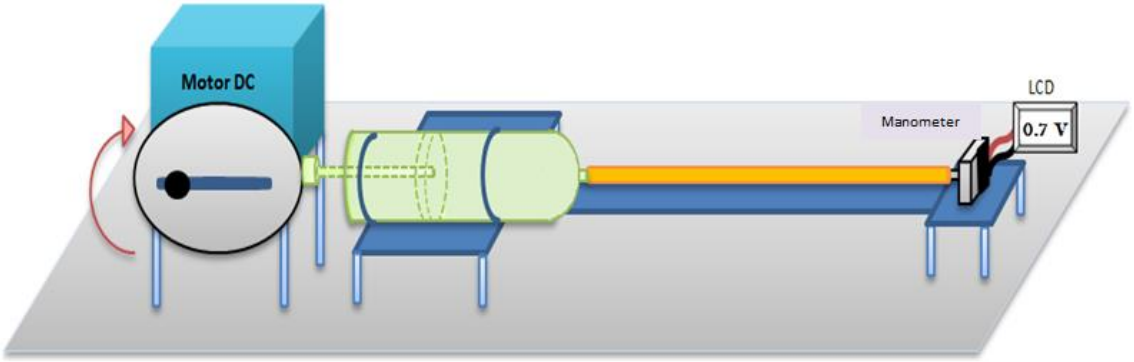

Figure 6.2: Schema of the first test bench system. This system is composed by a flexible rubber tube attached, at one extremity, to a syringe and to a manometer at the other; the syringe and tube are filled with water. The syringe piston is moved cyclic and automatically due to a DC motor with an eccentric attached to its rotation axis.

Below, in figure 6.3, an image of the test bench system after its assembly is visible.

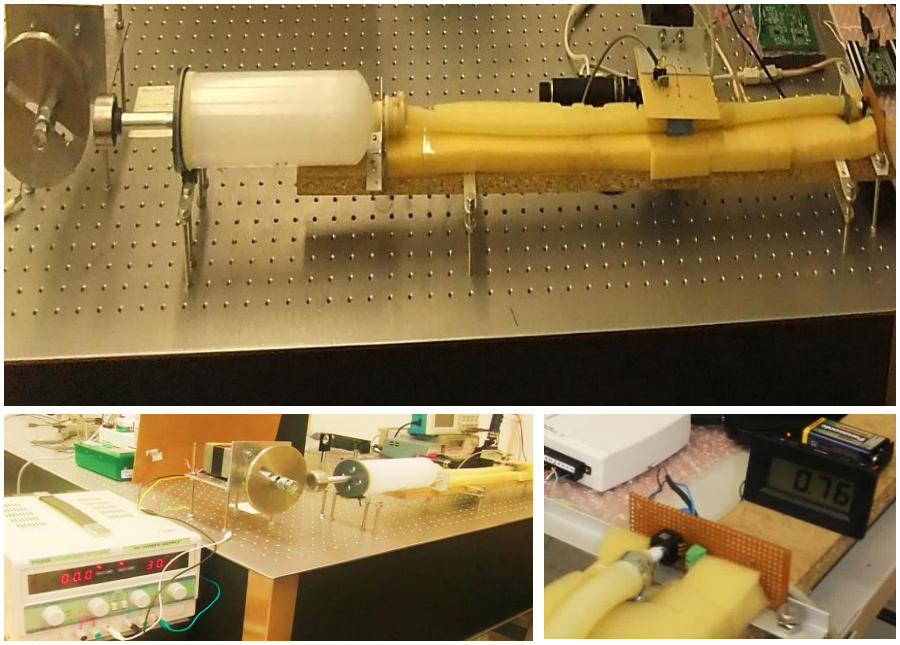

Figure 6.3: Photo of the first bench test system. The first picture shows the assembly of the first bench test system according to the schema presented previously. The second and third ones shows the details of the DC motor, its power supply and the manometer, at the end of the rubber tube. The values registered are converted to voltage and displayed at a LCD.

6.3.2 Results using acquisition system version I

In order to facilitate the system's usage and manipulation, this test bench system version was planned and assembled to generate, automatically, cyclical pressure waveforms.

Experimental tests were accomplished and the output signal, presented on the figure below, is the result of a single eccentric rotation cycle.

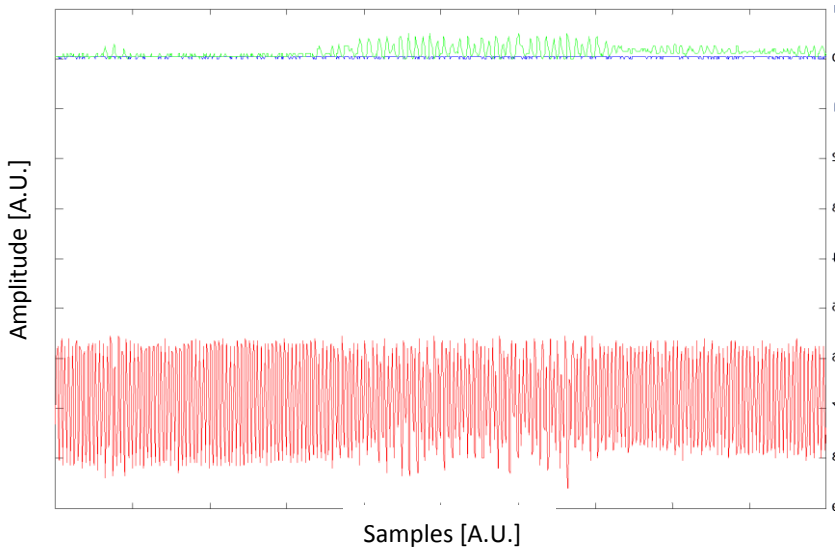

Figure 6.4: Output signal obtained from the first bench system experimental tests. The signal results from eccentric actuation over the syringe piston during a single rotation. Some problems such as significant noise and the irrelevant signal modulation are visible.

Through the analysis of the signal obtained from experimental test, some problems can be identified:

- The signal modulation is very small;
- The output signal is significantly affected by noise.

Their causes were found on some bench system failures:

- Water escapes from the syringe when eccentric actuates over the syringe's piston, leading to an insignificant increase of tube inner pressure;
- A significant friction between the eccentric and the syringe's piston surface explains the signal noise and;
- Turbulence on the water flow is perceptible.

These factors converge into a poor signal modulation and, consequently, a poor output demodulated signal.

Based on these facts it is possible to conclude that the test bench system needs further improvements.

6.4 Second Test bench system version

6.4.1 Instrumentation

The new bench system is identical to that developed at first, except for the smaller syringe and for the manual pressure creation process. Once the DC motor and the eccentric were discarded, the syringe's piston manipulation became manual.

The following two figures show, respectively, the schema of the bench system and its configuration after assembly.

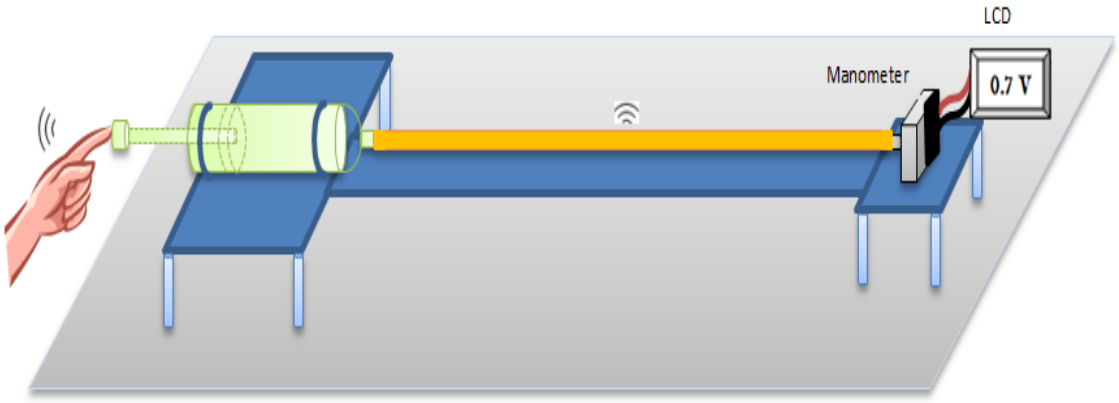

Figure 6.5: Schema of the second test bench system. It is very similar to the first bench system except for the smaller syringe size which is equivalent to 100ml. Another very important difference is the manual syringe's piston manipulation.

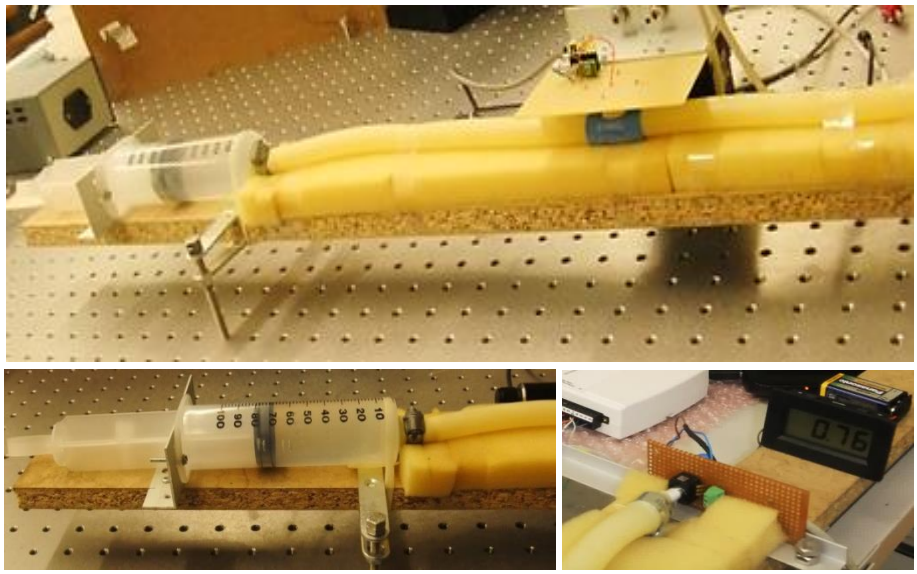

Figure 6.6: Photo of the second bench test system assembly. The syringe used is much smaller than the previous one, being equivalent to 100ml; its piston is covered with rubber allowing smoother motion and avoiding water escape. No DC motor is added to the system meaning that the piston movement is manual.

The new syringe has an equivalent volume of 100ml and its piston is covered with rubber which allows to: reduce the signal noise due to piston smoother movement; create a higher tube inner pressure once there's no water escape and increase the signal modulation.

6.4.2 Tests using acquisition system version I

6.4.2.1 Data Processing

The data processing was done having in mind the need to compare the obtained signals and determine their RMSE value. As such, a simple algorithm was developed and implemented, consisting in the following steps:

Step 1: File load and visualization;

Step 2: Software demodulation through the extraction of superior and inferior envelope from the modulated signal;

Step 3: Hardware demodulated signals filtering: application of a smooth filter with 150 point;

Step 4: Determination of the demodulated signal by subtracting the superior and inferior envelope;

Step 5: Visualization and comparison of demodulated signals from software and hardware and calculus of the RMSE value;

Step 6: Visualization and comparison of demodulated signal from hardware with the pressure sensor signal and calculus of RMSE value.

Step 7: Visualization and comparison of demodulated signal from software with the pressure sensor signal and calculus of RMSE.

6.4.2.2 Signal results

The signals resulting from *Matlab* data processing, whose steps are described above, are presented in the figure 6.7.

It is very important to mention that signals comparisons were made based on the RMSE and, acceptable values are smaller than 10%.

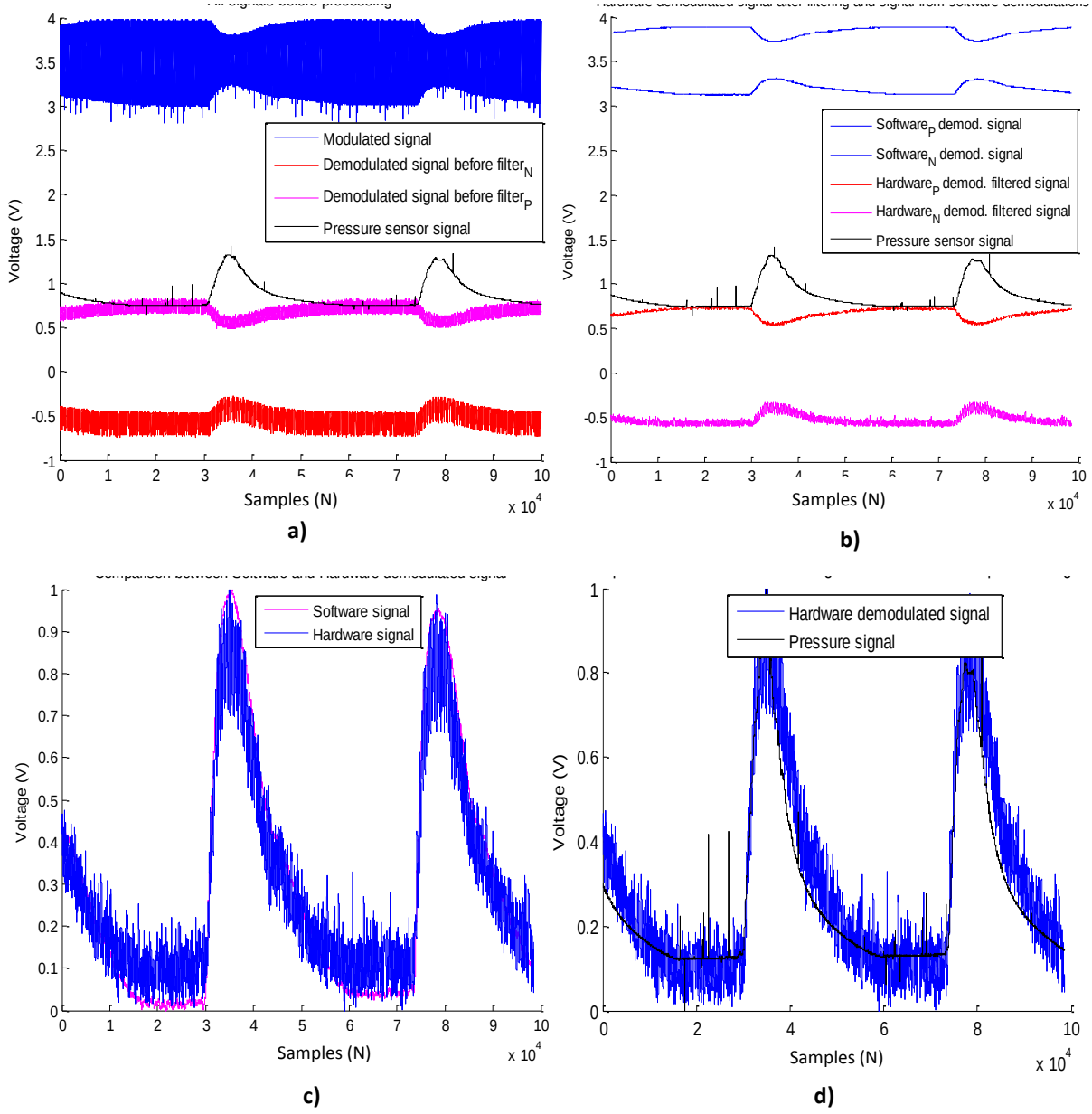

Figure 6.7: Signals resulting from data processing. Image a) presents all the acquired signals without processing; on image b), hardware demodulated signals are filtered using a "smooth" function and the modulated signal is demodulated through *Matlab* software by detecting its superior and inferior envelopes; image c) shows both hardware and software demodulated signals while image d) compares hardware demodulated signal to pressure sensor signal.

The RMSE values resulting from comparison between demodulated signals obtained from hardware and software corresponds to 9.05% and the RMSE value resulting from comparison between hardware's demodulated signal and pressure sensor signal is 8.15%.

The results obtained allow the conclusion that, despite requiring manual operation, it is possible to reproduce the ABP waveform by using this bench system's design. Besides that, comparing the demodulation obtained through software and hardware proves the correct performance of the envelope detector circuit. The comparison between pressure sensor signal and hardware demodulated signal demonstrates, once again, that the developed hemodynamic probe works well.

6.4.3 Tests using acquisition system version II

6.4.3.1 Data Processing

As described on subchapter 3.3.2, to acquire signals using the acquisition box it was necessary to develop an algorithm whose main steps allow the determination of probe resonant frequency, signal addressing, digilent activation, analog signal acquisition and conversion into digital data.

Through this algorithm five options were made available to the user, allowing him to choose which pair of signals to visualize compare and analyze. The five options were:

- Option 1: Positive and negative demodulated signals;
- Option 2: Pressure and positive demodulated signals;
- Option 3: Pressure and negative demodulated signals;
- Option 4: Modulated and positive demodulated signals;
- Option 5: Modulated and negative demodulated signals;

Acquired signals which result from demodulation process had a significant inherent noise being necessary to filter them. As a result, a *smooth* filter with 150 points was used.

6.4.3.2 Signals Result

Experimental tests using the acquisition box were done and the output signals, presented on the following pages, were acquired according to the various options described previously.

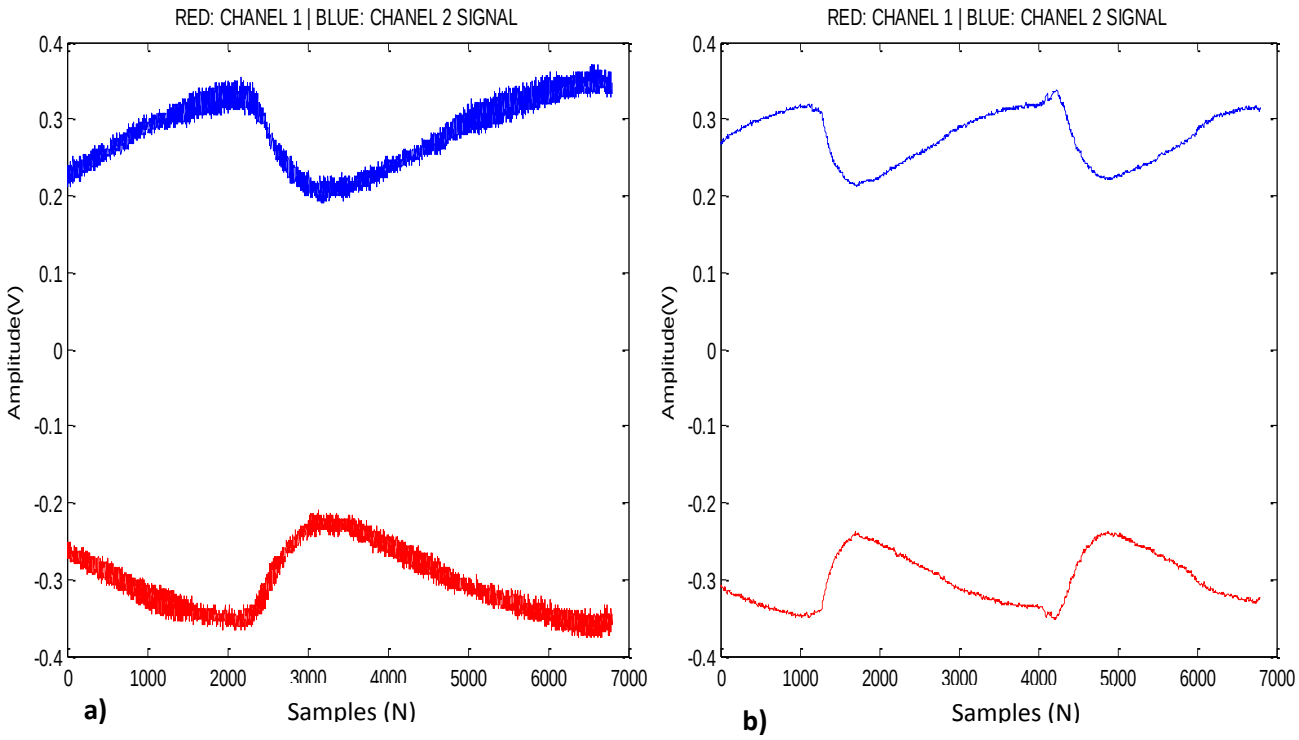

Figure 6.8: Positive and negative demodulated signals. On image a) both positive and negative demodulated signals were not filtered while on image b) they were processed by applying a smooth filter.

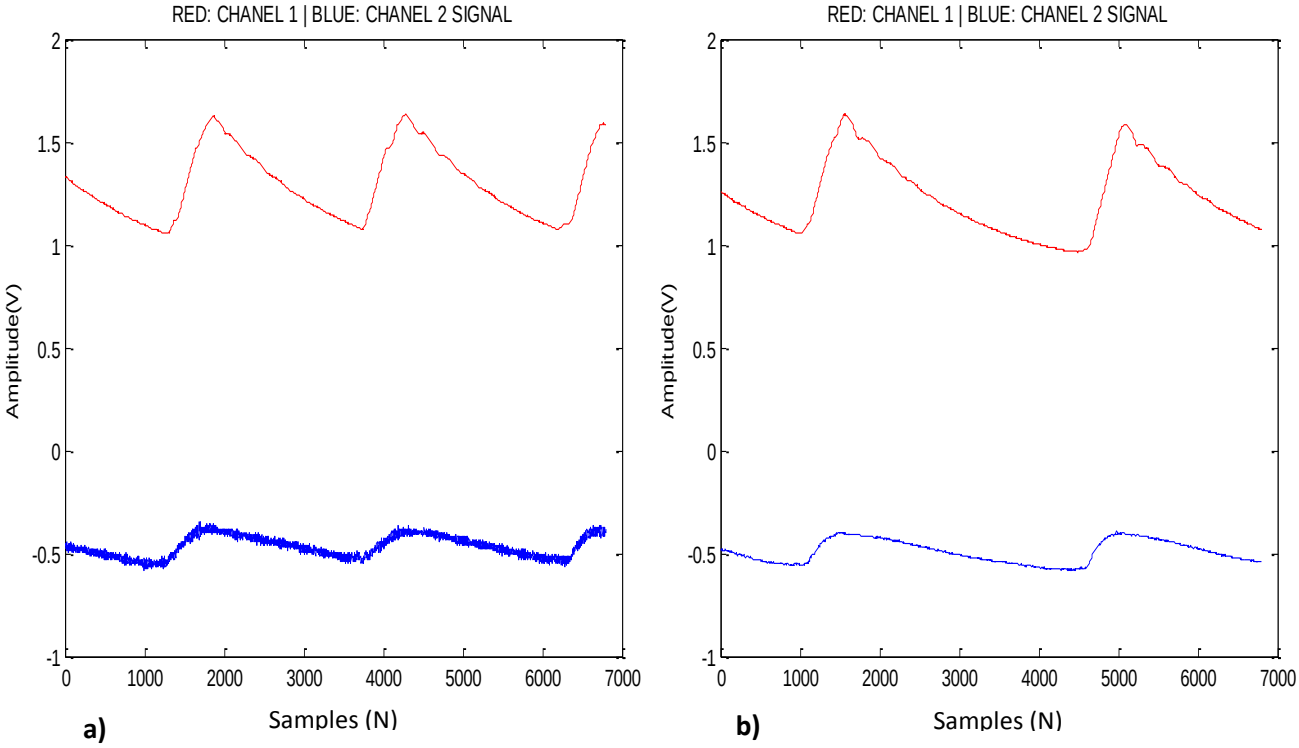

Figure 6.9: Pressure sensor and negative demodulated signals. Images a) and b) differ from each other on the negative demodulated signal. Image a) presents the raw signal (with noise) while image b) present the filtered signal.

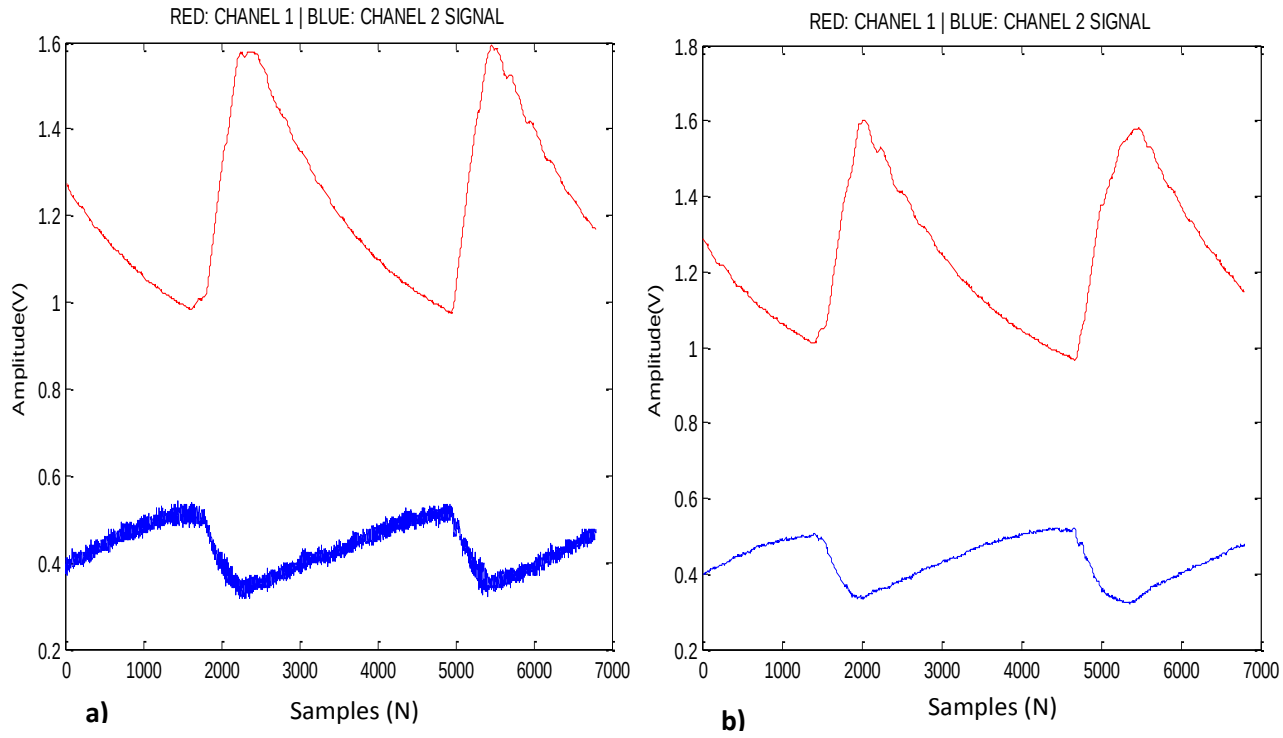

Figure 6.10: Pressure sensor and positive demodulated signals. Image a) has the positive demodulated signal before being filtered while image b) presents the positive demodulated after applying the *smooth* filter.

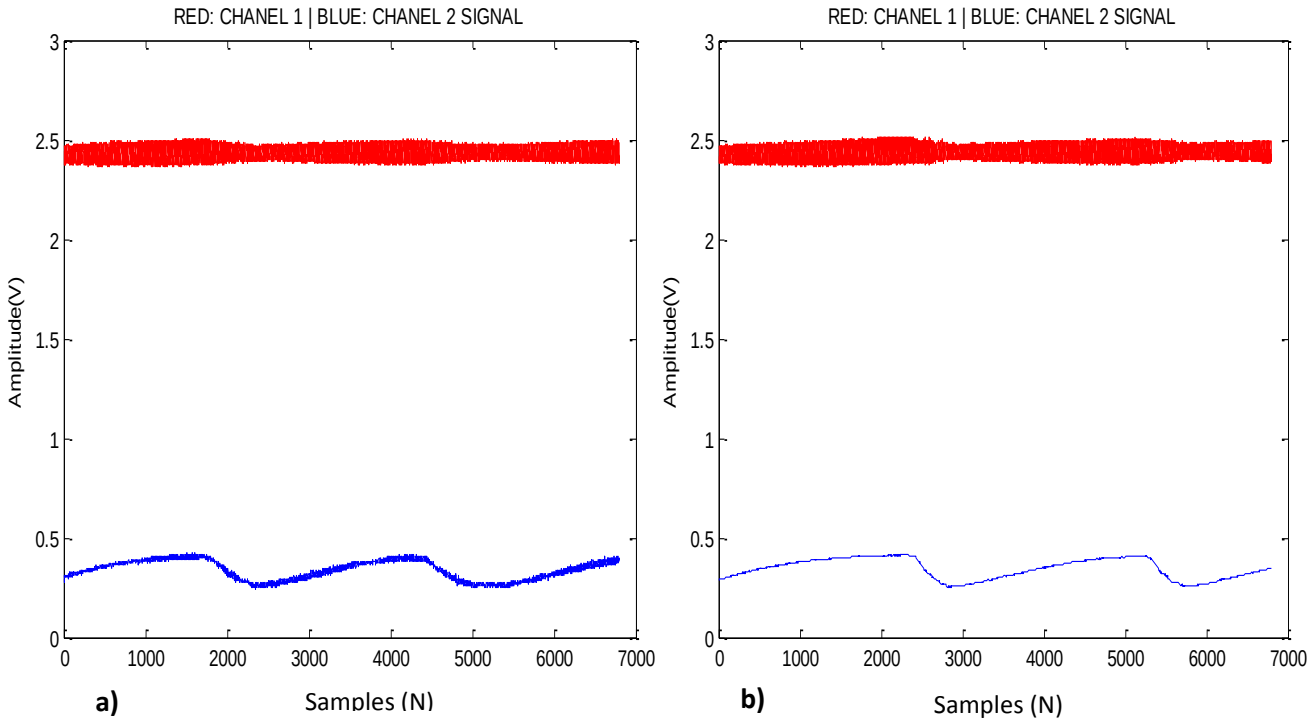

Figure 6.11: Modulated and positive demodulated signals. The demodulated signal is on its original form on image a) while on image b) it is filtered.

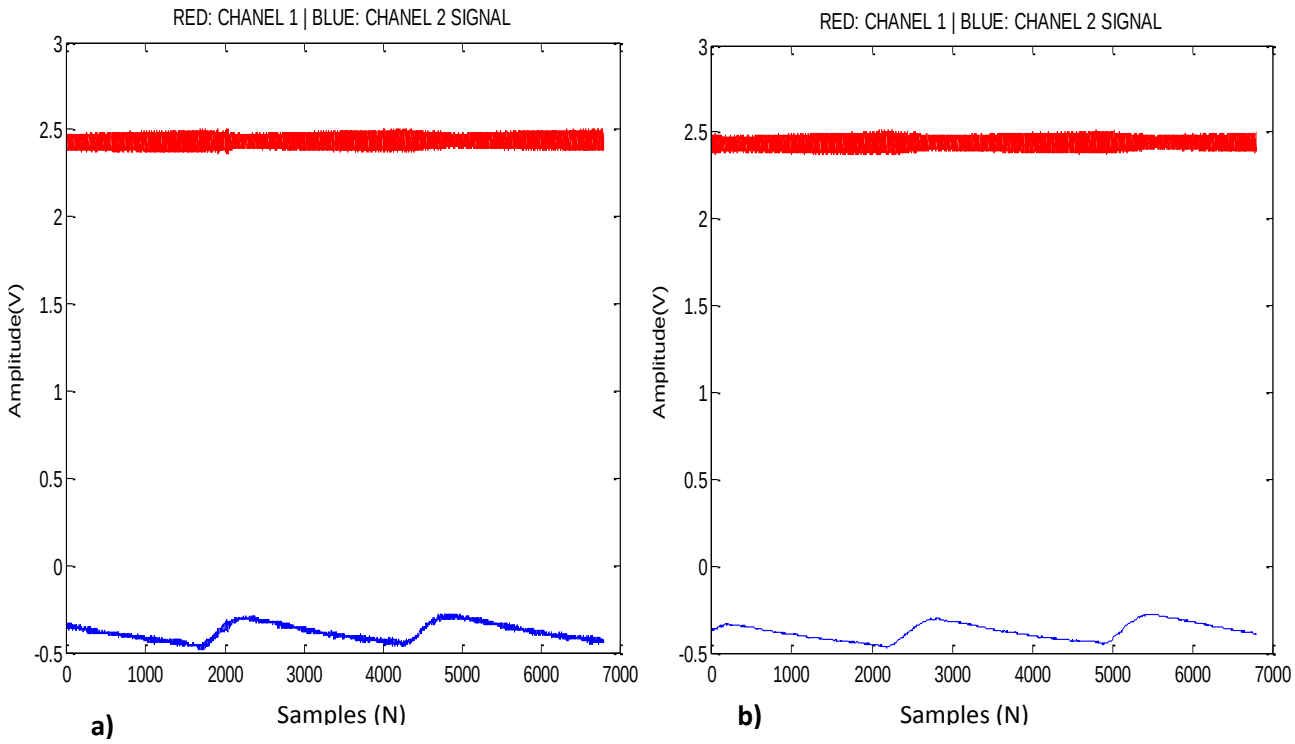

Figure 6.12: Modulated and negative demodulated signals. Image a) presents the original version of the negative demodulated signal where is possible to see the noise that is associated to it. Contrarily, on image b) the negative demodulated signal is filtered.

Based on the previous images, it is possible to conclude favorably towards the efficiency of the developed acquisition box and the best version of the test bench system in the simulation of the arterial system dynamic.

Chapter 7

Conclusion

Contents

7.1 Conclusion

The main objective of this project was to develop a functional instrumental method, based on concepts such as piezoelectricity, accelerometry, modulation and demodulation in order to assess APW and measure ABP.

To enable experimental tests, two different test bench systems were developed to simulate the cardiovascular system, namely carotid artery dynamics. The first test bench system did not succeed since a significant noise was introduced and it was not capable of modulating the carrier wave in effective way (Figure 6.4). However, the second bench system was efficient, simulating perfectly ABP and leading to robust signals without noise.

The hemodynamic probe, composed by a PZ sensor and an accelerometer, was developed and combined with an envelope detector circuit. Considering the signals obtained in experimental tests (Figure 3.8), is possible to confirm its correct performance. As expected, the probe output is a sinusoidal signal with high frequency whose amplitude is modulated by the pressure variation inside the vessel. Similarly, the demodulator circuit detects the envelope of the modulated signal with efficiency, according to the results obtained in experimental test results (Figure 4.8 and Figure 4.12).

The acquisition and conversion of analog output signals into digital data was only possible thanks to the two acquisition systems developed during this project. The first bench system revealed to be efficient, according to result signals on figure 6.7. However, limitations such as large dimension waste of energy and high cost of the materials that integrate this first system exposed the necessity to improve it. The second acquisition system integrates a PCB with the demodulator circuit and a Digilent module. It is smaller, cheaper, more available and portable besides being efficient on acquiring, logging and converting the signals, as figures 6.8, 6.9, 6.10, 6.11 and 6.12 show.

Considering these facts, at the end we do succeed on detecting APW developing a very promising prototype for further ABP.

7.2 Future Work

Despite all the work done during this project, there are still many improvements to be done in order to achieve an efficient and robust instrument capable of accurately measuring ABP, analyzing and assessing APW. Future interventions should lie essentially on following aspects:

- Encapsulation of the hemodynamic probe;
- Hemodynamic probe interface;
- Development of robust algorithm;
- Clinical tests;
- Hardware improvements to discard computer usage.

Bibliographic References

[1] *Using Nontraditional Risk Factors to Estimate Risk for Coronary Heart Disease*. Annals of Internal Medicine. 151(7) (2009).

[2] Taylor, Robert B. – *Taylor's cardiovascular diseases: A Handbook.* [Online]. United States of America: Springer & Business Media, 2005. [Accessed on 29 10 2013]. ISBN: 978-0-387-27276-4.

[3] Figueiras, E. - *Doppler flowmetry: line imaging techniques.* University of Coimbra, 2007. Tese de Mestrado.

[4] World Health Organization. [Online] Available: http://www.who.int/cardiovascular_diseases/en/. [Accessed on 30 10 2013.]

[5] Demoduladores I-10: princípios básicos para AM e FM. [online]. Available: http://www.mspc.eng.br/eletrn/demod_110.shtml. [Accessed on 2 2 2014]

[6] Pereira, H. C. B. M. - *Cardioaccelerometry: the assessment of pulse wave velocity using accelerometers.* Coimbra: University of Coimbra, 2007. Tese de Mestrado.

[7] Pereira, H. C.B. M. - *Methods and Instrumentation for Non-Invasive Assessment of the cardiovascular condition.* Coimbra: University of Coimbra, 2014. PhD Thesis.

[8] Texas Heart Institute. [Online] 15 11 2013. http://www.texasheartinstitute.org/HIC/Anatomy/anatomy2.cfm

[9] Amplitude Modulation. Answers. [online] Available: http://www.answers.com/topic/amplitude-modulation. [Accessed on 2 2 2014]

[10] National Instruments. What is I/Q data? [Online] Available: http://www.ni.com/white-paper/4805/en/. [Accessed on 2 2 2014]

[11] Amplitude modulated Wave. [Online]. Available: http://en.wikipedia.org/wiki/File:Amplitude_Modulated_Wave-hm-64.svg. [Accessed on 3 2 2014]

[12] Demodulator. Tutor Vista. [Online] Available: http://www.tutorvista.com/content/physics/physics-iv/communication-systems/demodulation.php. [Accessed on 5 3 2014]

[13] DEMODULAÇÃO AM e FM. [Online]. Available: http://www.decom.fee.unicamp.br/~candido/resources/EXP5-EE882-2S2012.pdf. [Accessed on 3 3 2014].

[14] Coração. Sistema Vascular. [Online]. Available: http://www.auladeanatomia.com/cardiovascular/coracao.htm. [Accessed on 5 3 2014]

[15] Inner Body, Cardiovascular System, Heart. [Online] Available: http://www.innerbody.com/image/card01.html#full-description. [Accessed on 25 11 2013]

[16] Cardiovascular System (Heart). [Online] Available: http://www.austincc.edu/apreview/PhysText/Cardiac.html [Accessed on 25 11 2013.]

[17] Hypertension. [Online] 25 11 2013). http://en.wikipedia.org/wiki/Hypertension

[18] Cardiovascular Disease. [Online]. Available: http://en.wikipedia.org/wiki/Cardiovascular_disease. [Accessed on 10 11 2013]

[19] Safar, M.E.; Frohlich, E. D. - *Arterial Stiffness: A Simplified Overview in Vascular Medicine*. Advances in cardiology. J.S. Borer. Vol. 44 (2007), p. 16.

[20] Piezo Theory. APC International. [Online]. Available: https://www.americanpiezo.com/knowledge-center/piezo-theory.html. [Accessed on 16 2 2014]

[21] Ferreira, E. S. B - *Assessment of hemodynamic parameters.* University of Coimbra, 2008. Tese de Mestrado.

[22] Almeida,V. M. G. A. - *Hemodynamic parameters assessment: an improvement of methodologies.* University of Coimbra, 2009. Tese de Mestrado.

[23] Accelerometers. Theory of Operation (ADXL family and others). [Online] Available: https://ccrma.stanford.edu/~gary/controllers/accelerometers.html. [Accessed on 15 1 2014]

[24] Cardiovascular Physiology Concepst. [Online] 8 11 2013 http://www.cvphysiology.com/Heart%20Disease/HD002.htm

[25] News Medical. "How is heart rate measured?" [Online] Available: http://www.news-medical.net/health/What-is-Heart-Rate.aspx. [Accessed on 2 12 2013]

[26] Pulse Wave analysis. [Online] Available: http://www.ncbi.nlm.nih.gov/pmc/articles/PMC2014492/. [Accessed on 8 3 2014]

[27] Safar, M.E.; Frohlich, E.D. - *Atherosclerosis, Large Arteries and Cardiovascular Risk.* Advance in Cardiology. New York: Jeffrey S. Borer. Vol. 44 (2007). p. 9-12.

[28] Elasticity (Physics). [Online] Available: http://en.wikipedia.org/wiki/Elasticity_ (physics). [Accessed on 15 12 2013].

[29] Laurent, S. [et al.]. - *Expert consensus document on arterial stiffness: methodological issues and clinical applications*. European Heart Journal. (2006), 2588-2605.

[30] Lopes, T. M. P. - *Methodologies for Hemodynamic Parameters Assessment.* University of Coimbra, 2007. Tese de Mestrado.

[31] Murgo JP. [et al.] - *Aortic input impedance in normal man: relationship to pressure wave forms*. Circulation. Vol. 62 (1980). p. 105-116.

[32] Resonance. [Online] Available: http://www.vinayakgarg.com/resonance/3 . [Accessed on 15 02 2014]

[33] O'Rourke, M. F.; Pauca, A.; Xiong-Jing, J. - *Pulse wave analysis.* British Journal of Clinical Pharmacology. 51(6) (2001): 507-522.

[34] Walker, R.D. [et al.]. - *Latex vessels with customized compliance for use in arterial flow models*. Physiol Meas. Vol. 20 (1999), p. 277-286.

[35] Feng, J.; Khir, A.W. - *Determination of wave intensity in flexible tubes using measured diameter and velocity.* Proceedings of the 29th Annual International, Conference of the IEEE EMB (2007). p. 985-988.

[36] Feng J and Khir AW. - *Determination of wave intensity in flexible tubes using measured diameter and velocity*. Proceedings of the 29th Annual International, Conference of the IEEE EMB. p. 210-215.

[37] Perloff, M.D. [et al] - *Human blood pressure determination by sphygmomanometry*. Circulation. Vol. 88 (1993), p. 2460-2470.

[38] McCutcheon, E.P.; Rushmer, R.F. - *Korotkoff sounds: an experimental critique.* Circulation Research. 20(2) (1967): 149-161.

[39] Kirkendall, W.M.; Burton, A.C.; Epstein, F.H.; FREIS, E. D. - *Recommendations for human blood pressure determination by sphygmomanometers*. Circulation. Vol. 36 (1967). p. 980-988.

[40] Askey, J.M. - *The auscultatory gap in sphygmomanometry*. Ann Intern Med. 80(1) (1974): 94-97.

[41] O'Brien, E. [et al]. - *The British Hypertension Society protocol for the evaluation ofautomated and semi-automated blood pressure measuring devices with special reference to ambulatory systems*. JHypertens. 8(7) (1990): 607-19.

[42] *An epidemiological approach to describing risk associated with blood pressure levels: final report of the Working Group on Risk and High Blood Pressure*. Hypertension. 7(4) (1985): 641-651.

[43] Stamler, J.; Neaton, J.D.; Wentworth, D.N. - *Blood pressure (systolic and diastolic) and risk of fatal coronary heart disease*. Hypertension. 13(5) (1989): 2-12.

[44] *The fifth report of the Joint National Committee on Detection, Evaluation, and Treatment of High Blood Pressure (JNCW).* [s. l.]: Arch Intern Med. 153(2) (1993): 154-83.

[45] Pickering G. - *Normotension and hypertension: the mysterious viability of the false.* AMERICAN JOURNAL OF MEDICINE. 65(4) (1978): 561-563.

[46] Nichols WW and O'Rourke MF, McDonald's Blood Flow in Arteries: Theoretical, Experimental and Clinical Principles. 5 th ed. London: Hodder Arnold, 2005.

[47] Digilent. Analog Discovery USB Oscilloscope. [Online]. Available: http://www.digilentinc.com/data/products/analog-discovery/AnalogDiscovery.pdf. [Accessed on 4 3 2014]

[48] Digilent. [Online]. Available: http://www.digilentinc.com/Products/Detail.cfm?NavPath=2,842,1018&Prod=ANALOG-DISCOVERY. [Accessed on 8 3 2014].

[49] Analog Discovery. KAMAMI Development tools. [Online]. Available: http://www.kamami.pl/index.php?productID=196455. [Accessed on 8 3 2014].

[50] Multiplexador. [Online] Available: http://pt.wikipedia.org/wiki/Multiplexador. [Accessed on 5 4 2014].

[51] Multiplexing. [Online] Available: http://en.wikipedia.org/wiki/Multiplexing. [Accessed on 5 04 2014].

[52] The demultiplexer. Electronics Tutorial. [Online] Available: http://www.electronics-tutorials.ws/combination/comb_2.html. [Accessed on 12 4 2014].

[53] World Health Organization. [Online] 30 10 2013. http://www.who.int/mediacentre/factsheets/fs317/en/index.html

[54] Impedance plethysmography. [Online] Available: http://www.medis-de.com/en/ipg.html. [Accessed on 30 10 2013.]

[55] Van De Graaff, K.M. - *Human Anatomy.* Miamisburg: Mc Graw Hill Science/Engineering/Math, 2001. p. 840. ISBN: 9780072486650

[56] Burkhoff, D. - *Mechanical properties of heart and its interation with vascular system*. Cardiac physiology, Columbia University, 2002.

[57] O'Rourke, M. F.; Pauca, A.; Jiang, X. - *Pulse Wave Analysis.* St Vincent's Clinic, Sydney, Winston-Salem and 3Fu Wai Hospital, Beijing (China), Blackwell Science Ltd, March 2001

[58] Pereira, H. C.; Correia, C. M.; Cardoso, J. M. and Falcão, M. Apparatus and Method for Non-Invasive Pressure Measurement of a Fluid Confi ned in a Vessel with Elastic Walls or Rigid Walls Fitted with an Elastic Window. Provisional Patent Application, nº 106504. 2012.

[59] Anderson, R. H.; Razavi, R.; Taylor, A. M. - *Cardiac anatomy revisited.* Journal of Anatomy. 205(3) (2004): 159–177.

[60] Nabel, E. G. M. D. - *Cardiovascular Disease.* The NEW ENGLAND JOURNAL of MEDICINE. New England: Alan E. Guttmacher, M.D., and Francis S. Collins, M.D., Ph.D., Editors. DOI: 10.1056/NEJMra035098 . N.º 349:60-72 (July 2003).

[61] Laurent, S. [et al]. *Expert consensus document on arterial stiffness: methodological issues and clinical applications*. European Heart Journal. 27(21) (2006): 2588-2605.

[62] Safar, M.E.; Frohlich, E.D. - *Atherosclerosis, Large Arteries and Cardiovascular Risk.* Advance in Cardiology. Vol. 44 (2007). p. 234–244.

[63] Safar ME, Frohlich ED (eds): *Atherosclerosis, Large Arteries and Cardiovascular Risk*. Adv Cardiol. Basel, Karger, 2007, vol. 44, p. 212–222.

[64] Safar ME, Frohlich ED (eds): *Atherosclerosis, Large Arteries and Cardiovascular Risk*. Adv Cardiol. Basel, Karger, 2007, vol. 44, p. 140-142.

[65] Pereira, H. - "Acelerómetros". Monography, *Sensores e Sinais Biomédicos discipline*, University of Coimbra, January 2006 (tese de mestrado).

[66] Webster, J. G. - Measurement, Instrumentation and Sensors Handbook CRCnetBASE. 1 st ed. New York: CRC Press LLC, 1999, p. 454-481.

[67] Piezoelectric sensors. [Online] Available: http://ccrma.stanford.edu/CCRMA/Courses/252/sensors/node7.html. [Accessed on 25 01 2014].

[68] Vânia Patrícia Silva Relvas. Hemodynamic parameters assessment: characterization of a new piezoelectric probe. Master's degree dissertation in Biomedical Engineering, University of Coimbra, 2011.

[69] H. C. Pereira, J. Maldonado, T. Pereira, M. Contente, V. Almeida, T. Pereira, J. B. Simoes, J. Cardoso, and C. Correia. A novel and low cost acoustic based probe for local pulse wave velocity estimation - experimental characterization and in-vivo feasibility. In BIODEVICES, pages 78 88, Barcelona, Spain, 2013. SciTePress.

[70] H. C. Pereira, T. Pereira, V. Almeida, E. Borges, E. Figueiras, J. B. Simoes, J. L. Malaquias, J. M. Cardoso, and C. M. Correia. Characterization of a double probe for local pulse wave velocity assessment. Physiol Meas, 31(11):1449 65, 2010.

Appendix

Contents

Appendix A- Circuits Schematics

a) Demodulator Circuit

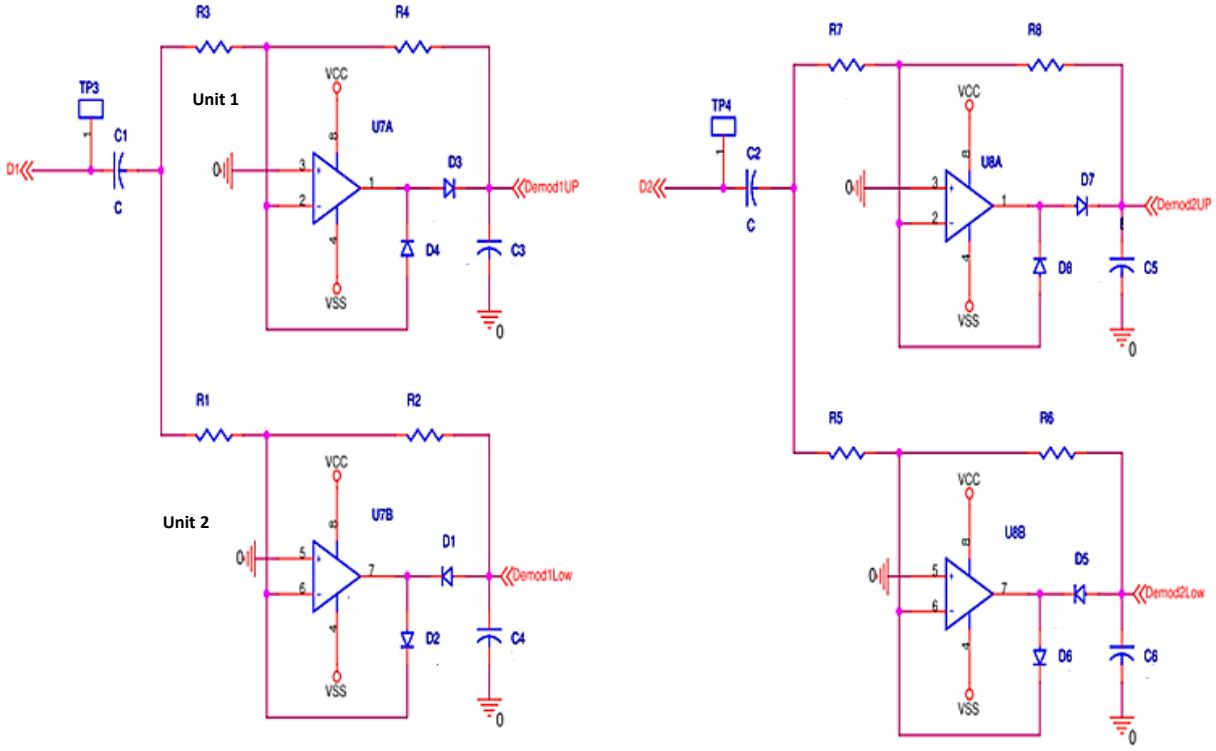

b) Power Source

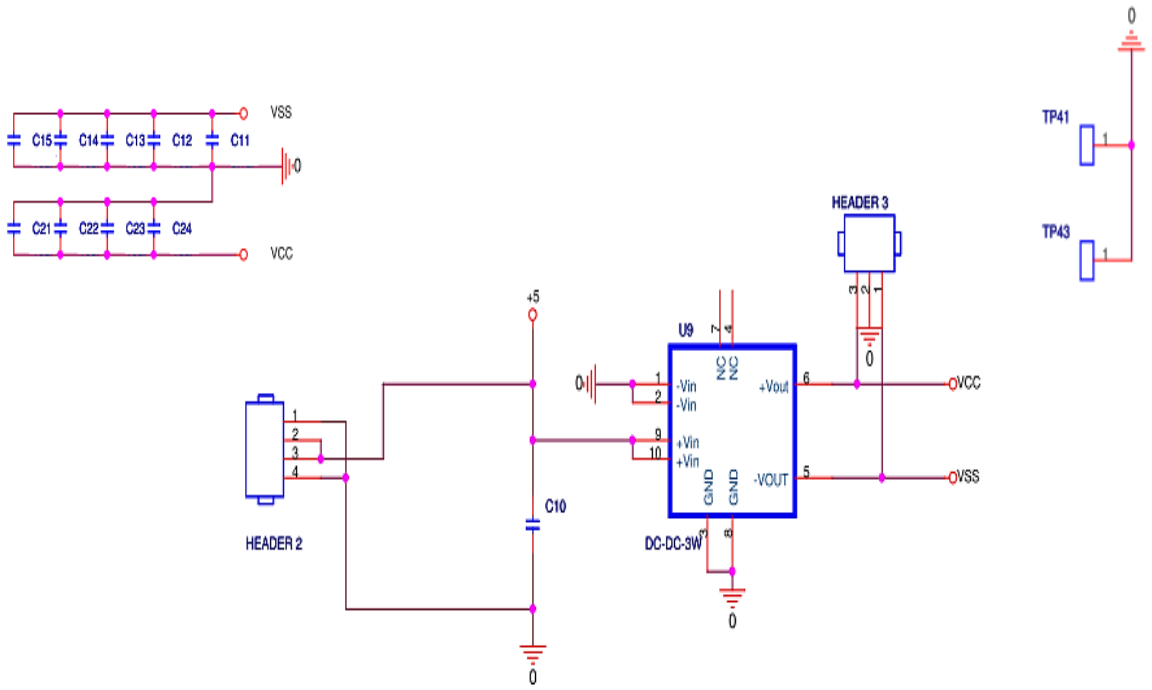

c) Envelope detector Printed circuit board (2^{nd} Acquisition system version)

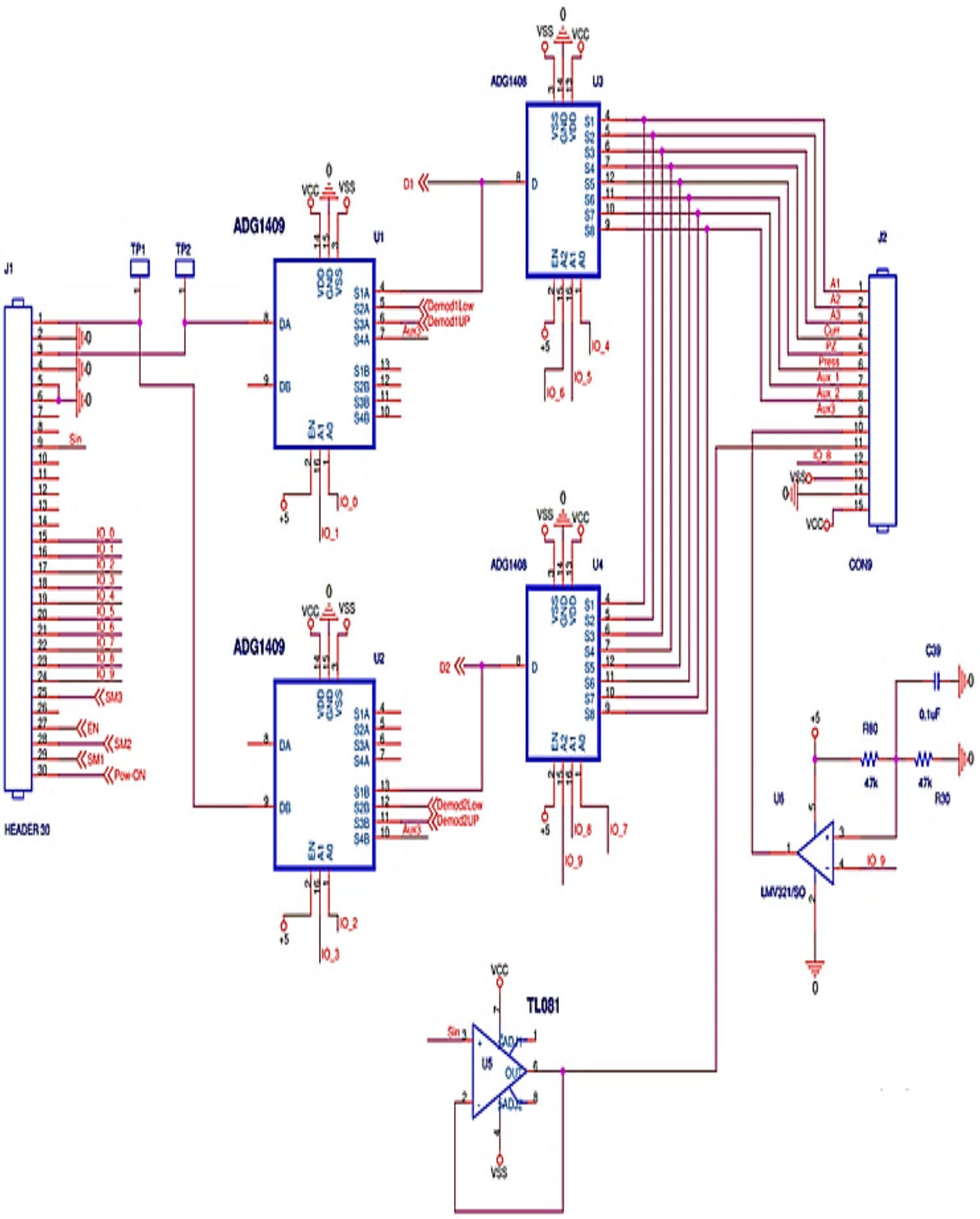

Appendix B- Specifications of DC Motor RS

BRUSHLESS range from CROUZET

1 - Composition

This new product range is based on the 3-phase motor with **internal rotor**. The high-energy plasto-ferrite magnet is completely integral with the motor shaft. The chosen structure gives high dynamic performance : made possible by the low inertia of the rotor (unlike motors with external rotors, which have high inertia) .
The stator lamination stack acts as a heat dissipator for energy losses induced by the winding.

■ **Motor principle :**

With internal rotor,

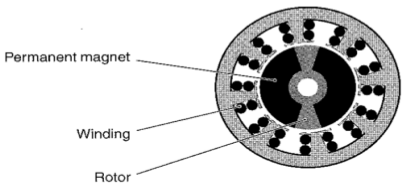

Both zamac flanges mounted on the stator lamination stack are fitted with a ball bearing, ensuring the motor will have a long service life.

■ **Composition :**

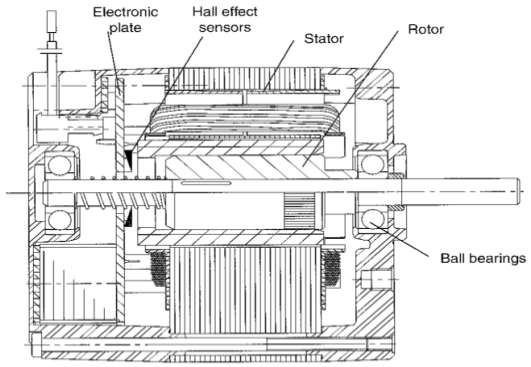

The electronics required for operation are completely integrated in the motor.

2 - Operating principle

The chosen architecture is based on a "3-phase" motor, with a 4-pole rotor.

■ **Sequencing :** the "3-phase" motor is wired as "delta".
Three hall effect sensors are used to locate the position of the rotor.

The transistors conduct up to 120°

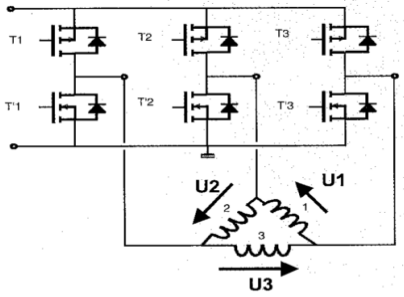

Communication logic

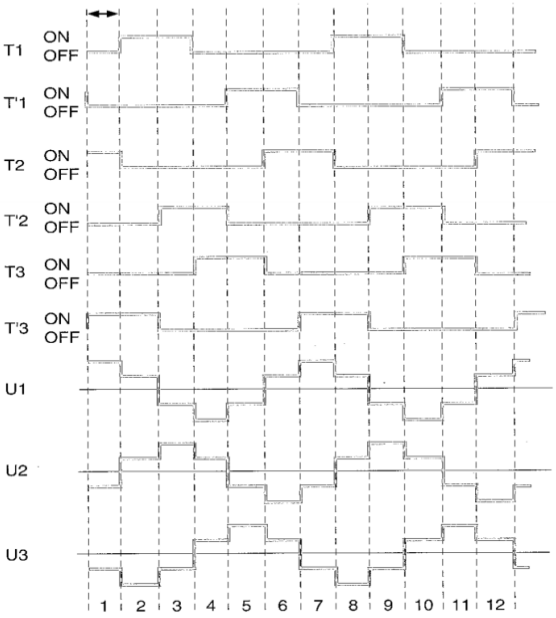

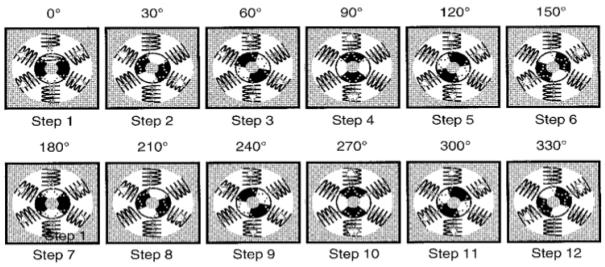

■ **Resulting torque form**

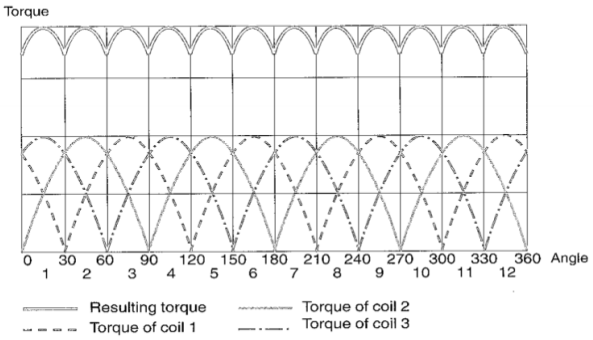

The "3-phase" motor provides the best possible compromise in terms of regularity of the resulting torque (low ripple percentage). As the electronics are completely integrated, all the sequencing is performed by the electronics inside the motor.

3 - Functions and inputs/outputs

The speed of the motors offered with integrated electronics can be controlled : by an analogue (0 - 10 volts), or digital (PWM : 15 kHz) speed signal.

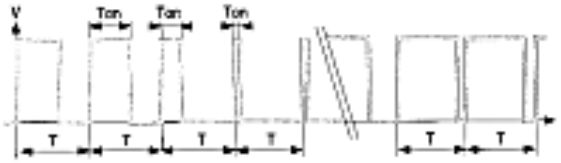

■ Definition of PWM

T is constant, but Ton varies ; the Ton/T ratio is the cyclical ratio (as a %).
In this case, PWM is a control signal, converted by the electronics to set the speed.

- If the cyclical ratio is 0%, the speed is 0 rpm.
- If the cyclical ratio is 100%, the speed is N0 (no-load speed).
- If the cyclical ratio is 50%, the speed is N0/2 (half the no-load speed).

The voltage V is not significant (between 5 and 28 V), and does not affect the speed.
The PWM input is a digital input : it can be used by PLCs and micro-controllers.

■ Motor protection :

The motors are completely protected during operation : by current limiting and thermal protection. During abnormal operation, in a machine or device : for example locking, the motor stops after approximately 3 seconds, (power stage off) and must be reinitialised via the On/Off input : **this is a failsafe system.**

■ Inputs / Outputs :

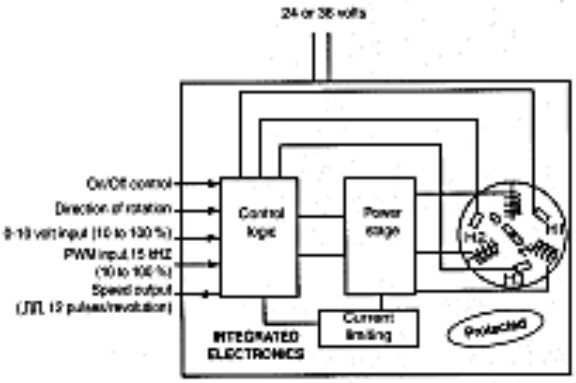

■ Truth table for Inputs / Outputs :

On/Off	PWM	0-10 V	Direction	
0	x	x	x	motors off
1	1	0	0	reverse rotation
1	0	1	0	reverse rotation
1	1	1	0	unauthorised configuration
1	0	0	x	motors stopped
1	1	0	1	clockwise rotation
1	0	1	1	clockwise rotation
1	1	1	1	unauthorised configuration

X= don't care 1=Vit 0=Vil

■ Speed regulation :

Two types of product with integrated electronics are offered for the whole range, both motors and geared motors.

a) No speed regulation : this option is offered for users who do not need to regulate speed in a closed loop, or who wish to reuse their own regulation electronics on an external card, to limit modifications to the architecture of their machine.

Motors without integrated speed regulation : no data feedback on action taken.

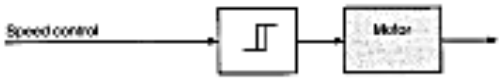

b) With integrated speed regulation (eg : Part no. 80 030 003) see page 10.
This integrated option can be used simply for a speed regulation function suitable for most applications. In effect : there is no longer any need to wire a motor to a card, no electromagnetic compatibility problems linked to wiring, hence reduced net cost!

Motor with integrated speed loop :
Hall effect sensors monitor the action taken, enabling the electronics to modify the command to achieve the desired effect.

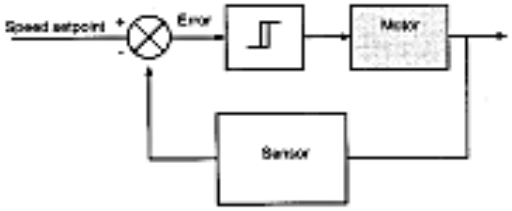

4- Safety

Crouzet BRUSHLESS DC motors are designed and manufactured to be integrated into devices or machines which meet, for example, the specifications of the machine standard : EN 60335-1 (IEC 335-1, "Safety of domestic electrical appliances").
The integration of Crouzet DC motors into devices or machines, should generally take account of the following motor characteristics :

- no earth connection
- "main isolation" motors (simple isolation)
- protection index : IP40
- isolation system class : B (120°C)

European low voltage directive 73/23/EEC of 19/02/73 :

CROUZET DC motors and geared motors are outside the field of application of this directive (LVD 73/23/EEC applies to voltages over 75 volts DC).

5 - Electromagnetic Compatibility (EMC) :

On request, Crouzet will provide the EMC characteristics of the various types of product.

European directive 89/336/EEC of 03/05/89, "electromagnetic compatibility" :

DC motors and geared motors which are components designed for professionals, to be incorporated in more complex devices, and not for end users, are excluded from the field of application of this directive.

However, conscious of potential customer difficulties concerning problems linked to electromagnetic compatibility, Crouzet has designed its products to meet the requirements of the standards : for example EN 55011 Gr. 1 class B (medical) as well as EN 55022, class B (data processing) in terms of emitted electromagnetic interference, as well as standards linked to immunity : IEC 1000- 4 -2/3/4/5/6/8.

■ Wiring precautions

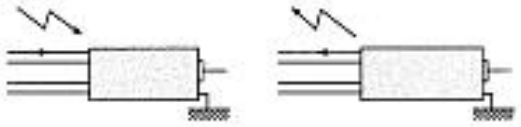

For EMC conformity :
- The motor must be connected to earth via its front flange.
- The length of the wires is 20 cm.

6- Electrical characteristics

	Symbol	Conditions Ta = -10 to 40 °C	Min.	Nominal	Max.	Units
Power supply						
Supply voltage	Vmot	Version 1	10.8	24	28	V
		Version 2	32.4	36	39.6	V
Direction, on/off inputs						
Logic level 1	Vih		3		Vmot	V
Logic level 0	Vil		-1		1.7	V
Current for logic level 1	Iih				0.5	mA
Current for logic level 0	Iil				0.05	mA
0-10 V input						
Voltage	Vma		-1		Vmot	V
Input impedance	Za			10		kΩ
PWM (Pulse width modulation) input						
Logic level 1	Vih		3		28	V
Logic level 0	Vil		-1		1.7	V
Current for logic level 1	Iih				0.5	mA
Current for logic level 0	Iil				0.05	mA
PWM input frequency	Fin		13	15	17	kHz
Encoder output						
Voltage for level 0	Vol	Vih = 5 V, R pull up = 1.2 kΩ			0.4	V
Voltage for level 1	Voh				35	V
Current for level 0	Iol				5	mA
Current for level 1	Ioh				0.8	mA
Width of low level	Wle			320		µs
Current limiting						
Limit value	Imax	Ta = 20 °C, electronics at ambient 20 °C			3	A
Derating	Idt			-23		mA/°C

Connection diagrams

General precautions : see pages 1/53, 1/54, 1/58.
Connector labelling : see page 1/58.

■ *Adjusting the speed using a potentiometer : using the 0-10 V input*

This type of connection only requires a power supply (24 or 36 V, 3 A).
Point 3 should not be connected.
This diagram can be further simplified by connecting input 7 directly to the power supply positive and input 6 to either the positive or the negative of the power supply, depending on the desired direction of rotation.

Comment : If a maximum fixed speed is desired, the potentiometer can be omitted and input 4 connected to the power supply positive.

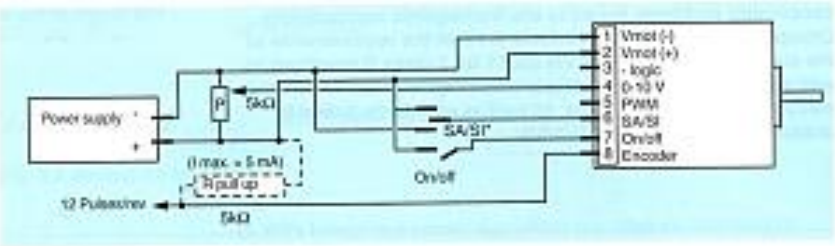

■ *Using the 0-10 V input, with separate power supply*

This type of connection requires a power supply (24 or 36 V, 3 A) and an adjustable 0-10 V power supply.

Comment : Inputs 6 and 7 can also be connected to the TTL signals.

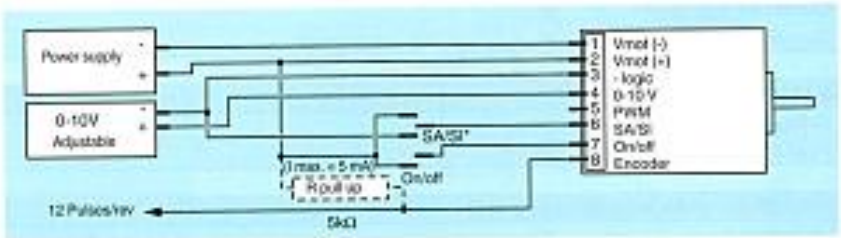

■ *Using the PWM input, with TTL commands from a microcontroller*

This type of connection requires a power supply (24 or 36 V, 3 A).
With the aid of the machine microcontroller or the device being used, the customer can generate command signals : inputs and PWM, and use the motor encoder output signal.

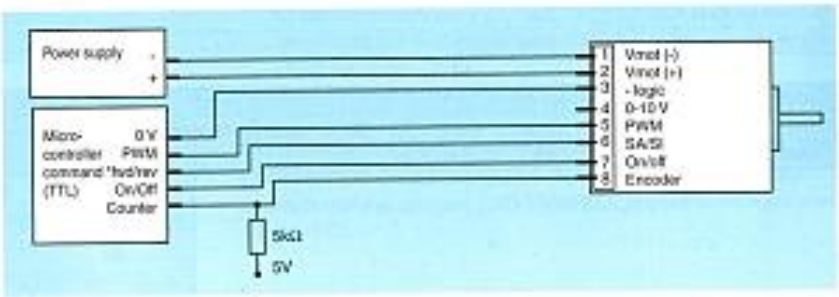

* Do not change the direction of rotation without first stopping the motor, to avoid the risk of permanent damage.

Appendix C- Specifications of ADXL 103/203

ANALOG DEVICES

Precision ±1.7 *g*, ±5 *g*, ±18 *g* Single-/ Dual-Axis *i*MEMS® Accelerometer

Data Sheet **ADXL103/ADXL203**

FEATURES

- High performance, single-/dual-axis accelerometer on a single IC chip
- 5 mm × 5 mm × 2 mm LCC package
- 1 m*g* resolution at 60 Hz
- Low power: 700 µA at V_S = 5 V (typical)
- High zero *g* bias stability
- High sensitivity accuracy
- −40°C to +125°C temperature range
- X and Y axes aligned to within 0.1° (typical)
- Bandwidth adjustment with a single capacitor
- Single-supply operation
- 3500 *g* shock survival
- RoHS compliant
- Compatible with Sn/Pb- and Pb-free solder processes
- Qualified for automotive applications

APPLICATIONS

- Vehicle dynamic controls
- Electronic chassis controls
- Platform stabilization/leveling
- Navigation
- Alarms and motion detectors
- High accuracy, 2-axis tilt sensing
- Vibration monitoring and compensation
- Abuse event detection

GENERAL DESCRIPTION

The ADXL103/ADXL203 are high precision, low power, complete single- and dual-axis accelerometers with signal conditioned voltage outputs, all on a single, monolithic IC. The ADXL103/ADXL203 measure acceleration with a full-scale range of ±1.7 *g*, ±5 *g*, or ±18 *g*. The ADXL103/ADXL203 can measure both dynamic acceleration (for example, vibration) and static acceleration (for example, gravity).

The typical noise floor is 110 µg/√Hz, allowing signals below 1 mg (0.06° of inclination) to be resolved in tilt sensing applications using narrow bandwidths (<60 Hz).

The user selects the bandwidth of the accelerometer using Capacitor C_X and Capacitor C_Y at the X_{OUT} and Y_{OUT} pins. Bandwidths of 0.5 Hz to 2.5 kHz can be selected to suit the application.

The ADXL103 and ADXL203 are available in a 5 mm × 5 mm × 2 mm, 8-terminal ceramic LCC package.

FUNCTIONAL BLOCK DIAGRAMS

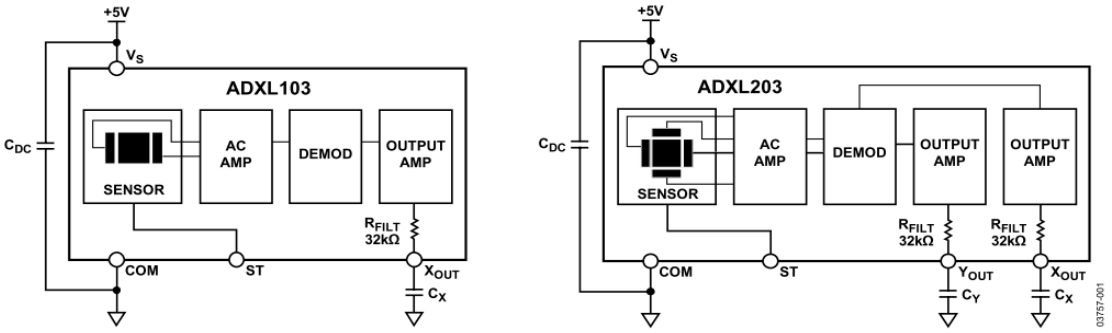

Figure 1.

Rev. E Document Feedback

One Technology Way, P.O. Box 9106, Norwood, MA 02062-9106, U.S.A.
Tel: 781.329.4700
Technical Support www.analog.com

SPECIFICATIONS

T_A = −40°C to +125°C, V_S = 5 V, C_X = C_Y = 0.1 µF, acceleration = 0 *g*, unless otherwise noted. All minimum and maximum specifications are guaranteed. All typical specifications are not guaranteed.

Table 1.

		ADXL103/ADXL203			AD22293			AD22035/AD22037			
Parameter	**Test Conditions**	**Min**	**Typ**	**Max**	**Min**	**Typ**	**Max**	**Min**	**Typ**	**Max**	**Unit**
SENSOR	Each axis										
Measurement Range[1]		±1.7			±5	±6		±18			*g*
Nonlinearity	% of full scale		±0.2	±1.25		±0.2	±1.25		±0.2	±1.25	%
Package Alignment Error			±1			±1			±1		Degrees
Alignment Error (ADXL203)	X to Y sensor		±0.1			±0.1			±0.1		Degrees
Cross-Axis Sensitivity			±1.5	±3		±1.5	±3		±1.5	±3	%
SENSITIVITY (RATIOMETRIC)[2]	Each axis										
Sensitivity at X_{OUT}, Y_{OUT}	V_S = 5 V	960	1000	1040	293	312	331	94	100	106	mV/*g*
Sensitivity Change Due to Temperature[3]	V_S = 5 V		±0.3			±0.3			±0.3		%
ZERO *g* BIAS LEVEL (RATIOMETRIC)	Each axis										
0 *g* Voltage at X_{OUT}, Y_{OUT}	V_S = 5 V	2.4	2.5	2.6	2.4	2.5	2.6	2.4	2.5	2.6	V
Initial 0 *g* Output Deviation From Ideal	V_S = 5 V, 25°C		±25			±50			±125		m*g*
0 *g* Offset vs. Temperature			±0.1	±0.8		±0.3	±1.8		±1		m*g*/°C
NOISE											
Output Noise	<4 kHz, V_S = 5 V		1	3		1	3			2	mV rms
Noise Density			110			200			130		µ*g*/√Hz rms
FREQUENCY RESPONSE[4]											
C_X, C_Y Range[5]		0.002		10	0.002		10	0.002		10	µF
R_{FILT} Tolerance		24	32	40	24	32	40	24	32	40	kΩ
Sensor Resonant Frequency			5.5			5.5			5.5		kHz
SELF TEST[6]											
Logic Input Low				1			1			1	V
Logic Input High		4			4			4			V
ST Input Resistance to GND		30	50		30	50		30	50		kΩ
Output Change at X_{OUT}, Y_{OUT}	ST 0 to ST 1	450	750	1100	125	250	375	60	80	100	mV
OUTPUT AMPLIFIER											
Output Swing Low	No load	0.05	0.2		0.05	0.2		0.05	0.2		V
Output Swing High	No load		4.5	4.8		4.5	4.8		4.5	4.8	V
POWER SUPPLY (V_{DD})											
Operating Voltage Range		3		6	3		6	3		6	V
Quiescent Supply Current			0.7	1.1		0.7	1.1		0.7	1.1	mA
Turn-On Time[7]			20			20			20		ms

[1] Guaranteed by measurement of initial offset and sensitivity.
[2] Sensitivity is essentially ratiometric to V_S. For V_S = 4.75 V to 5.25 V, sensitivity is 186 mV/V/*g* to 215 mV/V/*g*.
[3] Defined as the output change from ambient-to-maximum temperature or ambient-to-minimum temperature.
[4] Actual frequency response controlled by user-supplied external capacitor (C_X, C_Y).
[5] Bandwidth = 1/(2 × π × 32 kΩ × C). For C_X, C_Y = 0.002 µF, bandwidth = 2500 Hz. For C_X, C_Y = 10 µF, bandwidth = 0.5 Hz. Minimum/maximum values are not tested.
[6] Self-test response changes cubically with V_S.
[7] Larger values of C_X, C_Y increase turn-on time. Turn-on time is approximately 160 × C_X or C_Y + 4 ms, where C_X, C_Y are in µF.

ABSOLUTE MAXIMUM RATINGS

Table 2.

Parameter	Rating
Acceleration (Any Axis, Unpowered)	3500 *g*
Acceleration (Any Axis, Powered)	3500 *g*
Drop Test (Concrete Surface)	1.2 m
V_S	−0.3 V to +7.0 V
All Other Pins	(COM − 0.3 V) to (V_S + 0.3 V)
Output Short-Circuit Duration (Any Pin to Common)	Indefinite
Temperature Range (Powered)	−55°C to +125°C
Temperature Range (Storage)	−65°C to +150°C

Stresses above those listed under Absolute Maximum Ratings may cause permanent damage to the device. This is a stress rating only; functional operation of the device at these or any other conditions above those indicated in the operational section of this specification is not implied. Exposure to absolute maximum rating conditions for extended periods may affect device reliability.

Table 3. Package Characteristics

Package Type	θ_{JA}	θ_{JC}	Device Weight
8-Terminal Ceramic LCC	120°C/W	20°C/W	<1.0 gram

ESD CAUTION

ESD (electrostatic discharge) sensitive device. Charged devices and circuit boards can discharge without detection. Although this product features patented or proprietary protection circuitry, damage may occur on devices subjected to high energy ESD. Therefore, proper ESD precautions should be taken to avoid performance degradation or loss of functionality.

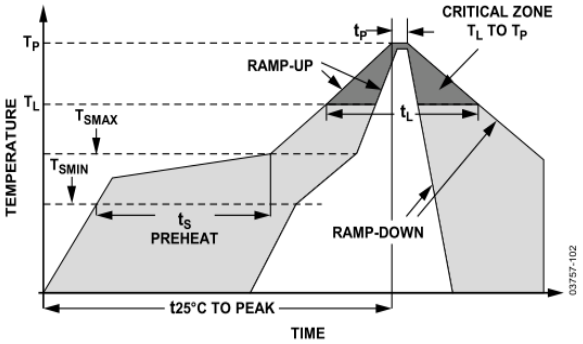

Figure 2. Recommended Soldering Profile

Table 4. Solder Profile Parameters

	Test Condition	
Profile Feature	**Sn63/Pb37**	**Pb-Free**
Average Ramp Rate (T_L to T_P)	3°C/second maximum	3°C/second maximum
Preheat		
Minimum Temperature (T_{SMIN})	100°C	150°C
Maximum Temperature (T_{SMAX})	150°C	200°C
Time (T_{SMIN} to T_{SMAX}) (t_S)	60 seconds to 120 seconds	60 seconds to 150 seconds
T_{SMAX} to T_L		
Ramp-Up Rate	3°C/second	3°C/second
Time Maintained above Liquidous (T_L)		
Liquidous Temperature (T_L)	183°C	217°C
Time (t_L)	60 seconds to 150 seconds	60 seconds to 150 seconds
Peak Temperature (T_P)	240°C + 0°C/−5°C	260°C + 0°C/−5°C
Time Within 5°C of Actual Peak Temperature (t_P)	10 seconds to 30 seconds	20 seconds to 40 seconds
Ramp-Down Rate	6°C/second maximum	6°C/second maximum
Time 25°C to Peak Temperature	6 minutes maximum	8 minutes maximum

PIN CONFIGURATIONS AND FUNCTION DESCRIPTIONS

ADXL103
TOP VIEW
(Not to Scale)

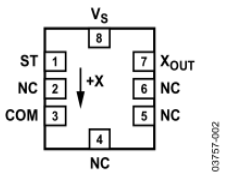

NOTES
1. NC = NO CONNECT. DO NOT CONNECT TO THIS PIN.

Figure 3. ADXL103 Pin Configuration

ADXL203
TOP VIEW
(Not to Scale)

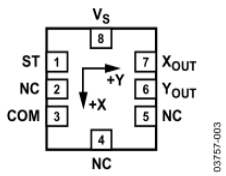

NOTES
1. NC = NO CONNECT. DO NOT CONNECT TO THIS PIN.

Figure 4. ADXL203 Pin Configuration

Table 5. ADXL103 Pin Function Descriptions

Pin No.	Mnemonic	Description
1	ST	Self Test
2	NC	Do Not Connect
3	COM	Common
4	NC	Do Not Connect
5	NC	Do Not Connect
6	NC	Do Not Connect
7	X_{OUT}	X Channel Output
8	V_S	3 V to 6 V

Table 6. ADXL203 Pin Function Descriptions

Pin No.	Mnemonic	Description
1	ST	Self Test
2	NC	Do Not Connect
3	COM	Common
4	NC	Do Not Connect
5	NC	Do Not Connect
6	Y_{OUT}	Y Channel Output
7	X_{OUT}	X Channel Output
8	V_S	3 V to 6 V

Appendix D- Specifications of PZ sensor

⚠Note • Please read rating and ⚠CAUTION (for storage, operating, rating, soldering, mounting and handling) in this catalog to prevent smoking and/or burning, etc.
• This catalog has only typical specifications. Therefore, please approve our product specifications or transact the approval sheet for product specifications before ordering.

Piezoelectric Sound Components

Piezoelectric Diaphragms

■ Features
1. Clear sound
2. Ultra thin and lightweight
3. No contacts; therefore, noiseless and highly reliable
4. Low power consumption for voltage type

■ Applications
Clocks/Calculators/Digital camera/Various alarms
(Burglar alarms, etc.)

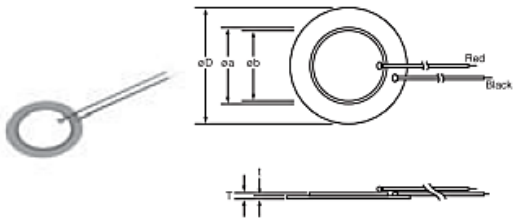

External Drive Type

Part Number	Resonant Frequency (kHz)	Resonant Impedance (ohm)	Capacitance (nF)	Plate Size dia. D (mm)	Element Size dia. a (mm)	Electrode Size dia. b (mm)	Thickness T (mm)	Plate Thickness t (mm)	Plate Material
7BB-12-9	9.0 ±1.0kHz	1000 max.	8.0 ±30% [1kHz]	12.0	9.0	8.0	0.22	0.10	Brass
7BB-15-6	6.0 ±1.0kHz	800 max.	10.0 ±30% [1kHz]	15.0	10.0	9.0	0.22	0.10	Brass
7BB-20-3	3.6 ±0.6kHz	500 max.	20.0 ±30% [1kHz]	20.0	14.0	12.8	0.22	0.10	Brass
7BB-20-6	6.3 ±0.6kHz	350 max.	10.0 ±30% [1kHz]	20.0	14.0	12.8	0.42	0.20	Brass
7BB-20-6L0	6.3 ±0.6kHz	1000 max.	10.0 ±30% [1kHz]	20.0	14.0	12.8	0.42	0.20	Brass (with Lead Wire: AWG32 Length 50mm)
7BB-27-4	4.6 ±0.5kHz	200 max.	20.0 ±30% [1kHz]	27.0	19.7	18.2	0.54	0.30	Brass
7BB-27-4L0	4.6 ±0.5kHz	300 max.	20.0 ±30% [1kHz]	27.0	19.7	18.2	0.54	0.30	Brass (with Lead Wire: AWG32 Length 50mm)
7BB-35-3	2.8 ±0.5kHz	200 max.	30.0 ±30% [1kHz]	35.0	25.0	23.0	0.53	0.30	Brass
7BB-35-3L0	2.8 ±0.5kHz	200 max.	30.0 ±30% [1kHz]	35.0	25.0	23.0	0.53	0.30	Brass (with Lead Wire: AWG32 Length 50mm)
7BB-41-2	2.2 ±0.3kHz	250 max.	30.0 ±30% [1kHz]	41.0	25.0	23.0	0.63	0.40	Brass
7BB-41-2L0	2.2 ±0.3kHz	300 max.	30.0 ±30% [1kHz]	41.0	25.0	23.0	0.63	0.40	Brass (with Lead Wire: AWG32 Length 50mm)
7NB-31R2-1	1.3 ±0.5kHz	300 max.	40.0 ±30% [120Hz]	31.2	19.7	18.2	0.22	0.10	Nickel Alloy

⚠Note • Please read rating and ⚠CAUTION (for storage, operating, rating, soldering, mounting and handling) in this catalog to prevent smoking and/or burning, etc.
• This catalog has only typical specifications. Therefore, please approve our product specifications or transact the approval sheet for product specifications before ordering.

1

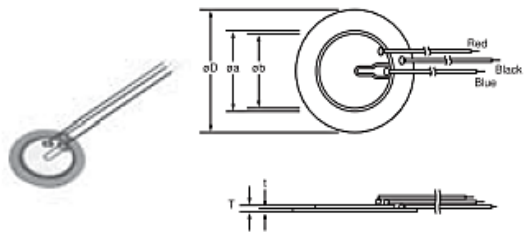

Self Drive Type

Part Number	Resonant Frequency (kHz)	Resonant Impedance (ohm)	Capacitance (nF)	Plate Size dia. D (mm)	Element Size dia. a (mm)	Electrode Size dia. b (mm)	Thickness T (mm)	Plate Thickness t (mm)	Plate Material
7BB-20-6C	6.3 ±0.6kHz	500 max.	8.5 ±30% [1kHz]	20.0	14.0	12.8	0.42	0.20	Brass
7BB-20-6CL0	6.3 ±0.6kHz	800 max.	8.5 ±30% [1kHz]	20.0	14.0	12.8	0.42	0.20	Brass (with Lead Wire: AWG32 Length 50mm)
7BB-27-4C	4.6 ±0.5kHz	200 max.	18.0 ±30% [1kHz]	27.0	19.7	18.2	0.54	0.30	Brass
7BB-27-4CL0	4.6 ±0.5kHz	350 max.	18.0 ±30% [1kHz]	27.0	19.7	18.2	0.54	0.30	Brass (with Lead Wire: AWG32 Length 50mm)
7BB-35-3C	2.8 ±0.5kHz	200 max.	26.0 ±30% [1kHz]	35.0	25.0	23.0	0.53	0.30	Brass
7BB-35-3CL0	2.8 ±0.5kHz	200 max.	26.0 ±30% [1kHz]	35.0	25.0	23.0	0.53	0.30	Brass (with Lead Wire: AWG32 Length 50mm)
7BB-41-2C	2.2 ±0.3kHz	250 max.	24.0 ±30% [1kHz]	41.0	25.0	23.0	0.63	0.40	Brass
7BB-41-2CL0	2.2 ±0.3kHz	350 max.	24.0 ±30% [1kHz]	41.0	25.0	23.0	0.63	0.40	Brass (with Lead Wire: AWG32 Length 50mm)
7SB-34R7-3C	3.1 ±0.3kHz	150 max.	24.0 ±30% [1kHz]	34.7	25.0	23.4	0.50	0.25	Stainless

■ Node Diameter

Part Number	Node Diameter (mm)
7BB-20-6C	ø13.5
7BB-27-4C	ø17.5
7BB-35-3C	ø22.5
7BB-41-2C	ø26.5

• Sound diaphragms without feedback electrode also have the same node diameters.

⚠Note • Please read rating and ⚠CAUTION (for storage, operating, rating, soldering, mounting and handling) in this catalog to prevent smoking and/or burning, etc.
• This catalog has only typical specifications. Therefore, please approve our product specifications or transact the approval sheet for product specifications before ordering.

Piezoelectric Sound Components

Piezoelectric Sounders External Drive Pin Type

2

Microcomputers are widely used for microwave ovens, air conditioners, cars, toys, timers, and alarm equipment. Externally driven piezoelectric sounders are used in digital watches, electronic calculators, telephones and other equipment. They are driven by a signal (ex.: 2048Hz or 4096Hz) from an LSI and provide melodious sound.

■ Features

1. Low power consumption
2. No contacts; therefore, noiseless and highly reliable

■ Applications

1. Various office equipment such as PPCs, printers and keyboards
2. Audible feedback-response to some action or input.
3. Confirmation sound of various audio equipment

PKM13EPYH4002-B0

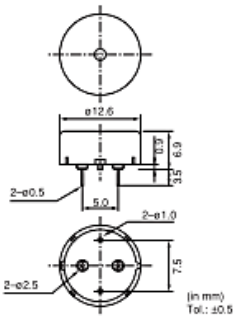

PKM17EPP-2002-B0

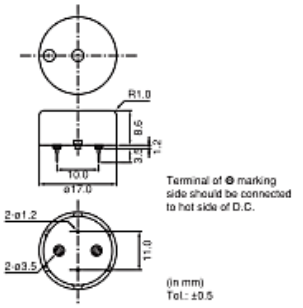

PKM17EPPH4001-B0

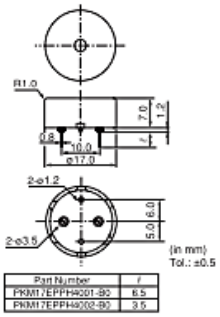

Part Number	ℓ
PKM17EPPH4001-B0	6.5
PKM17EPPH4002-B0	3.5

PKM22EPH2001

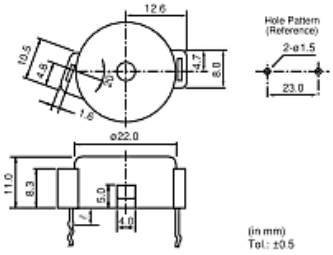

Part Number	ℓ
PKM22EPH2001	4.0
PKM22EPH2002	8.0
PKM22EPH2003	12.0

PKM22EPPH2001-B0

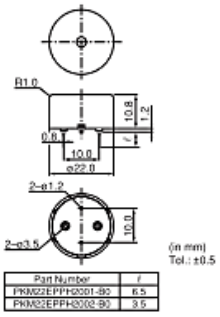

Part Number	ℓ
PKM22EPPH2001-B0	6.5
PKM22EPPH2002-B0	3.5

PKM22EPPH4001-B0

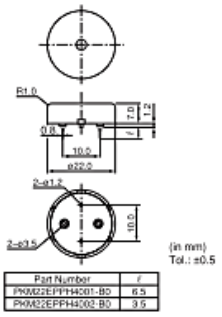

Part Number	ℓ
PKM22EPPH4001-B0	6.5
PKM22EPPH4002-B0	3.5

Continued on the following page.

⚠Note • Please read rating and ⚠CAUTION (for storage, operating, rating, soldering, mounting and handling) in this catalog to prevent smoking and/or burning, etc.
• This catalog has only typical specifications. Therefore, please approve our product specifications or transact the approval sheet for product specifications before ordering.

Continued from the preceding page.

PKM22EPPH4005-B0

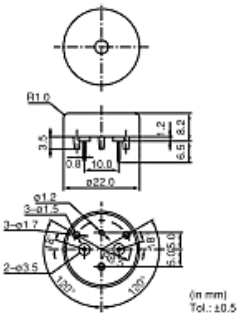

PKM22EPPH4007-B0

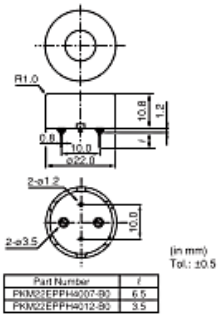

Part Number	Sound Pressure Level (dB)	Sound Pressure Level (Ref. only) (dB)	Operating Voltage Range	Capacitance (nF)	Operating Temp. Range (°C)	Storage Temp. Range (°C)
PKM13EPYH4002-B0	70 min. [3Vp-p,4kHz,square wave,10cm]	70 min. [1Vrms,4kHz,sine wave,10cm]	30.0Vp-p max.	5.5 ±30% [1kHz]	-40 to +85	-40 to +85
PKM17EPP-2002-B0	70 min. [3Vo-p,2kHz,square wave,10cm]	70 min. [1Vrms,2kHz,sine wave,10cm]	25.0Vo-p max. [with polarity]	34.0 ±30% [120Hz]	-20 to +70	-30 to +80
PKM17EPPH4001-B0	72 min. [3Vp-p,4kHz,square wave,10cm]	72 min. [1Vrms,4kHz,sine wave,10cm]	25.0Vp-p max.	7.0 ±30% [1kHz]	-20 to +70	-30 to +80
PKM22EPH2001	75 min. [3Vp-p,2kHz,square wave,10cm]	75 min. [1Vrms,2kHz,sine wave,10cm]	25.0Vp-p max.	17.0 ±30% [120Hz]	-20 to +70	-30 to +80
PKM22EPPH2001-B0	70 min. [3Vp-p,2kHz,square wave,10cm]	70 min. [1Vrms,2kHz,sine wave,10cm]	30.0Vp-p max.	19.0 ±30% [120Hz]	-20 to +70	-30 to +80
PKM22EPPH4001-B0	75 min. [3Vp-p,4kHz,square wave,10cm]	75 min. [1Vrms,4kHz,sine wave,10cm]	30.0Vp-p max.	12.0 ±30% [1kHz]	-20 to +70	-30 to +80
PKM22EPPH4005-B0	75 min. [3Vp-p,4kHz,square wave,10cm]	75 min. [1Vrms,4kHz,sine wave,10cm]	30.0Vp-p max.	12.0 ±30% [1kHz]	-20 to +70	-30 to +80
PKM22EPPH4007-B0	85 min. [3Vp-p,4kHz,square wave,10cm]	85 min. [1Vrms,4kHz,sine wave,10cm]	30.0Vp-p max.	12.0 ±30% [1kHz]	-20 to +70	-30 to +80

■ Freq. Response (Square Wave 3Vp-p, 10cm)

PKM13EPYH4002-B0

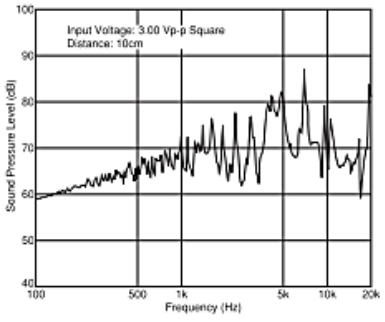

PKM17EPP-2002-B0

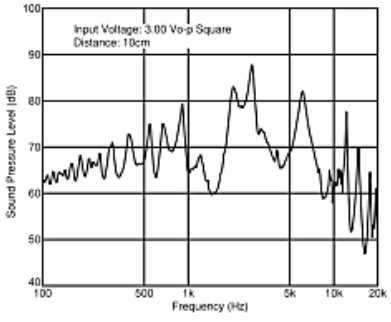

Continued on the following page.

⚠Note • Please read rating and ⚠CAUTION (for storage, operating, rating, soldering, mounting and handling) in this catalog to prevent smoking and/or burning, etc.
• This catalog has only typical specifications. Therefore, please approve our product specifications or transact the approval sheet for product specifications before ordering.

Continued from the preceding page.

■ Freq. Response (Square Wave 3Vp-p, 10cm)

PKM17EPPH4001-B0

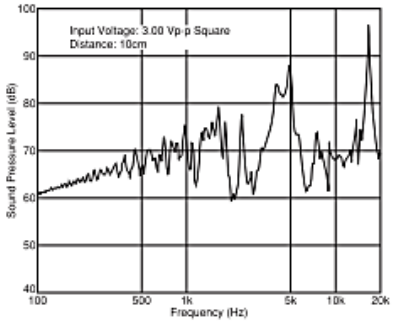

PKM22EPH2001

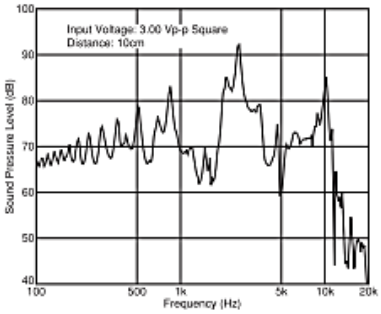

PKM22EPPH2001-B0

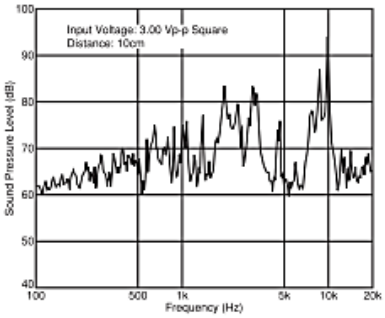

PKM22EPPH4001-B0

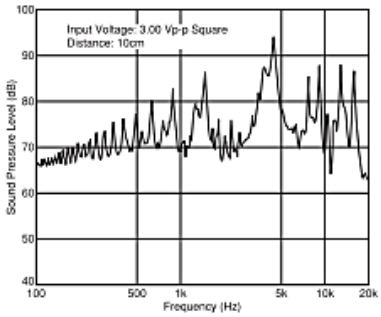

PKM22EPPH4005-B0

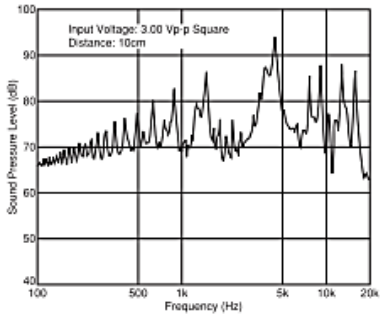

PKM22EPPH4007-B0

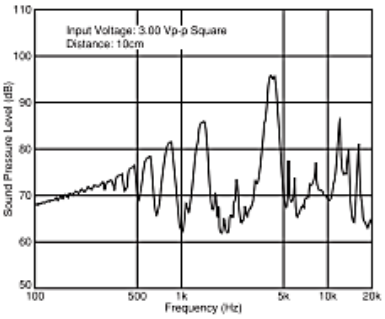

■ Freq. Response (Sine Wave 1Vrms, 10cm)

PKM13EPYH4002-B0

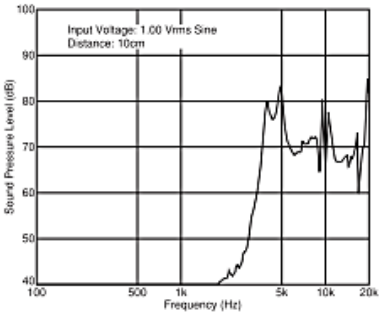

PKM17EPP-2002-B0

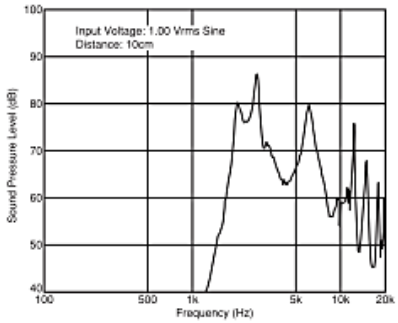

Continued on the following page.

⚠Note • Please read rating and ⚠CAUTION (for storage, operating, rating, soldering, mounting and handling) in this catalog to prevent smoking and/or burning, etc.
• This catalog has only typical specifications. Therefore, please approve our product specifications or transact the approval sheet for product specifications before ordering.

Continued from the preceding page.

■ Freq. Response (Sine Wave 1Vrms, 10cm)

PKM17EPPH4001-B0

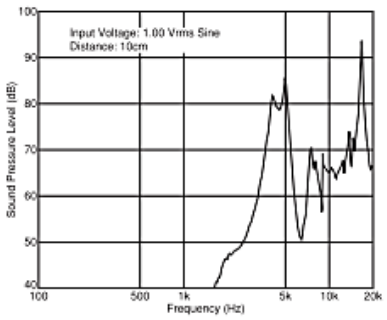

PKM22EPH2001

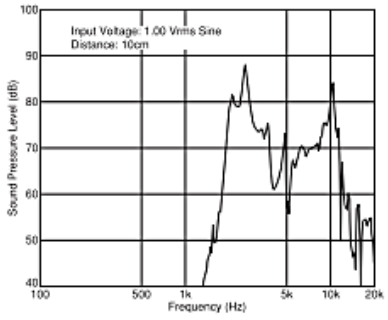

PKM22EPPH2001-B0

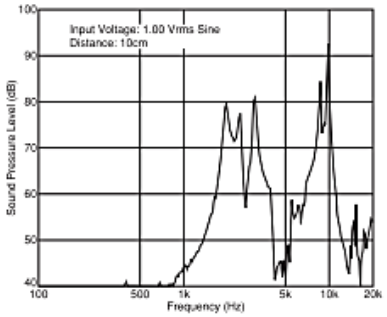

PKM22EPPH4001-B0

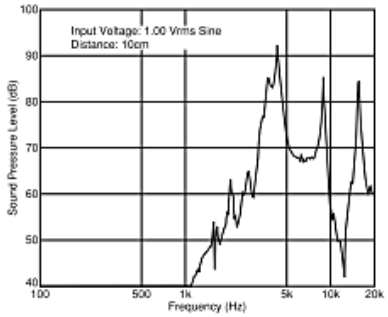

PKM22EPPH4005-B0

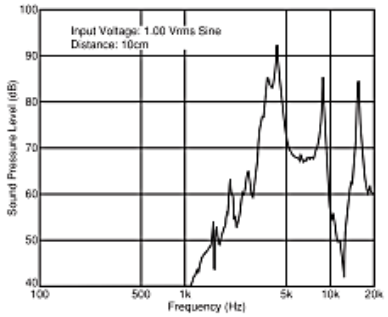

PKM22EPPH4007-B0

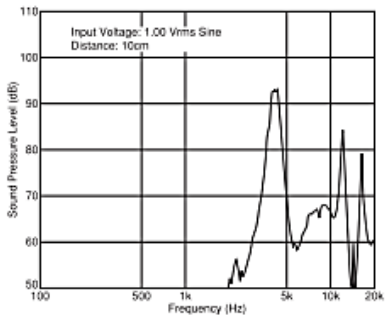

Appendix E- 40PC Series Pressure Sensor

310 7425 310 7437 310 7449 310 7450
310 7462

Pressure Sensors
Miniature Signal Conditioned

40PC Series

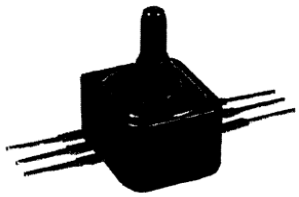

NEW

FEATURES
- Smallest amplified sensor package
- Minimal PCB space
- Fully signal conditioned
- Operating temperature range from −45° to +125°C
- Silicon piezoresistive technology
- Monolithic design
- 6 Pin DIP package
- Port designed for O-ring interface
- Excellent media compatibility
- Accuracy of 0.2%

PERFORMANCE CHARACTERISTICS

Pressure Range	±50 mm Hg	0-15 psi	0-100 psi	0-150 psi	0-250 psi
Overpressure, max.	±170 mm Hg	45 psi	200 psi	300 psi	500 psi
Supply Voltage	5 VDC ±0.25				
Supply Current	10 mA max.				
Output Source Current	0.5 mA max.				
Output Sink Current	1.0 mA max.				
Operating Temperature	−45° to +125°C (−49° to +257°F)				
Storage Temperature	−55° to +125°C (−67° to +257°F)				
Hysteresis & Repeatability	0.15% Span, Typ.				
Ratiometricity (at 4.75 to 5.25 Supply Voltage)	±0.25% Span, Typ.				
Output Load Capacitance	0.05 microtarads, max.				
Full Scale					
−50 mm Hg	0.50 VDC Typ.				
+50 mm Hg	4.50 VDC Typ.				
All other pressure ranges	4.50 VDC Typ.				
Media Compatibility P1 port	DRY GASES ONLY: Media must be compatible with epoxy based adhesive				
P2 port	Media must be compatible with glass, silicon, stainless steel, invar, Sn/Ni plating or Sn/Ag solder				

CAUTION
ELECTROSTATIC SENSITIVE DEVICES
DO NOT OPEN OR HANDLE EXCEPT AT A STATIC FREE WORKSTATION

ESD SENSITIVITY: CLASS I

Amplified

40PC SERIES ORDER GUIDE

Catalog Listing	Pressure Range psi	Pressure Type	Lead Style
40PC001B1A	±50 mm Hg	Bi-directional	1-unformed
40PC001B2A	±50 mm Hg	Bi-directional	2-formed away from port
40PC001B3A	±50 mm Hg	Bi-directional	3-formed towards port
40PC015G1A	0-15	Gage	1-unformed
40PC015G2A	0-15	Gage	2-formed away from port
40PC015G3A	0-15	Gage	3-formed towards port
40PC100G1A	0-100	Gage	1-unformed
40PC100G2A	0-100	Gage	2-formed away from port
40PC100G3A	0-100	Gage	3-formed towards port
40PC150G1A	0-150	Gage	1-unformed
40PC150G2A	0-150	Gage	2-formed away from port
40PC150G3A	0-150	Gage	3-formed towards port
40PC250G1A	0-250	Gage	1-unformed
40PC250G2A	0-250	Gage	2-formed away from port
40PC250G3A	0-250	Gage	3-formed towards port

Note: For tubing and O-Ring interface recommendations, see the 40PC Application Note in the Reference Section.

Pressure Sensors
Miniature Signal Conditioned

40PC Series

OUTPUT PERFORMANCE CHARACTERISTICS @ 25°C, 5VDC (unless otherwise noted)

Pressure Range	Null (VDC)	Span (VDC)	Sensitivity, Typ.	Linearity, B.F.S.L. (% Span) Max.		Null Shift (% Span) Max.	Span Shift (% Span) Max.	Combined Null and Span Shift (% Span) Max.
±50 mm Hg	2.50 ± 0.050	4.00 Typ.	40.0 mV/mm Hg	0.80	+25° to +50°C	±1.50	±1.50	—
					+25° to 0°C	±1.50	±1.50	—
0 to 15 psi	0.50 ± 0.11	4.00 ± 0.11	266.6 mV/psi	0.20	+25° to −18°C	±2.00	±0.75	±2.00
					+25° to +63°C	±2.00	±0.75	±2.00
					+25° to −45°C	±2.75	±1.00	±3.00
					+25° to +85°C	±2.75	±1.00	±3.00
					+25° to +125°C	—	—	—
0 to 100 psi	0.50 ± 0.04	4.00 ± 0.09	40.0 mV/psi	0.10	+25° to −18°C	±1.25	±0.75	±1.50
					+25° to +63°C	±1.25	±0.75	±1.50
					+25° to −45°C	±2.00	±1.00	±2.50
					+25° to +85°C	±2.00	±1.00	±2.50
					+25° to +125°C	±3.00	±2.00	±3.00
0 to 150 psi	0.50 ± 0.04	4.00 ± 0.07	26.6 mV/psi	0.10	+25° to −18°C	±0.75	±0.75	±0.75
					+25° to +63°C	±0.75	±0.75	±0.75
					+25° to −45°C	±1.00	±1.00	±1.00
					+25° to +85°C	±1.00	±1.00	±1.00
					+25° to +125°C	±1.50	±1.50	±1.50
0 to 250 psi	0.50 ± 0.04	4.00 ± 0.07	16.0 mV/psi	0.10	+25° to −18°C	±0.75	±0.75	±0.75
					+25° to +63°C	±0.75	±0.75	±0.75
					+25° to −45°C	±1.00	±1.00	±1.00
					+25° to +85°C	±1.00	±1.00	±1.00
					+25° to +125°C	±2.00	±2.00	±3.00

PERFORMANCE SPECIFICATIONS, TEMPERATURE/ACCURACY

Temperature Range	Total Accuracy (% Span) Max.			
	0 to 15 psi	0 to 100 psi	0 to 150 psi	0 to 250 psi
25°C	±0.4 (RSS)	±0.2 (RSS)	±0.2 (RSS)	±0.2 (RSS)
−18° to +63°C	±4.0	±2.5	±2.0	±2.0
−45° to +85°C	±4.0	±2.5	±2.0	±2.0
−45° to +125°C		±3.0	±2.5	±3.0

Note 1: Accuracy at 25°C is defined as RSS error for linearity, hysteresis, and repeatability.

Note 2: Total accuracy is the maximum deviation from the 25°C reference transfer function at any pressure or temperature over the specified ranges. This calculation includes null, span, linearity, hysteresis, repeatability, null shift, and span shift.

ELECTRICAL CONNECTION

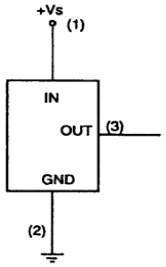

NOTES:
1. Square corner marks pin 1 (Vs).
2. Output is short circuit protected.

MOUNTING DIMENSIONS (for reference only) mm/In.

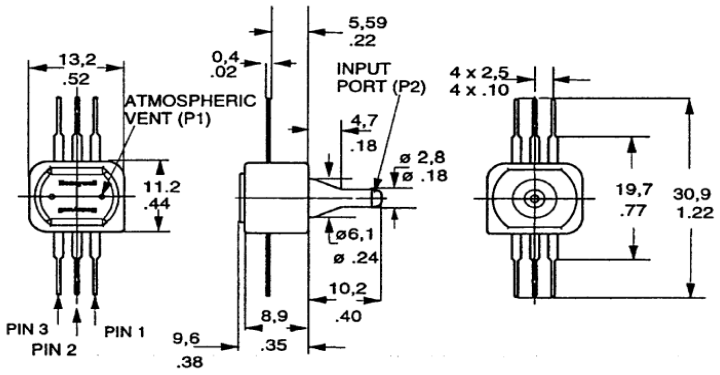

Lead Style 1

NOTE:
P1 - DRY GASES ONLY: Media must be compatible with epoxy based adhesive.
P2 - Media must be compatible with glass, silicon, stainless steel, invar, Sn/Ni plating or Sn/Ag solder.

Lead Style 2

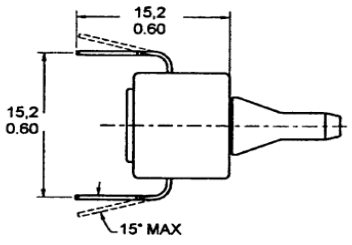

Lead Style 3

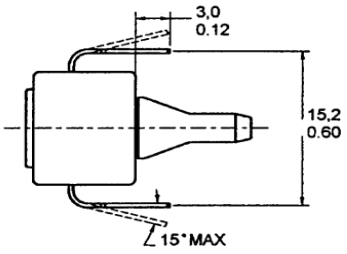

Amplified